THE UNIVERSITY
of EDINBURGH

Calculation of the $K \to \pi\ell^+\ell^-$ rare kaon decay amplitude using lattice quantum chromodynamics

Fionn Ó hÓgáin

Doctor of Philosophy
The University of Edinburgh
September 2021

Abstract

The $K \to \pi\ell^+\ell^-$ decay is a flavor changing neutral current process which is forbidden at tree level in the Standard Model and instead occurs as a second-order electroweak process. This suppression causes the decay to be sensitive to potential New Physics, however the decay channels are dominated by long-distance contributions which require non-perturbative methods of investigation. The details of a lattice calculation on a $48^3 \times 96$ zMöbius domain wall fermion action, with near-physical pion and kaon masses, $M_\pi \approx 140$ MeV and $M_K \approx 500$ MeV respectively, will be presented in this thesis.

The challenges that occur when evaluating four-point correlation functions which include two effective operators, that are required to study second-order electroweak processes, will be discussed. These challenges include extracting unphysical intermediate states that grow exponentially in the Euclidean-space correlators, the ultra-violet divergence that occurs when the operators approach each other and the extrapolation to the physical charm quark mass needed to deal with this divergence. A comparison of different methods of creating quark propagators, the All-to-All method and using Coulomb gauge-fixed wall sources, will also be presented, showing that the All-to-All method is not suited for a study of this type of decay.

The form factor $V(z)$ for the $K \to \pi\ell^+\ell^-$ decay, where $z = q^2/M_K^2$ and q is difference in the 4-momenta of the kaon and pion, is found to be $V(z) = -0.8(5.9)$ for $z = 0.0151(5)$. The large error on this result, that leads to our calculation of $V(z)$ being consistent with zero, stems from a statistical decorrelational between the single-propagator traces of physical light- and charm-quarks. This statistical decorrelational will be presented along with a discussion on how it may be tackled in the future.

Lay Summary

The Standard Model is a theory of the unification of three fundamental forces: the electromagnetic, the strong, and the weak, and a set of fundamental particles needed to describe these forces. It is the origin of many discoveries and predictions that give insight into the structure and inner-workings of our universe. There are some phenomena, however, that are not currently explainable by the Standard Model. For example we do not understand why there is more matter than antimatter in the universe, nor can we explain the existence of dark matter, which is needed to understand the observed rotation of galaxies. Finding new discrepancies between theoretical predictions and experimental observations may illuminate a path to expanding the Standard Model such that these mysteries can be solved.

One potential source of such a discrepancy is lepton-flavor universality. This is the expectation that a process involving a charged lepton, such as the electron or its heavier counterparts, the muon and tauon, and interaction mediating particles, known as gauge bosons, should behave in exactly the same way, independent of which lepton flavor is involved. The decay of a kaon to a pion and a lepton/anti-lepton pair (the titular $K \to \pi\ell^+\ell^-$ decay) is one such process. This decay has garnered interest in recent years and it has been observed at with increased precision in particle colliding experiments at CERN. We wish to improve our theoretical understanding of the decay in tandem with experiment in order to stringently test for any disagreement.

The current theoretical description of this decay is lacking in the low-momentum transfer region, as typical "pen-and-paper" methods require high-momentum transfer in order to make certain approximations that make a calculation feasible. One method that is capable of investigating this region is Lattice Quantum

Chromodynamics, where we take the sub-theory of the Standard Model, Quantum Chromodynamics, and define it with spacetime discretized on a finite 4D lattice. This method allows for computational simulations and calculations, leading to predictions that were previously out of reach. Our theoretical knowledge can then be pushed to new limits along with computational capabilities, with the cutting edge of software and hardware being employed to make more precise and more ambitious analyses of physical processes.

In this thesis I outline a Lattice Quantum Chromodynamics calculation of the $K \to \pi\ell^+\ell^-$ decay amplitude. This is the first calculation of its kind to be done with quark masses that give near-physical kaon and pion masses, which are needed in order to have a sound comparison to experimental results. A bound for the prediction of the amplitude is given, and the contributions that require a refined approach in order to tighten this bound are identified.

Declaration

I declare that this thesis was composed by myself, that the work contained herein is my own except where explicitly stated otherwise in the text, and that this work has not been submitted for any other degree or professional qualification except as specified. The results presented in Section (4.4) are in preparation to be published, with P. A. Boyle, F. Erben, J. M Flynn, V. Gülpers, R. Hill, R. Hodgson, A. Jüttner, and A. Portelli as coauthors.

Parts of this work have been published in [23].

(*Fionn Ó hÓgáin, September 2021*)

Acknowledgements

I would like to thank my supervisor Antonin Portelli, for his guidance and encouragement these past years. I will forever be grateful for his advice and support. I am also grateful for the help and insight given by me second supervisor Peter Boyle, who laid much of the computational foundation upon which this project was built.

My thanks also go to everyone in RBC-UKQCD, for their discussion, input, and inspiration. In particular, but of course not limited to, I would like to thank Norman Christ, Jonathan Flynn, Vera Gülpers, Andreas Jüttner, Chris Sachrajda, and Justus Tobias Tsang for their advice. I would like to thank Felix Erben, Raoul Hodgson, and James Richings for their help gathering key data that was used in this project. I cannot express enough gratitude to Ryan Hill, for his help verifying analysis that was done, when I know he was much too busy to help as much as he did. Special thanks go to my officemate Andrew Zhen Ning Yong, for sharing his camaraderie and putting up with mine.

Finally I would like to thank all of my friends and family for providing so much love and support during such a socially distant time. All of the movie nights, discord games, zoom "pub" quizzes, streamed comedy gigs, online book clubs, dog walks, picnics, group chat memes, and video calls helped me feel grounded in an unsettled world. Getting through the double whammy of a pandemic lockdown and thesis-writing lockdown was made so much more manageable with you all in my life.

Go raibh míle maith agaibh.

Contents

List of Figures

List of Tables

Introduction

The $K \to \pi\ell^+\ell^-$ ($\ell = e, \mu$) rare kaon decays are flavor changing neutral current processes that occur in the occur in the Standard Model (SM) through W-W and γ exchange diagrams. Theses second-order electroweak interactions are suppressed in the SM and so the decays can be used to probe areas of potential New Physics, such as lepton flavor universality violation. Short distance top quark contributions to the CP-conserving $K_S \to \pi^0\ell^+\ell^-$ and $K^+ \to \pi^+\ell^+\ell^-$ decays are suppressed by the CKM factor $\mathrm{Re}(\lambda_t)$, and short distance light quark contributions are suppressed by a logarithmic GIM cancellation. As such the long-distance single-photon exchange dominates these processes.
These decays have been observed in experiment at the NA48 experiment at the Super Proton Synchrotron at CERN in the late 1990s and early 2000s, with ~ 1000 $K^\pm \to \pi^\pm\ell^+\ell^-$ [11, 12] and 13 $K_S \to \pi^0\ell^+\ell^-$ [13, 14] decay modes being observed. The NA62 experiment, the successor of NA48, measured $\sim$ 28000 $K^+ \to \pi^+\mu^+\mu^-$ events during the 20016-2018 Run 1, with prospects for further measurements during the 2012-2024 Run 2. The PDG average of the branching ratios of these decays are [92]

$$\begin{aligned} BR\left[K^+ \to \pi^+e^+e^-\right] &= (3.00 \pm 0.09) \times 10^{-7}, \\ BR\left[K^+ \to \pi^+\mu^+\mu^-\right] &= (9.4 \pm 0.6) \times 10^{-8}, \\ BR\left[K_S \to \pi^0e^+e^-\right] &= \left(3.0^{+1.4}_{-1.2}\right) \times 10^{-9}, \\ BR\left[K_S \to \pi^0\mu^+\mu^-\right] &= \left(2.9^{+1.5}_{-1.2}\right) \times 10^{-9}. \end{aligned}$$

There are no theoretical estimates for these branching ratios, due to the long-distance nature of the decays. Lattice QCD is uniquely poised in its abilities to compute long distance contributions to this decay, and an exploratory calculation of the $K^+ \to \pi^+\ell^+\ell^-$ decay amplitude with unphysically heavy pion and kaon masses was performed in [34]. This thesis outlines the first lattice QCD study of this decay using physical light quark masses, and thus near-physical pion and

kaon masses.

The structure of the thesis is as follows. Chapters (1) through (3) will provide the background knowledge required to give context to the results that are presented in Chapter (4). Chapter (1) will introduce the Standard Model, giving a description of the fundamental interactions, particles, and symmetries in Section (1.1). Following that a summary of quantum chromodynamics and the electroweak theory are given in Sections (1.2) and (1.3). As they play a key role in the study of rare kaon decays Fermi's theory of the weak interaction and the operator product expansion method are introduced in Sections (1.4) and (1.5.1). Finally a description of chiral perturbation theory, which has previously been used to study the long-distance part of rare kaon decays, is given in Section (1.6).

Chapter (2) introduces lattice QCD, describing fundamental concepts of discretizing QCD in Section (2.1), along with a review of the fermion actions used in this project. An overview of the process simulating QCD on the lattice and extracting observables from these simulations is is given in Section (2.2). Sections (2.3) and (2.4) describe the various methods used to construct quark propagators for this calculation and the structure of the sources used to create the propagators.

A summary of the $K \to \pi\ell^+\ell^-$ decay is given in Chapter (3), with an overview of the effective Hamiltonians needed to study the decay in Section (3.1), along with a non-lattice description of the decay amplitude. Experimental and non-lattice theoretical predictions for this amplitude are also presented. Section (3.2) defines this amplitude in Euclidean spacetime and describes how to extract the it using lattice QCD.

Chapter (4) gives an outline of the lattice QCD calculation that was performed. Details of the simulation are given in Section (4.1). with a description of the calculation setup in Section (4.2). This setup is contrasted with an all-to-all approach as presented in Section (4.3), where results from an all-to-all study of the decay are used to justify the choice not to perform the full calculation with all-to-all vectors and meson fields. The numerical results of the calculation are given in Section (4.4), with a discussion of the results and future outlook in Chapter (5).

Chapter 1

The Standard Model

The Standard Model (SM) is a theory of the unification of three fundamental forces: the electromagnetic, the strong, and the weak, and a set of fundamental particles needed to describe these forces. The SM gives us a highly accurate representation of the territory it is capable of mapping, guiding the way to the discovery of fundamental particles, such as the tau[90], the Z-boson[54], Higgs-boson[49, 60], and quarks [52] and giving theoretical predictions that have been verified to incredible precision. For example the prediction for the anomalous magnetic moment of the electron agrees with experiment to 10 significant figures [7].

However there are many phenomena that are not contained in this territory. There is no SM answer to the question of why we observe an asymmetry in the amount of matter/antimatter in the universe [85] or a satisfactory explanation for dark matter, needed to describe the observed rotation of galaxies[16], let alone a clear way to fold the fourth fundamental force of gravity into the model. There are also parts of the SM that still come under scrutiny, with some discrepancies invoking the curiosity of many scientist interested in finding ways to expand the borders of the theory. In contrast to the electron, there is disagreement between the SM and experimental predictions for the anomalous magnetic moment of the muon, interim results from a Fermilab experiment shows that this discrepancy is currently 4.2σ[3] and further data collection is expected to improve the statistical error on this result. Lattice Quantum Chromodynamics is expected to improve the theoretical prediction by reducing uncertainties surrounding hadronic contributions [6], with results from the Budapest-Marseille-Wuppertal collaboration showing that the discrepancy can potentially be reduced to 1.5σ

with these improvements [22].
Lepton flavor universality is another source of tension in the SM. Decays involving different flavors of lepton should not prefer any particular flavor, according to the SM, and so ratios of decay probabilities ought to be measured to be close to one. Experiments at LHCb that look at $B \to K\ell^+\ell^-$, for $\ell = e, \mu$, show a 3.1σ discrepancy between this prediction and their results [2]. The analogous decay of $K \to \pi\ell^+\ell^-$, which is the focus of this thesis, is also an avenue in which lepton flavor universality can be explored for inconsistencies in the SM[38].
In order to discover New Physics, to increase the overlap in what we observe and how we describe it, both experiment and theory must be push to the cutting edge in tandem. In this chapter I will give an introduction to the SM, beginning with Section (1.1) where I will give an overview of the model, discussing fundamental interactions, particles and symmetries. Following that I will give further details needed to understand rare kaon decays, presenting quantum chromodynamics in Section(1.2), electroweak theory in Section (1.3), and Fermi effective theory of the weak interaction in Section(1.4).

1.1 Fundamental Interactions, Particles and Symmetries

The Standard Model is constructed using the mathematical framework of quantum field theory (QFT), where particles are treated as excited states of dynamical quantum fields. The interaction terms in a general, renormalizable, Lagrangian which obeys the appropriate symmetries describe the interactions between these particles. For the SM the Lagrangian takes the form of

$$\mathcal{L}_{SM} = \mathcal{L}_{QCD} + \mathcal{L}_{EW} + \mathcal{L}_{Higgs} + \mathcal{L}_{Yukawa}. \tag{1.1}$$

The particles that are described in the SM can be split into fermions, with $\frac{1}{2}$-integer spin, and bosons, with integer spin. Fermions obey Fermi-Dirac statistics and come in two types: quarks and leptons (along with their antimatter counterparts: anti-quarks and anti-leptons). There are 3 generations of two quarks types: the up, charm, and top quarks make up the "up" type quarks and the down, strange, and bottom quarks make up the "down" type quarks. The leptons, again, have three generations, consisting of the e^-, μ^-, and τ^- leptons, each of which has an associated neutrino. The neutrinos participate only in weak

interactions, the charged leptons participate in electroweak (EW) interactions, and the quarks participate in strong and EW interactions.
Bosons obey Bose-Einstein statistics and consists of four, force carrying, gauge bosons with spin 1 and one scalar boson with spin 0. The gauge bosons include the photon, which mediates electromagnetic forces, the W and Z bosons, that mediate the EW forces, and the gluon which mediates the strong force. The scalar boson is known as the Higgs bosons which, when it acquires a non-zero vacuum expectation value (VEV), gives rise to the quarks, leptons, the W boson, and the Z boson acquiring mass at low energies.
I will now focus on the QCD Lagrangian, describing it and the relevant symmetries and conserved currents needed for this thesis.

1.2 Quantum Chromodynamics

The QCD Lagrangian is given by

$$\mathcal{L}_{QCD} = \sum_f \overline{\psi}_f(x) \left(i\not{D} - m_f \right) \psi_f(x) - \frac{1}{4} G^a_{\mu,\nu} G^{\mu,\nu}_a. \tag{1.2}$$

Here the quarks are represented as Dirac 4-spinors, ψ_f, and we have summed over the six flavors, f, of quark, the spinor indices, $\mu, \nu = 1, 2, 3, 4$, and the color index, a, which goes from 1 to 8 (one index for each generator of SU(3)). The covariant derivative is given by

$$D_\mu = \partial_\mu + igT^a A^a_\mu \tag{1.3}$$

where g is the QCD coupling, T^a are the generators of the SU(3) algebra and A^a_μ is the gauge field of the gluon. This gauge field is also used to define the gluon field strength tensor, $G^a_{\mu,\nu}$,

$$G^a_{\mu,\nu} = \partial_\mu A^a_\nu - \partial_\nu A^a_\mu + g f^{abc} A_{\mu b} A_{\mu c} \tag{1.4}$$

where f^{abc} are the SU(3) structure constants.
The quark-gluon interaction is induced by the covariant derivative and (unlike in QED) the gluon-gluon interaction is induced by the gluon field strength tensor. Expanding a functional integral of the QCD Lagrangian over the $\psi, \overline{\psi}$, andA^a_μ fields in perturbation theory, starting with the free Lagrangian and $g = 0$, the Feynman rules can be derived. These show three basic interactions: quarks

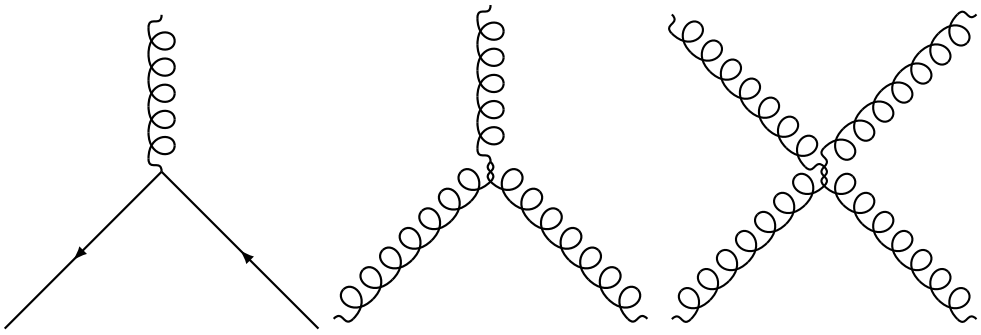

(a) *Quark-gluon vertex* **(b)** *Three-gluon vertex* **(c)** *Four-gluon vertex*

Figure 1.1 *Feynman diagrams showing the basic interaction vertices in QCD.*

absorbing and emitting gluons, gluons absorbing and emitting gluons and two gluons interacting. In principle the gluon fields in equation (1.2) should be written with color indices and the quark feilds with both Dirac and color indices, as $A^a_{\mu,c,d}$ and $\psi^f_{c,\mu}$. These are suppressed for brevity though it is color that dictates the bound states in which quarks can exist. The colors are conventionally called red, green, and blue and these must be combined such that "colorless" (or white) bound states, called hadrons, can be created.

Hadrons can be made up of either two quarks, a color-anti-color pair, called mesons, or three quarks, one of each color, called baryons. Tetra- and pentaquark are exotic particles that have been observed in experiment [1, 72]. Hexa- and heptaquark, consisting of six and seven quarks respectively, can exist in theory but have never been observed in experiment.

1.2.1 The Running Coupling

After a renormalization procedure to subtract UV divergences the QCD coupling, g, gains a dependence on energy scale, as can be seen in Figure (1.2). This dependence is determined by the renormalization group equation, for a given scheme, $\mathcal{S}$,

$$\mu \frac{\partial g_{\mathcal{S}}(\mu)}{\partial \mu} = \frac{\partial g_{\mathcal{S}}(\mu)}{\partial ln \mu} = \beta_{\mathcal{S}}(g_{\mathcal{S}}) \tag{1.5}$$

where in perturbation theory the β function takes the form

$$\beta_{\mathcal{S}}(g_{\mathcal{S}}) = -b_0 g_{\mathcal{S}}^3 - b_1 g_{\mathcal{S}}^3 - b_2 g_{\mathcal{S}}^5 - \dots \tag{1.6}$$

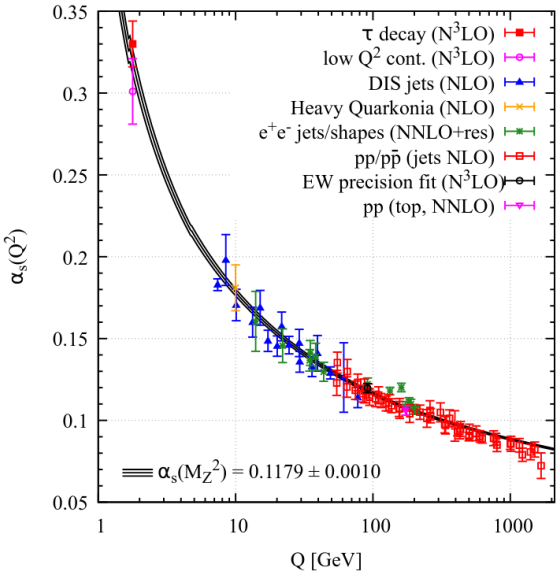

Figure 1.2 *The Q dependence of the strong coupling, α_s[92]. The respective degree of QCD perturbation theory used in the extraction of α_s is indicated in brackets.*

The first two coefficients are scheme independent and are given by

$$b_0 = \frac{1}{(4\pi)^2}\left(11 - \frac{2}{3}n_f\right), \quad b_1 = \frac{1}{(4\pi)^2}\left(102 - \frac{38}{3}n_f\right) \tag{1.7}$$

where n_f is the number of "active" quark flavors, that is, the number of quarks in which the energy-momentum involved in allows for the production of. The coefficients are known up to b_4 in the $\overline{MS}$ scheme [10, 59], one of the most commonly used schemes. Solving equation (1.5) to first order for $\alpha_{\mathcal{S}} = \frac{g^2}{4\pi}$ gives

$$\alpha_{\mathcal{S}}(\mu) = \frac{\alpha_{\mathcal{S}}(\Lambda)}{1 + \left(11 - \frac{2}{3}n_f\right)\frac{\alpha_{\mathcal{S}}(\Lambda)}{4\pi} ln\left(\frac{\mu^2}{\Lambda^2}\right)} \tag{1.8}$$

It can be seen for $n_f = 6$, and up to $n_f = 16$, that the coupling is positive, a phenomena observed by experiment. As μ grows the coupling shrinks and so quarks and gluons become asymptotically free, with quarks feeling no gluon exchange they can be considered quasi-free particles. At low energies the coupling grows, leading to quarks and gluons being confined to hadrons.

There must also exist a scale, Λ, such that $\alpha_{\mathcal{S}} \to \infty$ as $\mu \to \Lambda$. The point where the coupling goes to infinity is called the Landau pole, and although perturbation theory breaks down before the Landau pole is reached, and so the very definition of the coupling represented in terms of the β function breaks down, it is still

convenient to to define a mass scale, Λ, such that

$$\left(11 - \frac{2}{3}n_f\right) \frac{\alpha_{\mathcal{S}}(\Lambda)}{4\pi} ln\left(\frac{\mu^2}{\Lambda^2}\right) = 1 \tag{1.9}$$

which allows us to write equation (1.8) at this scale as

$$\alpha_{\mathcal{S}}(\mu) = \frac{2\pi}{\left(11 - \frac{2}{3}n_f\right) ln\left(\frac{\mu^2}{\Lambda^2}\right)} \tag{1.10}$$

This description depends on the scheme chosen, the number of active quarks, and the order to which the perturbative calculation has been established, but it is still useful to determine an energy scale at which perturbation is theory is valid above and not valid below. Values for $\Lambda_{\overline{MS}}$ range from $\sim$ 200 MeV for $n_f = 5$ to $\sim$ 400 MeV for $n_f = 3$ [15, 27, 31]. This is roughly the mass of the lightest hadrons, and so there is a need for non-perturbative methods in order to study QCD phenomena at low energies.

1.2.2 Global Symmetries

In order or QCD to be a valid relativistic QFT it must contain the global Poincaré symmetry, that is: translational symmetry in time and space, rotational symmetry in space, and an inertial reference frame invariance where Lorentz transformations relate uniformly moving bodies. Noether's theorem states that each continuous symmetry of an action gives rise to a conservation law [81]. In the case of the Poincaré symmetries, in four dimensional spacetime, there are 10 such symmetries, giving 10 conservation laws: time invariance associated to energy conservation, 3 translational invariances associated to 3 momenta being conserved, 3 rotational invariances associated to the angular momenta being conserved, and the boost invariances associated to the 3 components of velocity of the center of mass being conserved.
It is possible to extend the Lorentz group to the "nonorthochronous improper Lorentz group" by including the discrete transformations Parity, $\mathcal{P}$, and time reversal, $\mathcal{T}$;

$$\mathcal{P}(t, \vec{x}) = (t, -\vec{x}), \quad \mathcal{T}(t, \vec{x}) = (-t, \vec{x}). \tag{1.11}$$

It is also convenient to discuss a third discrete transformation, charge conjugation, $\mathcal{C}$, under which particles and anti-particles are interchanged. Although the gravitational, electromagnetic and strong interactions are invariant under individual

$\mathcal{C}, \mathcal{P}, \mathcal{T}$ transformations, a relativistic field theory generally does not have to be. For example, the weak interactions violate $\mathcal{C}$ and $\mathcal{P}$ separately, but preserve $\mathcal{CP}$ and $\mathcal{T}$. $\mathcal{CP}$ and $\mathcal{T}$ violations have been observed in neutral kaon decays [45], but they preserve $\mathcal{CPT}$, along with all other processes in nature. In fact, a Lorentz-invariant QFT with a hermitian Hamiltonian cannot be build such that it violates $\mathcal{CPT}$[88].
In QCD these operation transform the fermion fields as

$$\begin{aligned} \psi(t, \vec{x}) &\to \eta \gamma_0 \psi(t, -\vec{x}) \\ \overline{\psi}(t, \vec{x}) &\to \eta^* \overline{\psi}(t, -\vec{x}) \gamma_0 \end{aligned} \tag{1.12}$$

for the parity transformation, where η is a complex phase,

$$\begin{aligned} \psi(t, \vec{x}) &\to \gamma_1 \gamma_3 \psi(-t, \vec{x}) \\ \overline{\psi}(t, \vec{x}) &\to \overline{\psi}(-t, \vec{x}) \gamma_1 \gamma_3 \end{aligned} \tag{1.13}$$

for time reversal, and

$$\begin{aligned} \psi(t, \vec{x}) &\to -i \left(\overline{\psi}(t, \vec{x}) \gamma_0 \gamma_2 \right)^T \\ \overline{\psi}(t, \vec{x}) &\to -i \left(\gamma_0 \gamma_2 \psi(t, \vec{x}) \right)^T \end{aligned} \tag{1.14}$$

for charge conjugation. It can be seen that fermion fields are not eigenstates of these transformations but that fermion bilinears are. These symmetries are important for the construction of hadron interpolators, as we will see in Section (2.2.2).
The charged pion, for example, has zero spin ($\mathcal{J} = 0$), negative parity ($\mathcal{P} = -1$), isospin $I = 1$, and charge $Q = +e$, in units of electromagnetic charge, e. Using a $\overline{d}$-u quark combination, to match the charge and isospin, we can construct the appropriate pseudoscalar state

$$\phi(x) = \overline{d}(x) \gamma_5 u(x). \tag{1.15}$$

The pion is the lowest energy state that is created by this operator, and we will see in Section (2.2.2) how this helps us extract observables from the lattice in QCD. A generic meson interpolator has the form $\overline{\psi} \Gamma \psi$ and Table (1.1) shows quantum numbers for interpolators in this form.

State	$\mathcal{J}^{\mathcal{PC}}$	Γ	Particles
Scalar	0^{++}	$\mathbb{1}, \gamma_0$	$f_0, a_0, K_0^*, \ldots$
Pseudoscalar	0^{-+}	$\gamma_5, \gamma_5\gamma_0$	$\pi^{+-}, \pi^0, \eta, K^{+-}, K^0, \ldots$
Vector	1^{--}	$\gamma_i, \gamma_0\gamma_i$	$\rho^{+-}, \rho^0, \omega, K^*, \phi, \ldots$
Axial Vector	1^{++}	$\gamma_i\gamma_5$	$f_1, a_1, \ldots$
Tensor	1^{+-}	$\gamma_i\gamma_j$	$h_1, b_1, \ldots$

Table 1.1 *Quantum numbers for of meson interpolating operators, in the form $\overline{\psi}\Gamma\psi$ and some of the particles that are represented by those interpolators.*

1.2.3 Chiral Symmetry

If we consider the chiral transformation of quarks in QCD

$$\begin{aligned} \psi(x) &\to \psi' = e^{i\alpha\gamma_5}\psi \\ \overline{\psi}(x) &\to \overline{\psi}' = \overline{\psi}e^{i\alpha\gamma_5}, \end{aligned} \tag{1.16}$$

where α is a real constant, the Lagrangian transforms as

$$\mathcal{L}_{QCD}\left(\psi', \overline{\psi}', A, m\right) = \mathcal{L}_{QCD}\left(\psi, \overline{\psi}, A, m = 0\right) - m\overline{\psi}e^{i2\alpha\gamma_5}\psi. \tag{1.17}$$

and we see that the massless Lagrangian is invariant under the transformation, but the massive part is not. The Lagrangian can be split into "left-handed" and "right-handed" fermion fields using projectors

$$P_R = \frac{1}{2}\left(\mathbb{1} + \gamma_5\right), \quad P_L = \frac{1}{2}\left(\mathbb{1} - \gamma_5\right) \tag{1.18}$$

such that

$$\psi_{L/R} = P_{L/R}\psi, \quad \overline{\psi}_{L/R} = \overline{\psi}P_{R/L}. \tag{1.19}$$

Using these projectors we can write the massless Lagrangian as

$$\mathcal{L}_{QCD}(\psi, \overline{\psi}, A, m = 0) = \overline{\psi}_L D\psi_L + \overline{\psi}_R D\psi_R \tag{1.20}$$

and the massive term can be written as

$$m\overline{\psi}\psi = m\left(\overline{\psi}_R\psi_L + \overline{\psi}_L\psi_R\right) \tag{1.21}$$

The mass term mixes the left- and right-handed fields, and explicitly breaks the chiral symmetry. The symmetry is also implicitly broken by the quark condensate.

If the quarks were massless the energy cost of creating a $\psi\overline{\psi}$ would be small and these quarks would have a strong attractive interaction. It is thus expected that the QCD vacuum will contain a condensate of $\psi\overline{\psi}$ pairs, leading to a non-zero expectation value for the scalar operator

$$\langle 0|\, \psi\overline{\psi}\, |0\rangle = \langle 0|\, \psi_L\overline{\psi}_R + \psi_R\overline{\psi}_L\, |0\rangle \neq 0 \tag{1.22}$$

which, again, mixes the left- and right-handed fields.
Thus the $SU(n_f)_L \times SU(n_f)_R$ symmetry is spontaneously broken to $SU(n_f)$. The Goldstone theorem predicts that there will be $n_f - 1$ pseudo-Goldstone bosons[55]. With only u and d quarks the three pions (π^-, π_0, π^+) are these pseudo-Goldstone bosons. With an additional s quark the four kaons $\left(K^-, K_0, \overline{K}_0, K^+\right)$ and the η meson make up the missing five pseudo-Goldstone bosons.
While taking the limit of vanishing quark mass, or the chiral limit, an effective theory, called chiral perturbation theory (or χPT), can be constructed by expanding QCD in the external momenta and quark masses. This theory will be discussed further in Section (1.6).

1.2.4 Chiral Ward Identities

Noether's theorem allows us to define conserved currents and charges for each continuous symmetry of a given action. It is convenient to now describe several such conserved currents for the QCD action in the continuum before discussing them on the lattice. We do so by considering an infinitesimal variation on the quark fields which can be written in the form

$$\psi(x) \to \psi'(x) = \psi(x) + \delta\psi(x) \tag{1.23}$$

The infinitesimal deformation of the of the fermion field associated with the vector symmetry is given by

$$\begin{aligned} \delta\psi(x) &= i\alpha\lambda\psi(x) \\ \delta\overline{\psi}(x) &= i\overline{\psi}(x)\alpha\hat{\lambda} \end{aligned} \tag{1.24}$$

where α is a real infinitesimal constant and $\lambda, \hat{\lambda}$ are matrices in Dirac and flavor spaces. In SU(2), where $\mathcal{M}$=diag(m_u, m_d) is the mass matrix in flavor space it

can be shown that

$$\partial_\mu \left(\overline{\psi}\gamma_\mu \lambda \psi\right) = \overline{\psi}\left(\hat{\lambda}\mathcal{M} + \mathcal{M}\lambda\right)\psi. \tag{1.25}$$

We consider four different matrix structures: $\lambda = \mathbb{1}$; the Pauli matrices, $\lambda = \sigma^a$; $\lambda = \gamma_5$; and $\lambda = \gamma_5\sigma^a$. These give the vector currents

$$\lambda = \mathbb{1}, \hat{\lambda} = -\mathbb{1} \quad : \quad \partial^\mu J_\mu \equiv \partial^\mu \left(\overline{\psi}\gamma_\mu\psi\right) = 0 \tag{1.26}$$

$$\lambda = \sigma^a, \hat{\lambda} = -\sigma^a \quad : \quad \partial^\mu J^a_\mu \equiv \partial^\mu \left(\overline{\psi}\gamma_\mu\sigma^a\psi\right) = \overline{\psi}\left[\mathcal{M}, \sigma^a\right]\psi \tag{1.27}$$

and the axial currents

$$\lambda = \hat{\lambda} = \gamma_5 \quad : \quad \partial^\mu A_\mu \equiv \partial^\mu \left(\overline{\psi}\gamma_\mu\gamma_5\psi\right) = 2\overline{\psi}\mathcal{M}\gamma_5\psi \tag{1.28}$$

$$\lambda = \hat{\lambda} = \gamma_5\sigma^a \quad : \quad \partial^\mu A^a_\mu \equiv \partial^\mu \left(\overline{\psi}\gamma_\mu\gamma_5\sigma^a\psi\right) = \overline{\psi}\{\mathcal{M}, \sigma^a\}\gamma_5\psi \tag{1.29}$$

The Ward identity in equation (1.26), $\partial_\mu J^\mu = 0$, holds regardless of of quark mass. The symmetry in equation (1.27) is broken by the mass, but holds for degenerate u/d quarks. Equation (1.28) is the chiral symmetry discuss in the previous section. Finally for equation (1.29), if we define

$$A^a_\mu = \frac{1}{2}\overline{\psi}\gamma_\mu\gamma_5\sigma^a\psi \tag{1.30}$$

as the partially conserved axial current, and

$$P^a = \frac{1}{2}\overline{\psi}\gamma_5\sigma^a\psi \tag{1.31}$$

as the pseudoscalar density, then equation (1.29) gives us the partially conserved axial current (PCAC) relation:

$$\partial^\mu \left\langle 0\right| A^a_\mu(x)\mathcal{O}\left|0\right\rangle = 2m \left\langle 0\right| P^a(x)\mathcal{O}\left|0\right\rangle. \tag{1.32}$$

This relation can be used to calculate the pion decay constant, f_π, as

$$\partial^\mu \left\langle 0\right| A^a_\mu(x)\left|\pi^b(\vec{p}=\vec{0})\right\rangle = \delta_{ab} m_\pi^2 f_\pi e^{-im_\pi t} \tag{1.33}$$

but it also useful for proving that the choices of quark masses on the lattice are reasonable, as will be discussed in Section (2.1.5).

1.3 Electroweak Theory

The electroweak (EW) theory unifies electromagnetism and the weak interactions with a $SU(2)\times SU(2)$ symmetry group that is spontaneously broken via the Higgs mechanism to $U(1)$ [49, 60] and its Lagrangian is given by

$$\mathcal{L}_{EW} = \mathcal{L}_{gauge} + \mathcal{L}_{fermion} + \mathcal{L}_{Higgs} + \mathcal{L}_{Yukawa} \tag{1.34}$$

It is a chirally coupled gauge theory where left-handed fermion fields transform as $SU(2)$ doublets and right-handed fermion fields transform as $SU(2)$ singlets. Be we describe these fermion fields in more detail we do well to define the gauge sector of the Lagrangian:

$$\mathcal{L}_{gauge} = -\frac{1}{4}W^a_{\mu\nu}W^{a\mu\nu} - \frac{1}{4}B_{\mu\nu}B^{\mu\nu}. \tag{1.35}$$

This Lagrangian describes the interactions o the gauge bosons, the three W vector bosons and the B vector boson, which are described bu the field strength tensors corresponding to the $SU(2)$ and $U(1)$ groups respectively:

$$W^a_{\mu\nu} = \partial_\mu W^a_\nu - \partial_\nu W^a_\mu - g_W \epsilon^{abc}\left[\sigma^b, \sigma^c\right], \quad a \in [1,2,3] \tag{1.36}$$

and

$$B_{\mu\nu} = \partial_\mu B_\nu - \partial_\nu B_\mu. \tag{1.37}$$

Here W^a_μ and g_W are the gauge field and coupling constant for the $SU(2)$ group and $B_{\mu\nu}$ is the gauge field for the $U(1)$ group. We will see how these four massless vector bosons will be broken to the familiar three massive and one massless bosons by the Higgs mechanism.

1.3.1 Higgs Sector

The Lagrangian for the Higgs sector is

$$\mathcal{L}_{Higgs} = \left(D_\mu\phi\right)^\dagger D^\mu\phi - V\left(\phi^\dagger\phi\right) \tag{1.38}$$

where the scalar field, ϕ, is an $SU(2)$ doublet

$$\phi = \begin{pmatrix} \phi^+ \\ \phi^0 \end{pmatrix} \tag{1.39}$$

and the Higgs potential is given as

$$V\left(\phi^\dagger\phi\right) = \mu^2\phi^\dagger\phi + \lambda\left(\phi^\dagger\phi\right)^2. \tag{1.40}$$

In order for the theory to be invariant under local transformations we need

$$D_\mu = \partial_\mu + ig_W\frac{1}{2}\vec{\sigma}\cdot\vec{W}_\mu + ig_B Y B_\mu \tag{1.41}$$

where g_B is the coupling constant for the $U(1)$ group and Y is the hypercharge, the generator for the $U(1$ group. For $\mu^2 < 0$ and $\lambda > 0$ we acquire a vacuum expectation value of

$$\langle\phi\rangle = \frac{1}{\sqrt{2}}\begin{pmatrix} 0 \\ v \end{pmatrix}, \quad v = \sqrt{\frac{-\mu^2}{\lambda}} \tag{1.42}$$

If we consider $Q \equiv T^3 + Y$, where $T^a = \frac{1}{2}\sigma^a$, then

$$Q\langle\phi\rangle = \left[\frac{1}{2}\begin{pmatrix} 1 & 0 \\ 0 & -1 \end{pmatrix} + \frac{1}{2}\begin{pmatrix} 1 & 0 \\ 0 & 1 \end{pmatrix}\right]\langle\phi\rangle = \langle 0\rangle \rightarrow e^{i\epsilon Q}\langle\phi\rangle = \langle\phi\rangle \tag{1.43}$$

but

$$T^1\langle\phi\rangle = \frac{1}{2}\begin{pmatrix} 0 & 1 \\ -1 & 0 \end{pmatrix}\langle\phi\rangle = \frac{1}{2\sqrt{2}}\begin{pmatrix} v \\ 0 \end{pmatrix} \neq \langle 0\rangle \tag{1.44}$$

and we see that Q gives a symmetry and T^1, along with T^2 and $T^3 - Y$, is a broken generator. From this we expect 1 massless Goldstone boson and 3 Goldstone bosons that need to be gauged away. A gauge transformation, U, can be chosen such that we can rewrite the Higgs doublet as

$$\phi'(x) = U\phi(x) = \frac{1}{\sqrt{2}}(0, \quad v + h(x)) \tag{1.45}$$

where we are expanding about the minimal potential, v, and $h(x)$ is the Higgs field. We can now write the Higgs Lagrangian as

$$\begin{aligned}\mathcal{L}_{Higgs} &= \left[D_\mu \begin{pmatrix} 0 \\ h+v \end{pmatrix}\right]^\dagger D^\mu \begin{pmatrix} 0 \\ h+v \end{pmatrix} - V\left(\frac{1}{2}(h+v)^2\right) \\ &= \frac{1}{2}\partial_\mu h \partial^\mu h - \frac{\mu^2}{2}(h+v)^2 - \frac{\lambda}{4}(h+v)^4 \\ &\quad + \frac{g_W^2}{8}(h+v)^2\left(W_\mu^1 W^{1\mu} + W_\mu^2 W^{2\mu}\right) \\ &\quad + \frac{1}{8}\left(g_B B^\mu - g_W W^{3\mu}\right)\left(g_B B_\mu - g_W W_\mu^3\right)(h+v)^2\end{aligned} \tag{1.46}$$

and we can see the coupling between the Higgs field and the vector bosons. The interactions of the W_μ^1 and W_μ^2 arise through combinations of $W_\mu^\pm = W_\mu^2 + iW_\mu^1$ with an associated mass $M_W = \frac{1}{2}vg_W$ being read directly from the $\frac{1}{8}v^2g_W^2\left(\left(W_\mu^1\right)^2 + \left(W_\mu^2\right)^2\right)$ term. Their linear combinations become the recognizable W^+ and W^- gauge bosons. For the interaction of the W_μ^3 and B_μ bosons we get

$$\mathcal{L}_{W^3B} = \frac{v^2}{8}\begin{pmatrix} W_\mu^3 & B_\mu \end{pmatrix}\begin{pmatrix} g_W^2 & -g_W g_B \\ -g_B g_W & g_B^2 \end{pmatrix}\begin{pmatrix} W_\mu^3 \\ B_\mu \end{pmatrix}. \tag{1.47}$$

With the redefinition

$$\begin{pmatrix} W_\mu^3 \\ B_\mu \end{pmatrix} = \begin{pmatrix} cos\theta_W & sin\theta_W \\ -sin\theta_W & cos\theta_W \end{pmatrix}\begin{pmatrix} Z_\mu \\ A_\mu \end{pmatrix}, \quad sin\theta_W = \frac{g_B}{\sqrt{g_W^2+g_B^2}}, \tag{1.48}$$

where θ_W is known as the Weinberg angle, we can rewrite equation (1.47) as

$$\mathcal{L}_{W^3B} = \frac{v^2}{8}\left(g_w^2+g_B^2\right)\begin{pmatrix} Z_\mu & A_\mu \end{pmatrix}\begin{pmatrix} 1 & 0 \\ 0 & 0 \end{pmatrix}\begin{pmatrix} Z_\mu \\ A_\mu \end{pmatrix}. \tag{1.49}$$

and we can then see that A_μ is the massless photon and Z_μ is the massive vector boson with mass $M_Z^2 = \frac{g_W^2+g_B^2}{4}v^2 = \frac{1}{4}\frac{v^2g_W^2}{cos^2\theta_W} = \frac{M_W^2}{cos^2\theta_W}$. Finally we can also pick out the Higgs boson, with mass $M_H^2 = -2\mu^2$.
If we rewrite the covariant derivative again, in terms of mass eigenstates, it becomes

$$\begin{aligned}D_\mu &= \partial_\mu + i\frac{g_W}{\sqrt{2}}\left(W_\mu^+ T^+ + W_\mu^- T^-\right) \\ &\quad + \frac{i}{\sqrt{g_W^2+g_B^2}}Z_\mu\left(g_W^2T^3 + b_B^2Y\right) - i\frac{g_Wg_B}{\sqrt{g_W^2+g_B^2}}A_\mu\left(T^3+Y\right)\end{aligned} \tag{1.50}$$

where $W_\mu^\pm = W_\mu^1 \pm iW_\mu^2$, and $T^\pm$ has a similar definition. The final term here shows that the photon, A_μ, couples to the gauge generator from equation (1.43) and so we can identify $Q = T^3 + Y$ as the electric charge quantum number and the coefficient of the electromagnetic interaction, e:

$$e = \frac{g_W g_B}{\sqrt{g_W^2 + g_B^2}} \tag{1.51}$$

as the electric charge.

1.3.2 Fermion Sector

Ignoring fermion mass, the fermionic matter of the EW theory are described by

$$\begin{aligned}\mathcal{L}_{ferm} = \sum_{i=1}^{3} & \overline{Q}_{Li} i\not{D} Q_{Li} + \overline{u}_{Ri} i\not{D} u_{Ri} \\ & + \overline{d}_{Ri} i\not{D} d_{Ri} + \overline{E}_{Li} i\not{D} E_{Li} + \overline{e}_{Ri} i\not{D} e_{Ri}\end{aligned} \tag{1.52}$$

where the i index runs over the 3 generations of fermions that pave been split into separate terms:

$$Q_{Li} = \begin{pmatrix} u_L \\ d'_L \end{pmatrix}, \begin{pmatrix} c_L \\ s'_L \end{pmatrix}, \begin{pmatrix} t_L \\ b'_L \end{pmatrix}, \tag{1.53}$$

are the left-handed quark doublets;

$$u_{Ri} = u_R, c_R, t_r \tag{1.54}$$

$$d_{Ri} = d'_R, s'_R, b'_r, \tag{1.55}$$

are the right-handed up and down type quark singlets;

$$E_{Li} = \begin{pmatrix} \nu_e \\ e_L \end{pmatrix}, \begin{pmatrix} \nu_\mu \\ \mu_L \end{pmatrix}, \begin{pmatrix} \nu_\tau \\ \tau_L \end{pmatrix}, \tag{1.56}$$

are the left-handed lepton doublets; and

$$e_{Ri} = e_R, \mu_R, \tau_R, \tag{1.57}$$

are the right-handed lepton singlets. By splitting up the covariant derivative into left- and right-handed parts, such that

$$\mathcal{L}_{ferm} = \sum_{i}^{3} \overline{\psi}_L^i i \not{D}_L \psi_L^i + \overline{\psi}_R^i i \not{D}_R \psi_R^i \tag{1.58}$$

we see that

$$D_{L\mu} = \mathbb{1}\partial_\mu + \frac{i}{2} g_W \vec{\sigma} \cdot \vec{W} + i g_B Y B_\mu \mathbb{1} \tag{1.59}$$

and

$$D_{R\mu} = \partial_\mu + i g_B Y B_\mu \tag{1.60}$$

and so the right-handed fermions do not interact with the $SU(2)$ gauge bosons. As with the gauge sector there are no mass terms defined, they are added by the Yukawa sector that describes the couplings between the fermions and the Higgs.

1.3.3 The Yukawa Sector

The Yukawa Lagrangian is given by

$$\begin{aligned} \mathcal{L}_{Yukawa} = &- y_{ij}^u \overline{Q}_{Li} \left(i\sigma^2\right) \phi^* u_{Rj} y_{ij}^d \overline{Q}_{Li} \phi d_{Rj} \\ &- y_{ij}^e \overline{E}_{Li} h e_{Rj} + H.C. \end{aligned} \tag{1.61}$$

where the $y^{u,d,e}$ are matrices of Yukawa coupling. It is important to investigate whether or not the entries in these matrices are physical, i.e. they cannot be absorbed by a redefinition of fields and complex phases. It can be shown that a basis exists such that the lepton coupling matrix is diagonalizable, $y^e = \text{diag}\left(\lambda_e, \lambda_\mu, \lambda_\tau\right)$. This means that there is no allowance for lepton flavor mixing, and in this same basis the mass matrix for the leptons is also diagonalizable.
If we attempt to choose a basis for the quarks we find that there is a dependence shared between the up and down type quarks. If we choose a basis such that the up type coupling matrix is diagonal, $y^u = \text{diag}\left(\lambda_u, \lambda_c, \lambda_t\right)$, then the down type coupling matrix, y^d, takes the form

$$y_d = V D_d V^\dagger \tag{1.62}$$

where $D_d = diag\,(\lambda_d, \lambda_s, \lambda_b)$ and V is the unitary rotation matrix known as the Cabibbo-Kobyashi-Maskawa (CKM) matrix [30, 67]:

$$V = \begin{pmatrix} V_{ud} & V_{us} & V_{ub} \\ V_{cd} & V_{cs} & V_{cb} \\ V_{td} & V_{ts} & V_{tb} \end{pmatrix}. \tag{1.63}$$

This change of basis is also relevant when we introduce the Higgs mechanism to give the fermions mass as it leads to an additional interaction between the $W^{\pm}$ bosons and the $SU(2)$ quark doublets as the is a change in the term from equation (1.61) of the form

$$\frac{e}{\sqrt{2}sin\theta_W}\overline{Q}_{Li}\gamma^{\mu}W^{+}_{\mu}Q_{Li} \rightarrow \frac{e}{\sqrt{2}sin\theta_W}\overline{Q}_{Li}\gamma^{\mu}W^{+}_{\mu}V_{ij}Q_{Lj}. \tag{1.64}$$

The CKM matrix describes the weak interactions between the quark flavors that lead to flavor changing, with the probability of a quark q_i transitioning to quark q_j being proportional to $|V_{ij}|^2$. The mass terms for fermions given by the Higgs mechanism are

$$m_f = \lambda_f \frac{v}{\sqrt{2}} \tag{1.65}$$

and so the Yukawa Lagrangian after breaking the Higgs is

$$\begin{aligned} \mathcal{L}_{Yukawa} = -\Bigg[& (\overline{e}, \overline{\mu}, \overline{\tau}) \begin{pmatrix} m_e & 0 & 0 \\ 0 & m_\mu & 0 \\ 0 & 0 & m_\tau \end{pmatrix} \begin{pmatrix} e \\ \mu \\ \tau \end{pmatrix} \\ & + \left(\overline{u}, \overline{c}, \overline{t}\right) \begin{pmatrix} m_u & 0 & 0 \\ 0 & m_c & 0 \\ 0 & 0 & m_t \end{pmatrix} \begin{pmatrix} u \\ c \\ t \end{pmatrix} \\ & + \left(\overline{d}, \overline{s}, \overline{b}\right) \begin{pmatrix} m_d & 0 & 0 \\ 0 & m_s & 0 \\ 0 & 0 & m_b \end{pmatrix} \begin{pmatrix} d \\ s \\ b \end{pmatrix} \Bigg] \left(1 + \frac{h}{v}\right) \end{aligned} \tag{1.66}$$

where the mass eigenstates of the down type quarks are a linear combination of the EW eigenstates, given by the CKM matrix

$$\begin{pmatrix} d \\ s \\ b \end{pmatrix} = V \begin{pmatrix} d' \\ s' \\ b' \end{pmatrix}. \tag{1.67}$$

1.4 Fermi's Theory of the Weak Interaction

In 1938 Enrico Fermi proposed a theory with a four-fermion interaction in order to explain β-decay, the process where a neutron decays into a proton, an electron and an antineutrino. At the time this was a "bottom-up" effective field theory (EFT), that is, as this was a precursor to the theory of weak interaction and there was no UV description of weak processes. Fermi thus constructed his theory as a modification to QED which accounted for neutron decay. Now we can think of the Fermi theory as a "top-down" EFT and so it is useful for describing processes at energies far below the W mass.
In the SM the coupling of the $W^{\pm}$ and Z^0 bosons to the fermions are given in terms of the electromagnetic current for the right-handed $SU(2)$ singlets

$$j^{\mu}_{em} = \sum_{i}^{3} \frac{2}{3}\overline{u}_{Ri}\gamma^{\mu}u_{Ri} - \frac{2}{3}\overline{d}_{Ri}\gamma^{\mu}d_{Ri} - \overline{e}_{Ri}\gamma^{\mu}e_{Ri} \tag{1.68}$$

and in terms of the left-handed $SU(2)$ currents

$$j^{\mu}_{a} = \sum_{i}^{3} \overline{\psi}\gamma^{\mu}\left(\frac{1-\gamma_5}{2}\right)\frac{\sigma_a}{2}\psi \tag{1.69}$$

The couplings of the heavy gauge bosons to these currents is

$$\mathcal{L}_J = \frac{e}{sin\theta_W}\left(W^{+}_{\mu}J^{\mu}_{-} + W^{-}_{\mu}J^{\mu}_{+}\right) + \frac{e}{sin\theta_W cos\theta_W}Z_{\mu}(j^{\mu}_3 - sin^2\theta_W j^{\mu}_{em}) \tag{1.70}$$

where $J^{\mu}_{\pm} = \frac{1}{\sqrt{2}}\left(j^{\mu}_1 \pm j^{\mu}_2\right)$. This gives that the amplitude of a tree level exchange of a W boson at low momentum exchange is

$$i\mathcal{A} = -i\frac{e^2}{M^2_W sin^2\theta_W}J^{\mu}_{-}J_{\mu+} + O\left(\frac{q^2}{M^w_W}\right) \tag{1.71}$$

A low energy EFT with a "pinched" contact interaction, as in Figure (1.3), can reproduce this amplitude to lowest order in q^2/M^2_W as

$$\mathcal{L}_F = \frac{8}{\sqrt{2}}G_F J^{\mu}_{-}J_{\mu+}, \tag{1.72}$$

where

$$G_F = \frac{\sqrt{2}}{8}\frac{e^2}{M^2_W sin^2\theta_W} = 1.166 \times 10^{-5} GeV^2 \tag{1.73}$$

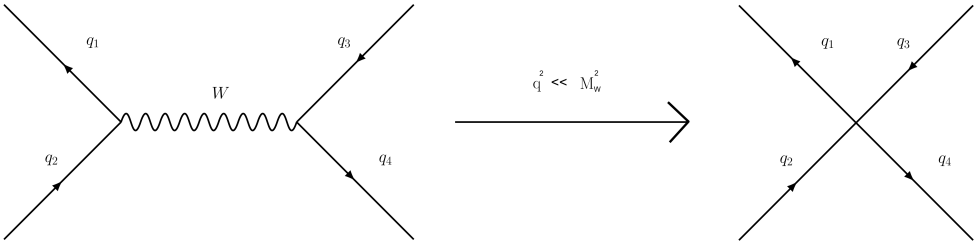

Figure 1.3 *We see how the effective vertex in the low energy EFT is the pinched version of the tree level W (or Z) exchange between four fermions.*

is the Fermi constant.

This effective theory is quite useful for LQCD calculations as the highest scales of the calculations are typically $O(2GeV)$, i.e, much lower than the mass of the W boson ($O(\sim 80GeV)$). As it is not possible to resolve heavy particles at this scale we instead exclude the weak interaction bosons and heavy quarks and instead use a low energy EFT, where light quark interactions that would be mediated by the exchange bosons are described by local operators. In order to express the short distance behavior of the product of these operators we will need to discuss operator product expansions.

1.5 Operator Product Expansion

To compute an amplitude for some process, for example the weak meson decay we are interested in, we must consider the integral over some time-ordered product of operators:

$$\begin{aligned}\mathcal{A} \propto \int d^4x_1 \ldots d^4_{n-1} e^{-iq_1\cdot x_1} \ldots e^{-iq_{n-1}\cdot x_{n-1}} \\ \times \langle 0|T\left[\mathcal{O}_1\left(x_1\right)\ldots\mathcal{O}_{n-1}\left(x_{n-1}\right)\right]|0\rangle\,.\end{aligned} \tag{1.74}$$

Operator product expansion (OPE) is the method of expanding these products of operators into a sum over local, composite, renormalized operators such that

$$\mathcal{A} = \sum_i C_i\left(\mu, M_W\right)\langle Q_i\left(\mu\right)\rangle\,. \tag{1.75}$$

Here we have factorized an effective Hamiltonian into the Wilson coefficients, C_i, and the matrix elements of local operators, Q_i. Particles with mass larger that the scale μ are removed from the theory as dynamical degrees of freedom and

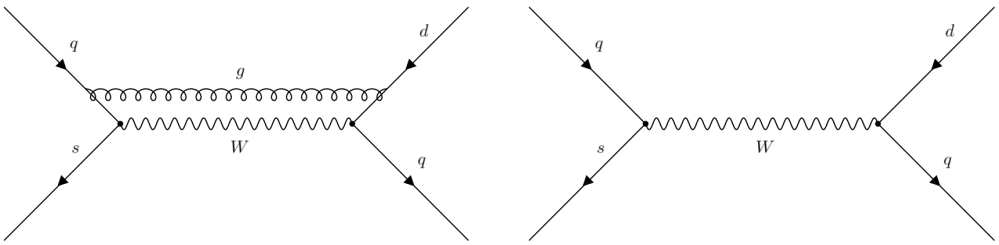

Figure 1.4 *Processes that the Q_1 and Q_2 operators describe.*

instead their effect are described by the Wilson coefficients. One interpretation of this approximation is that the sum $\sum_i C_i Q_i$ acts as an effective Hamiltonian for the process in question where the Q_i are the effective vertices that describe long distance contributions and the C_i are the effective couplings that describe short distance contributions. The final amplitude can not depend on scale so the scale dependence of the Wilson coefficients and the matrix elements cancel with each other

The Wilson coefficients are calculated using perturbation theory at a scale $\mu \gg \Lambda_{\overline{MS}}$ and the scale is then reduced. This must be done with care, as the perturbative calculation will have been done to some order where the $\alpha_S(\mu) log\left(\frac{M_W^2}{\mu^2}\right)$ terms are small. This term blows up, however, at scales where $\mu \ll M_W$ and the perturbative expansion is no longer valid. Renormalization group improved perturbation theory is needed for the transitions between theories with different choices of renormalization scales.

1.5.1 Effective Operators Renormalization

Take, for example, the four-quark interaction describing the $qs \to qd$ transition that we are interested in for the $K^+ \to \pi^+\ell^+\ell^-$ decay. We have an effective theory that describes the processes given in Figure (1.4) where the W propagator has been pinched as in Figure(1.5). We can write the amplitude for this process in the effective theory as [28]

$$\mathcal{A} = \int d^4x \sum_{i=1}^{2} C_i(\mu) \langle Q^u(\mu) - Q^c(\mu) \rangle \tag{1.76}$$

where the active quark flavors are $q = u, c$.

To compute the Wilson coefficients we perturbative compute the amplitude in both the full SM and in the effective theory to the same order. As this is done an

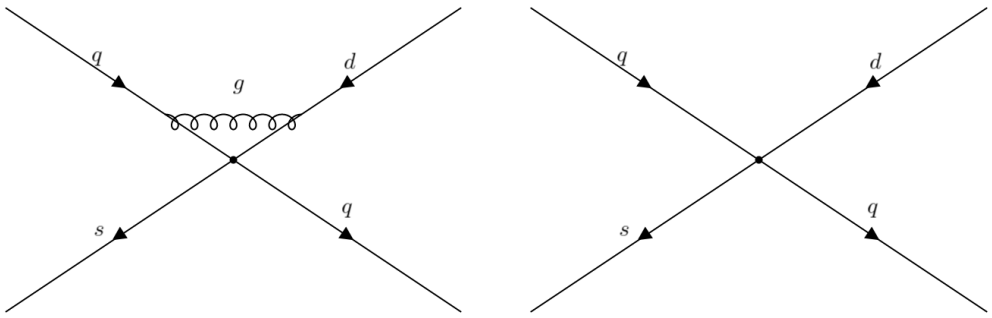

Figure 1.5 *The "pinched" equivalent of the processes in Figure (1.4), used in the calculation of Z_{ij}.*

additional renormalization step for the Q_1 and Q_2 operators must be taken.This is because divergences that do not exist in the full theory appear in the effective theory as the W propagator is pinched. The renormalization condition for these operators are given as

$$\langle Q_i \rangle = Z_q^2 Z_{ij}^{-1} \langle Q_j \rangle^b \tag{1.77}$$

where the superscript, b, indicates the unrenormalized (bare) quantity, Z_q comes from the quark renormalization condition, $q = Z^{-\frac{1}{2}} q^b$, and Z_{ij} is a renormalization matrix. We see from this matrix structure that the divergences introduced by $\langle Q_1 \rangle^b$ are removed by those introduced by $\langle Q_2 \rangle^b$. The Wilson coefficients are given by matching the SM amplitude to the effective theory one:

$$\mathcal{A} = C_i Z_q^2 Z_{ij} \langle Q_j \rangle^b \tag{1.78}$$

and reading off the C_i's.

1.5.2 Renormalization Group Equation

In order to compute the Wilson coefficients at a scale $\mu \ll M_W$ that we use in our lattice calculations we must take the C_i's that were computed at $\mu \gg \Lambda_{QCD}$ and evolve them down to our lower scale. This is done by solving the renormalization group equation for C_i with appropriate boundary conditions between schemes:

$$\frac{d}{dln\mu} C_i(\mu) = \gamma_{ji}(g)\, C_j(\mu) \tag{1.79}$$

where $\gamma_{ij}(g) = Z_{ik}^{-1} \frac{d}{dln\mu} Z_{kj}$ is the matrix of coupling anomalous dimensions for coupling g.

The solution to this equation with appropriate boundary conditions between schemes can be achieved by using the evolution matrix

$$\begin{aligned} U_{i,j}\left(\mu,\mu'\right) = 1 &+ \int_{g(\mu')}^{g(\mu)} dg_1 \frac{\gamma_{ji}\left(g_1\right)}{\beta\left(g_1\right)} \\ &+ \int_{g(\mu')}^{g(\mu)} dg_1 \int_{g(\mu')}^{g_1} dg_2 \frac{\gamma_{ji}\left(g_1\right)\gamma_{ji}\left(g_2\right)}{\beta\left(g_1\right)\beta\left(g_2\right)} + \ldots \end{aligned} \tag{1.80}$$

where we have already seen $\beta\left(g\right)$ in equation 1.5 when discussing the running of the QCD coupling. Now we can write

$$C_i\left(\mu\right) = U_{ij}\left(\mu, M_W\right) C_j\left(M_W\right) \tag{1.81}$$

and solve equation (1.80) order by order in perturbation theory to evolve C_i to our required scale. Care must also be taken when running the coupling down to consider the number of active quark flavors. As the scale falls below a quark mass we must move into an effective theory where this quark has been integrated out. The running of the coupling depends on the number of flavors, changing the structure of the perturbative theory. Flavor boundaries must then be established where the Wilson coefficients can be matched at given scale, μ_b, with

$$C_i^{f-1}\left(\mu+b\right) Q_i^{f-1}\left(\mu+b\right) = C_i^{f}\left(\mu+b\right) Q_i^{f}\left(\mu+b\right) \tag{1.82}$$

1.6 Chiral Perturbation Theory

Another EFT that is useful to consider is chiral perturbation theory (χPT)[21, 46], an effective theory of the pseudoscalar mesons. As discussed in Section (1.2.3) the QCD Lagrangian has a global $SU(n_f)_L \times SU(n_f)_R$ symmetry in the massless limit that is spontaneously broken to $SU(n_f)_L$. With non-zero masses this symmetry is explicitly broken, giving n_f^2-1 pseudo Goldstone bosons (pGBs). If the $SU(n_f)_L \times SU(n_f)_R$ symmetry proves to be an approximate symmetry then this would result in the pGBs being light. This is the case for the $n_f = 2$ case, where $m_u \approx m_d$, the 3 pGBs are the triplet of pions

$$\phi = \begin{pmatrix} \frac{1}{\sqrt{2}}\pi^0 & \pi^+ \\ \pi^- & -\frac{1}{\sqrt{2}}\pi^0 \end{pmatrix}, \tag{1.83}$$

all of which are roughly equal in mass and much lighter than the lightest baryons, with $m_\pi/m_p \sim 0.15$. For $n_f = 3$, where $m_s \gg m_d$, the pGBs are the octet of pions, kaons, and η mesons

$$\phi = \begin{pmatrix} \frac{1}{\sqrt{2}}\pi^0 + \frac{1}{\sqrt{6}}\eta & \pi^+ & K^+ \\ \pi^- & -\frac{1}{\sqrt{2}}\pi^0 + \frac{1}{\sqrt{6}}\eta & K^0 \\ K^- & \overline{K}^0 & -+\frac{2}{\sqrt{6}}\eta \end{pmatrix} \tag{1.84}$$

. Here we see that the assumption of an approximate symmetry is less accurate, with $m_{K^+}/m_p \sim 0.5$, however $n_f = 3$ χPT is phenomenologically useful, describing more phenomena than $n_f = 2$ but not breaking down as much as $n_f = 4$.

In order to construct the most general χPT Lagrangian for pseudoscalar mesons that is invariant under $SU(n_f)_L \times SU(n_f)_R$ transformations we use the matrix valued field, $U(x)$, that transforms as

$$\begin{aligned} U(x)U'(x) &= LU(x)R^\dagger \\ U^\dagger(x)U'^\dagger(x) &= RU(x)L^\dagger \end{aligned} \tag{1.85}$$

for the local independent transformations $L/R \in SU(n_f)_{L/R}$.

We chose the exponential representation of U

$$U(x) = exp\left(\frac{2i\phi(x)}{f}\right) \tag{1.86}$$

where $\phi(x)$ are the fields defined in (1.83) and (1.84) for $n_f = 2, 3$ and f is the parameter defined in the PCAC relation, given in Equation (1.32), that gives the $\phi(x)$ field the canonical mass dimensions of a scalar field.

An effective Lagrangian is then written in terms of the fields U that represent the pGBs.

$$\mathcal{L}_{eff} = \mathcal{L}_{eff}\left(U, U^\dagger; \partial U, \partial U^\dagger; \partial^2 U, \partial^2 U^\dagger\right) \tag{1.87}$$

which is expanded in chiral powers related to the number of derivatives acting on the pGB fields

$$\mathcal{L}_{eff} = \mathcal{L}^{(0)}_{eff} + \mathcal{L}^{(2)}_{eff} + \mathcal{L}^{(4)}_{eff} + \ldots \tag{1.88}$$

Only even chiral powers appear as the Lagrangian is a Lorentz scalar and so tensor indices of derivatives must appear in pairs. At each order the $\mathcal{L}_{eff}$ must be invariant under chiral transformations, implying that the zeroth order can only be a function of $UU^\dagger$, a constant that can be dropped. In the massless case the

second-order term consists of

$$\mathcal{L}_{eff}^{(2)} = c_1 tr\left(\partial_\mu U^\dagger \partial^\mu U\right) + c_2 tr\left(U^\dagger \partial^2 U\right) \tag{1.89}$$

where c_1 and c_2 are constants to be determined and the second term can be combined with the first using partial integration such that

$$\mathcal{L}_{eff}^{(2)} = c_1 tr\left(\partial_\mu U^\dagger \partial^\mu U\right). \tag{1.90}$$

If we expand the exponential representation

$$U\left(x\right) = \sum_{x=0}^{\inf} \frac{1}{n!}\left(\frac{2i}{f}\phi\right) \tag{1.91}$$

and demand that our Lagrangian take the standard kinematic form

$$\mathcal{L}_{eff}^{(2)} = \frac{1}{2}\partial_\mu\phi\partial^\mu\phi + O\left(\phi^4\right) \tag{1.92}$$

we get that $c_1 = \frac{f^2}{4}$ and that the effective Lagrangian at leading order is

$$\mathcal{L}_{eff}^{(2)} = \frac{f^2}{4} tr\left(\partial_\mu U^\dagger \partial^\mu U\right). \tag{1.93}$$

In order to include mass to the effective theory we consider, instead of the quark mass matrix, $\mathcal{M} = diag\left(m_1, \ldots, m_{n_f}\right)$, an external scalar source, χ, that transforms as

$$\begin{aligned} \chi \to \chi' &= L\chi R^\dagger \\ \chi^\dagger \to \chi'^\dagger &= R\chi^\dagger L^\dagger, \end{aligned} \tag{1.94}$$

where $\chi = 2B\mathcal{M}$ and B is a low energy constant that contains the matching of the chiral theory to QCD. The effective Lagrangian is extended to include this scalar source, at leading order this takes the form

$$\mathcal{L}_{eff}^{(2)} = \frac{f^2}{4} tr\left(\partial_\mu U^\dagger \partial^\mu U\right) + \frac{f^2}{4} tr\left(\chi U^\dagger + U\chi^\dagger\right) \tag{1.95}$$

where we have, again, expanded the exponential representation and matched constants to the expected form of the mass term.

For this thesis we are also interested in an EFT that includes not just hadronic interactions that would describe the $K^+ \to \pi^+\ell^+\ell^-$ decays. At leading order the

weak contribution to this transition can be written as [47]

$$\mathcal{L}^{(2)}_{\Delta_s=1} = \frac{G_F}{\sqrt{2}} V_{ud} V^{\dagger}_{us} G_8 \left(L_\mu L^\mu\right)_{23} \tag{1.96}$$

where $L^\mu = if^2 U \partial^\mu U^\dagger$, the 23 subscript are the indices of the entry of the matrix, and G_8 is a parameter consisting the Fermi constant, CKM matrix elements, and a dimensionless constant characterizing the enhancement of $\Delta I = 1/2$ non-leptonic amplitudes.

To include electromagnetism a $U(1)$ gauge interaction is introduced, such that the derivatives are replaced with covariant derivatives and the extra terms

$$\mathcal{L}^{(2)}_{EM} = -eA_\mu tr\left(\hat{Q}V^\mu\right) + e^2 A_\mu A^\mu \frac{1}{2} f^2 \left(1 - |U_{11}|^2\right) \tag{1.97}$$

are added, where $\hat{Q} = \mathrm{diag}\,(1,0,0)$ is the generator of the $U(1)$ interaction and $V_\mu = \frac{1}{2} i f^2 \left[U, \partial_\mu U^\dagger\right]$. We will see the application of this EFT to the $K^+ \to \pi^+ \ell^+ \ell^-$ decay in Chapter (3).

Chapter 2

Lattice Quantum Chromodynamics

As discussed in Section (1.2.1), and as can be seen in Figure (1.2), the QCD coupling grows as energy decreases, leaving analytic perturbative methods unable to investigate phenomena that appear occur in low energy regions of of the theory. EFTs can approximate QCD in order to make low energy predictions, but another approach is lattice QCD: a non-perturbative method that discretizes Euclidean spacetime on a finite, hypercubic, lattice, on which computational simulations of fermion and gauge interactions are created.

I will begin this chapter by introducing the fundamental concepts of discretizing QCD in Section (2.1.1) and presenting a naïve discretization of the fermion action in Section (2.1.3) and discuss why more nuanced actions are needed. In Section (2.1.4) I will introduce one such action in detail, as it is used in our study of rare kaon decays, as well as giving the formulation of the conserved currents for this action. Beyond that I will discuss both the hybrid Monte Carlo (HMC) method that is used to simulate sample gauge configurations in Section (2.2.1) and the methods that we use to compute gauge averaged correlation functions from which physical observables can be extracted in Sections (2.2.2) through (2.2.5). Finally, the various methods that can be used to create propagators on the lattice will be introduced in Section (2.3), with the lattice noises used as a foundation for these propagators being described in Section (2.4).

2.1 Discretizing QCD on the Lattice

2.1.1 Fundamental Concepts

In continuum QCD correlation functions can be computed using path integrals

$$\langle 0|\mathcal{O}_1(x_1)\dots\mathcal{O}_n(x_n)|0\rangle = \frac{1}{Z}\int D\left[A,\psi,\overline{\psi}\right]\mathcal{O}_1(x_1)\dots\mathcal{O}_n e^{iS\left[A,\psi,\overline{\psi}\right]} \tag{2.1}$$

where S is the action and Z is the partition function

$$Z = \int D\left[A,\psi,\overline{\psi}\right]e^{iS\left[A,\psi,\overline{\psi}\right]}. \tag{2.2}$$

Here we typically work in Minkowski spacetime in the continuum, however for our lattice calculations we wish to perform a Wick rotation, $x_0 \to -ix_4$, to express this path integral in a Euclidean spacetime lattice:

$$\Lambda_L = \left\{x \in \mathbb{N}^4 | x_1, x_2, x_3 = 0, 1, \dots, L-1; x_4 = 0, 1, \dots, T-1\right\} \tag{2.3}$$

where the lattice point are separated by the lattice spacing, a. The spatial extent of the lattice is aL and the temporal extant of the lattice is aT, giving a finite volume of $a^4V = (aL)^3 \times aT$ that regulates infrared divergence. On this lattice we replace the continuous integral with a Riemann sum, using a^4 as an elementary volume:

$$\int d^4x\psi(x) \to a^4\sum_{x\in\Lambda_L}\psi(x). \tag{2.4}$$

We have our choice of operator work as a discrete derivative on our lattice, one such choice is the central finite difference:

$$\begin{aligned}\partial_\mu\psi(x) \to \Delta_\mu\psi(x) &= \frac{1}{2a}\left(\psi(x+a\hat{\mu}) - \psi(x-a\hat{\mu})\right)\\ &= \partial_\mu\psi(x) + \frac{a^2}{6}\partial_\mu^3\psi(x) + O\left(a^4\right)\end{aligned} \tag{2.5}$$

where in the second line we have take the Taylor expansion for the continuum limit, $a \to 0$. We can also introduce discretized momenta

$$\Lambda^* = \left\{p \in \mathbb{N}^4 | p_\mu = \frac{2\pi}{aN_\mu}\left(x_\mu - \frac{N_\mu}{2} + 1\right)\right\} \tag{2.6}$$

where $N_{1,2,3} = L_{1,2,3}$ and $N_4 = T$, which gives a Brillouin zone such that $-\frac{\pi}{a} < p_\mu \leq \frac{\pi}{a}$ and we see that the lattice spacing acts as an ultraviolet regulator. We can also define the Fourier transform on Λ_L as

$$\tilde{f}(p) = a^4 \sum_{z \in \Lambda_L} f(x) e^{-ip \cdot ax}, \tag{2.7}$$

and the inverse Fourier transform as

$$f(x) = \frac{1}{V} \sum_{p \in \Lambda^*} \tilde{f}(p) e^{ip \cdot ax} \tag{2.8}$$

.

2.1.2 Gauge Invariance

On the lattice the full Lorentz symmetry group of the continuum is reduced to a subgroup called the hypercubic group. Care must be taken when defining, for example, angular momentum on the lattice as the hypercubic group has a finite number of irreducible representations of the rotational group, which has an infinite number of irreducible representations in the continuum. Gauge invariance is another such example of an invariance with which me must consider non-trivially. We require that the lattice QCD Lagrangian be invariant under the local gauge transformation

$$\begin{aligned} \psi(x) &\to \psi'(x) = \Omega(x) \psi(x) \\ \overline{\psi}(x) &\to \overline{\psi}'(x) = \overline{\psi}(x) \Omega^\dagger(x) \end{aligned} \tag{2.9}$$

where $\Omega(x)$ is a $SU(3)$ matrix. In our LQCD Lagrangian, where we have replace $\overline{\psi}(x) \partial_\mu \psi(x)$ with $\overline{\psi}(x) \Delta_\mu \psi(x)$, there will be terms that transform as

$$\overline{\psi}(x) \psi(x + a\hat{\mu}) \to \overline{\psi}(x) \Omega^\dagger(x + a\hat{\mu}) \psi(x + a\hat{\mu}) \neq \overline{\psi}(x) \psi(x + a\hat{\mu}) \tag{2.10}$$

which is not invariant. Instead, if we introduce a field, $U_\mu(x)$ that transforms as

$$U_\mu(x) \to U'_\mu(x) = \Omega(x) U_\mu(x) \Omega^\dagger(x + a\hat{\mu}), \tag{2.11}$$

then we can construct the gauge invariant term

$$\overline{\psi}\left(x\right)U_{\mu}\left(x\right)\psi\left(x+a\hat{\mu}\right)\rightarrow\overline{\psi}\left(x\right)U_{\mu}^{\prime}\left(x\right)\psi\left(x+a\hat{\mu}\right)=\overline{\psi}\left(x\right)U_{\mu}\left(x\right)\psi\left(x+a\hat{\mu}\right). \tag{2.12}$$

The $U_{\mu}\left(x\right)$ fields are "link variables" that connect the sites at x and $x+a\hat{\mu}$ and can be related to the gluon gauge field by

$$U_{\mu}\left(x\right)=e^{iaA_{\mu}(x)}. \tag{2.13}$$

We can now write down a lattice covariant derivative that is invariant under gauge transformations:

$$D_{\mu}=\frac{1}{2a}\left(U_{\mu}\left(x\right)\psi\left(x+a\hat{\mu}\right)-U_{-\mu}\left(x\right)\psi\left(x-a\hat{\mu}\right)\right), \tag{2.14}$$

where $U_{-\mu}\left(x\right)\equiv U_{\mu}^{\dagger}\left(x-a\hat{\mu}\right)$, which can be used to describe the fermionic part of our LQCD actions.
For the gluonic part of the action we consider closed loops on the lattice, know as Wilson loops, the shortest, non-trivial, of which is known as the plaquette

$$U_{\mu\nu}\left(x\right)=U_{\mu}\left(x\right)U_{\nu}\left(x+a\hat{\mu}\right)U_{\mu}^{\dagger}\left(x+a\hat{\nu}\right)U_{\nu}^{\dagger}\left(x\right). \tag{2.15}$$

The plaquette remains invariant under the gauge transformation and so expanding the link fields in their exponential form, as in Equation (2.13), as $a\rightarrow0$, it can be shown that

$$U_{\mu\nu}\left(x\right)=1+ia^{2}gG_{\mu\nu}\left(x\right)-\frac{a^{4}g^{2}}{2}G_{\mu\nu}\left(x\right)G^{\mu\nu}\left(x\right)+O\left(a^{6}\right) \tag{2.16}$$

and using this the the Wilson gauge action can be constructed as

$$\begin{aligned}S_{G}^{W}\left(U\right)&=\frac{2}{g^{2}}\sum_{x\in\Lambda_{L}}\sum_{\mu<\nu}Re\left(Tr\left[\mathbb{1}-U_{\mu\nu}\left(x\right)\right]\right)\\&=\frac{a^{4}}{2g^{2}}\sum_{x\in\Lambda_{L}}\sum_{\mu<\nu}Tr\left[G_{\mu\nu}\left(x\right)G^{\mu\nu}\left(x\right)\right]+O\left(a^{6}\right)\end{aligned} \tag{2.17}$$

and so the continuum QCD gauge action is matched as $a\rightarrow0$. More complicate Wilson loops may be used, for example the 1×2 rectangle $R_{\mu\nu}$, gives a gauge action of the form

$$S_{G}^{Improved}=\frac{2}{g^{2}}\sum_{x\in\Lambda_{L}}Tr\left[\left(1-8c_{1}\right)\sum_{\mu<\nu}U_{\mu\nu}+c_{1}\sum_{\mu\neq\nu}R_{\mu\nu}\right] \tag{2.18}$$

where c_1 is a coefficient to be chosen. For the actions used in this thesis $c_1 = -0.331$ is taken, giving what is known as the Iwasaki gauge action [63, 64].

2.1.3 Naïve Fermion Action

Using the covariant derivative we define in Equation (2.14) we can write a naïve LQCD fermion action

$$\begin{aligned} S_F\left[\psi, \overline{\psi}, U\right] &= a^4 \sum_{x \in \Lambda_L} \overline{\psi} \left(\sum_{\mu} \frac{\gamma_\mu}{2a} \left(U_\mu(x) \psi(x + a\hat{\mu}) - U_{-\mu}(x) \psi(x - a\hat{\mu}) \right) + m\psi(x) \right) \\ &= \overline{\psi}(x) D(x, y) \psi(y) \end{aligned} \tag{2.19}$$

where we consider only one quark flavor, for convenience, and we have defined the naïve Dirac operator, $D(x, y)$. If we take the Fourier transform of the Dirac operator, in the free fermion case where $U_\mu(x) = \mathbb{1}$, we find that

$$\begin{aligned} \tilde{D}(p, q) &= \frac{1}{V} \sum_{x \in \Lambda_L} e^{-(p-q)\cdot ax} \left(\sum_{\mu} \gamma_\mu \frac{1}{2a} \left(e^{iq_\mu a - e^{-iq_\mu a}} \right) + m \right) \\ &= \delta(p - q) \left(m + \frac{i}{a} \sum_{\mu} \gamma_\mu sin(p_\mu a) \right) = \delta(p - q) \tilde{D}(p). \end{aligned} \tag{2.20}$$

The quark propagator is given by the inverse of $\tilde{D}$, given as [83]

$$\tilde{D}^{-1}(p) = \frac{m - \frac{i}{a} \sum_\mu \gamma_\mu sin(p_\mu a)}{m^2 + \frac{1}{a^2} \sum_\mu \gamma_\mu sin^2(p_\mu a)}. \tag{2.21}$$

If we take the massless continuum limit

$$\tilde{D}^{-1}(p)\,|_{m=0} = -ia \frac{\sum_\mu \gamma_\mu sin(p_\mu a)}{\sum_\mu \gamma_\mu sin^2(p_\mu a)} \xrightarrow{a \to 0} -\frac{\not{p}}{p^2} \tag{2.22}$$

we see that this Dirac operator has the correct continuum limit. However, as lattice momenta are contained in the Brillouin zone of $-\frac{\pi}{a} < p^\mu \leq \frac{\pi}{a}$ we see that this operator has 16 poles, the expected $p^\mu = (0, 0, 0, 0)$ pole and an additional 15 poles when any of the p^μ entries are $\frac{\pi}{a}$ or 0. Thus the ψ fields can create 16 independent fermion states with the same energy, 15 of which are unphysical fermions, called "doublers". To remove these doublers the naïve Dirac operator

can be modified, adding a "Wilson term" to create the Wilson Dirac operator [51]:

$$D_W(x,y) = \left(\frac{4}{a} + m\right)\delta_{x,y} - \frac{1}{2a}\sum_{\mu}(1-\gamma_\mu)\left[U_\mu(x)\,\delta_{x+a\hat{\mu},y} - (1+\gamma_\mu)\,U_{-\mu}(x)\,\delta_{x-a\hat{\mu}}\right], \tag{2.23}$$

which in momentum spaces is

$$\tilde{D}_W(p) = m + \frac{i}{a}\sum_{\mu}\gamma_\mu sin(p_\mu a) + \frac{1}{a}(1 - cos(p_\mu a)). \tag{2.24}$$

This action gives the doubler fermions a mass of order a^{-1} so that when we take the continuum limit their masses become infinitely large and decouple from the theory. The Wilson term is equivalent to adding the discretized for of $-\frac{a}{2}\partial_\mu\partial^\mu$ to the operator, which disappears as we take the continuum limit, but this additional term also explicitly breaks chiral symmetry. A useful relation that can be defined when discussing a Dirac operator, D, that obeys chiral symmetry is

$$D\gamma_5 + \gamma_5 D = 0. \tag{2.25}$$

For the massless Wilson Dirac operator, we find:

$$D_W|_{m=0}\gamma_5 + \gamma_5 D_W|_{m=0} \neq 0. \tag{2.26}$$

In fact, the Nielsen-Ninomiya no-go theorem [80] states that it is impossible to construct a lattice action such that these four conditions are met:

- the action is local,
- the correct propagator is retrieved in the continuum limit,
- there are no doublers,
- chiral symmetry is obeyed for massless quarks.

This means that when constructing a lattice fermion action one must acquiesce and violate at least one of these conditions. Examples of fermion actions other than the Wilson action are the "Staggered Fermion" action [68], the "Overlap" action [79], and the "Domain Wall Fermion" (DWF) action [65]. The staggered fermion action reduces the number of doublers down to four "tastes", and a

subgroup of chiral symmetry is maintained. The overlap action is a solution to the Ginsparg-Wilson equation [53]

$$D\gamma_5 + \gamma_5 D = aD\gamma_5 D \tag{2.27}$$

which has the form

$$D_{ov} = \frac{1}{2}(1+m) + \frac{1}{2}(1+m)\gamma_5 \epsilon(H) \tag{2.28}$$

where ϵ is the sign function $\epsilon(H) = \frac{H}{\sqrt{H^\dagger H}}$, $H = \gamma_5 D_{kernel}$ and D_{kernel} is some Dirac operator that satisfies chiral symmetry. The overlap action allows for lattice fermions that are free of doublers ans achieve chiral symmetry in the continuum limit. The DWF action serves as the foundation of the action used for this thesis, and so warrants further discussion.

2.1.4 Domain Wall Fermions

In order to simulate fermions with approximate chiral symmetry at finite lattice spacing an auxiliary fifth dimension, that has length L_s and is denoted by s, is introduced. This dimension is constructed such that, at low energies, chiral symmetry breaking is suppressed exponentially in L_s. Left- and right-handed fermions can be thought to be localized at opposite ends of the fifth dimension with the exponential suppression causing a suppression of any overlap of their wavefunctions. The four dimensional theory is retrieved by considering the physics at these boundaries.
To see this we consider a fermion with an s-dependent mass that has the shape of a domain wall

$$m(s) = m\theta(s) = \begin{cases} +m, & s > 0 \\ -m, & s < 0 \end{cases} \tag{2.29}$$

A five dimensional free Dirac operator defined as

$$D(x,s) = \not{D} + \gamma_5 \partial_s + m(s) \tag{2.30}$$

for which the five dimensional spinor, $\Psi(x,s)$, that satisfies the Dirac equation

$$D(x,s)\,\Psi(x,s) = 0, \tag{2.31}$$

can be separated into functions of s multiplied by four dimensional spinors, $\psi(s)$,

$$\Psi(x,s) = \sum_n \left[b_n(s) P_R + f_n P_L\right] \psi(x) \tag{2.32}$$

satisfying the equations [66]

$$\begin{aligned} \left[\partial_s + m(s)\right] b_n(s) &= \lambda_n f_n(s) \\ \left[-\partial_s + m(s)\right] f_n(s) &= \lambda_n b_n(s) \end{aligned} \tag{2.33}$$

A solution for $b(s)$ can be found with eigenvalue $\lambda = 0$, given by

$$b_0 = N exp\left(-\int_0^s m(s')\, ds'\right) = N e^{-m|s|}. \tag{2.34}$$

So we have a solution that is localized near the mass defect at $s = 0$ which falls off exponentially with distance s, describing a single, massless, right-handed fermion at the right domain wall. There is no analogous solution for $f_n(s)$ as

$$f_0 \sim exp\left(+\int_0^s m(s')\, ds'\right) \tag{2.35}$$

as this grows exponentially with distance s and is not renormalizable for infinite s. For a fifth dimension that has periodic boundary conditions $\Psi(x, s + L_s) = \Psi(x,s)$, the theory can be defined on the interval $s \in \left[-\frac{L_s}{2}, \frac{L_s}{2}\right]$ with mass $m(s) = m\frac{s}{|s|}$. Now the f_0 solution

$$f_0 = N' exp\left(+\int_0^s m(s')\, ds'\right) = N' e^{m|s|} \tag{2.36}$$

is renormalizable, as the transverse direction is finite, and f_0 corresponds to a left-handed chiral fermion on the left domain wall.
A discretized DWF action is then given, in the Shamir formulation, as

$$S^{DWF}\left(\Psi, \overline{\Psi}, U\right) \sum_{x,y} \sum_{s,r} \overline{\Psi}(x,s)\, D_{DWF}(x,s;y,r)\, \Psi(y,r) \tag{2.37}$$

where we now consider the interval $s, r \in [0, L_s - 1]$ and the domain wall Dirac operator is given by

$$D_{DWF}(x,s;y,r) = \delta_{s,r} D_W(x,y) + \delta_{x,y} D^5_{DWF}(s,r) \tag{2.38}$$

where D_W is the Wilson operator with the mass term replaced with M_5, the height of the domain wall, and $D^5_{DWF}(s,r)$ is given by

$$\begin{aligned} D^5_{DWF}(s,r) =& \delta_{s,r} - (1-\delta_{s,L_s-1}) P_L \delta_{s+1,r} - (1-\delta_{s,0}) P_R \delta_{s-1,r} \\ &+ m\left(P_L \delta_{s,L_s-1}\delta_{0,r} + P_R \delta_{s,0}\delta_{L_s-1,r}\right). \end{aligned} \tag{2.39}$$

The four dimensional fermion fields are then given by

$$\psi(x) = P_L \Psi(x,0) + P_R \Psi(x, L_s-1) \tag{2.40}$$

$$\overline{\psi}(x) = \overline{\Psi}(x, L_s-1) P_L + \overline{\Psi}(x,0) P_R \tag{2.41}$$

In the $L_s \to \infty$ limit the DWF operator has arbitrarily exact chiral symmetry and is equivalent to overlap operator, with different DWF formulations making up different kernels in argument of the sign function. For example, for the Shamir formulation, we can write [86]

$$D^{Shamir}_{kernel} = \frac{a_5 D^W(M_5)}{2 + a_5 D^W(M_5)} \tag{2.42}$$

where a_5 is the lattice spacing in the fifth dimension, that is generally set to $a_5 = 1$ in units of the spacetime lattice spacing. For finite L_s there is an equivalence between the DW operators and an "effective" overlap operator that has a L_s dependence:

$$D_{ov}(L_s) = \frac{1}{2}(1+m) + \frac{1}{2}(1+m)\gamma_5 \epsilon^{L_s}(H) \tag{2.43}$$

where $\epsilon^{L_s}(x)$ is an approximate sign function. For the finite L_s Shamir formulation we have

$$\epsilon^{L_s}(x) = \frac{(1+x)^{L_s} - (1-x)^{L_s}}{(1+x)^{L_s} + (1-x)^{L_s}} = \tanh\left(L_s \tanh^{-1}(x)\right). \tag{2.44}$$

A general form of the the Shamir kernel is the Möbius kernel [26]

$$D^{Mob}_{kernel} = \frac{(b_s + c_s) D^W(M_5)}{2 + (b_s - c_s) D^W(M_5)} \tag{2.45}$$

where b_s and c_s are s-dependent real parameters, with the Shamir case given by $\alpha a_5 = b_s + c_s$, $a_5 = b_s - c_s$, where α is a scaling parameter. The Möbius fermion has an approximate sign function of the form

$$\epsilon^{L_s}(x) = \frac{f(x) + f(-x)}{f(x) - f(-x)}; \quad f(x) = \prod_{i=0}^{L_s-1} (\omega_i + x); \quad \omega_i \equiv \frac{1}{b_i + c_i}. \tag{2.46}$$

The extent to which the overlap between the left- and right-handed fermions manifest due to finite L_s can be seen through the residual mass, and additive renormalization to the bare quark mass

$$m_q = m + m_{res} \tag{2.47}$$

which we will discuss further in (2.1.5). With an appropriate choice of ω_i's Equation (2.46) for the Möbius kernel can better approximate the sign function than Equation (2.44) for the Shamir kernel. This can reduce the residual chiral symmetry breaking for a given L_s, or alternatively, produce an equivalent residual breaking for a reduced L_s. An "approximate equivalence relation" between the two operators can be given in terms of the scaling parameter, α [26]:

$$\text{Shamir at } L_s \approx \text{Möbius at } L_s/\alpha. \tag{2.48}$$

A smaller L_s is beneficial, not only for reducing the computational costs of using the action, but also it allows for more eigenvector generation, the uses of which will be discussed in sections (2.3.2) and (2.3.3).
Another method to reduce L_s is to introduce the zMöbius operator [77], the kernel of which is equivalent to the Möbius kernel with complex b_i and c_i. As the sign function must be real the ω_i's must be real or come in complex conjugate pairs. For a given L_s, L'_s, where $L'_s < L_s$, a set of ω_i's can be found such that the approximation

$$\epsilon^{L'_s}(x) \approx \epsilon^{L_s}(x) \tag{2.49}$$

is satisfied. This is a function approximation problem, and so can be achieved using the Remez algorithm.
After they have been computed these ω_s's can be used to construct a reduced-L_s Möbius operator, which can then be used in the "Möbius-accelerated DWF" (MADWF) algorithm [91] to speed up inversions of the original large-L_s operator, or, as is the case in this thesis, used as a cheaper approximation of the original action to which bias correction step can be applied. This is analogous to the all-mode-averaging (AMA) technique [20] where, for an observable $\mathcal{O}$, an approximation of the the observable $\mathcal{O}'$ is computed using an "inexact" method. $\mathcal{O}$ is typically expensive to compute using an "exact" method and so is only calculated on a small number of configurations in order to measure a correction term $\Delta\mathcal{O}$. The AMA estimator, or equivalently the Möbius bias correction

estimator, is given by

$$\mathcal{O}_{AMA} = \mathcal{O}' + \Delta\mathcal{O} \tag{2.50}$$

$$= \mathcal{O}' + \left(\tilde{\mathcal{O}}' - \tilde{\mathcal{O}}'\right), \tag{2.51}$$

where the observables with a tilde have been computed on a set of statistics that is smaller and separate than that of $\mathcal{O}'$. With an appropriate choice of $\mathcal{O}'$ and $\Delta\mathcal{O}$ the computational cost of calculation $\mathcal{O}_{AMA}$ with a particular statistical error can be greatly reduced compared to a direct computation of $\mathcal{O}$.

2.1.5 Conserved Currents

When defining conserved currents on the lattice it is not enough to simply take a discrete derivative of the currents defined in Equation (1.25). Instead we must vary the lattice action under some same symmetry transformations, corresponding to the matrices λ^a, and derive the lattice Ward identities. For example, the Wilson action gives

$$\begin{aligned} J_\mu^{W,a} = \frac{1}{2} \big(& \overline{\psi}\left(x + a\hat{\mu}\right)\left(\mathbb{1} + \gamma_\mu\right) U_\mu^\dagger \lambda^a \psi\left(x\right) \\ & - \overline{\psi}\left(x\right)\left(\mathbb{1} - \gamma_\mu\right) U_\mu^\dagger \lambda^a \psi\left(x + a\hat{\mu}\right) \big) . \end{aligned} \tag{2.52}$$

For some actions, including the Möbius DWF action, an alternative approach is taken. We take advantage of the fact that gauge symmetry leaves the action invariant at $O\left(\alpha\right)$ under the simultaneous transformations

$$\begin{aligned} U_\mu\left(x\right) &\to \left(1 + i\alpha\right) U_\mu\left(x\right) \\ U_\mu\left(x - a\hat{\mu}\right) &\to U_\mu\left(x - a\hat{\mu}\right)\left(1 - i\alpha\right) \end{aligned} \tag{2.53}$$

and those in Equation (1.26). A change of variables can be performed on the fermion fields such that the phase is absorbed

$$\begin{aligned} \psi'\left(x\right) &= \left(1 + i\alpha\right)\psi\left(x\right) \\ \overline{\psi}'\left(x\right) &= \overline{\psi}\left(x\right)\left(1 - i\alpha\right) \end{aligned} \tag{2.54}$$

The Jacobian matrix for this change of variable is the identity, and so, for example, the partition function can be written as

$$Z = Z' = \int d\overline{\psi}' d\psi' e^{-S[\psi',\overline{\psi}',U]} \left(1+ i\alpha \sum_{\mu} \left[\frac{\delta S}{\delta U_{\mu}(x)} U_{\mu}(x) - \frac{\delta S}{\delta U_{\mu}(x-a\hat{\mu})} U_{\mu}(x-a\hat{\mu})\right]\right). \tag{2.55}$$

When we insist that

$$\left\langle \sum_{\mu} \left(\frac{\delta S}{\delta U_{\mu}(x)} U_{\mu}(x) - \frac{\delta S}{\delta U_{\mu}(x-a\hat{\mu})} U_{\mu}(x-a\hat{\mu}) \right) \right\rangle = 0 \tag{2.56}$$

we can, for example, rederive Equation (2.52) for the Wilson action in this manner. In fact for a gauge invariant Lagrangian this can always be done. In order to derive the conserved current for the Möbius DWF action we consider this variation of the gauge links for the associated approximate overlap Dirac operator, giving [19]

$$\delta D_{ov}^{Mob} = \frac{1}{2}(1-m)\gamma_5 \delta \left(\frac{1}{1-T^{-L_s}} \right) \tag{2.57}$$

where T is the so-called transfer matrix,

$$T = -\frac{D_{kernel}^{Mob}+1}{D_{kernel}^{Mob}-1}. \tag{2.58}$$

It can be shown with this method that the conserved Möbius current is [19]

$$\begin{aligned} J_{\mu}^{Mob} &= \frac{1-m}{b_s+c_s}\gamma_5 \left(1+T^{-L_s}\right)^{-1} \left[\delta\left(T^{-L_s}\right)\right] \left(T^{-L_s}+1\right)^{-1} \\ &= \frac{1-m}{b_s+c_s}\gamma_5 \left(1+T^{-L_s}\right)^{-1} \left[\sum_{s=0}^{L_s-1} T^{-s}\delta\left(T^{-1}\right) T^{-(L_s-s-1)}\right] \left(T^{-L_s}+1\right)^{-1} \\ &= \frac{1-m}{b_s+c_s}\gamma_5 \left(1+T^{-L_s}\right)^{-1} \left[\sum_{s=0}^{L_s-1} T^{-s}\left[b_s\left(P_R - T^{-1}P_L\right) + c_s\left(T^{-1}P_R - P_L\right)\right]\right. \\ &\quad \left. \times\delta\left(D_W\right)\left[b_s\left(P_R + P_L T^{-1}\right) + c_s\left(P_R T^{-1} + P_L\right)\right] T^{-(L_s-s-1)}\right] \left(T^{-L_s}+1\right)^{-1} \end{aligned} \tag{2.59}$$

where we have used the fact that $\delta\left(T^{-L_s}\right) = \sum_{s=0}^{L_s-1} T^{-s}\delta\left(T^{-1}\right)T^{-(L_s-s-1)}$ and

$$\begin{aligned}\delta\left(T^{-1}\right) = &\left[b_s\left(P_R - T^{-1}P_L\right) + c_s\left(T^{-1}P_R - P_L\right)\right] \\ &\times \delta\left(D_W\right)\left[b_s\left(P_R + P_L T^{-1}\right) + c_s\left(P_R T^{-1} + P_L\right)\right],\end{aligned} \tag{2.60}$$

and we have used the variation of the Wilson action $\delta\left(D_W\right)$ that gives (2.52) with the form $\overline{\psi}\delta\left(D_W\right)\psi = \Delta_\mu^- J_\mu^W$, for the backwards derivative, Δ^-.
Taking b_s and c_s to represent the Shamir DWF formulation the conserved current constructed by Furman and Shamir for the $\lambda^a = \mathbb{1}$ related symmetry can be rederived. For a general λ^a the current in the four spacetime dimensions is [87]

$$\begin{aligned}j_{4,\mu}^a\left(x,s\right) = \frac{1}{2}\big(&\overline{\Psi}\left(x + a\hat{\mu}, s\right)\left(\mathbb{1} + \gamma_\mu\right)U_\mu^\dagger\left(x\right)\lambda^a\Psi\left(x,s\right) \\ &-\overline{\Psi}\left(x,s\right)\left(\mathbb{1} - \gamma_\mu\right)U_\mu^\dagger\left(x\right)\lambda^a\Psi\left(x + a\hat{\mu}, s\right)\big)\end{aligned} \tag{2.61}$$

and for the fifth dimension the current is

$$j_{5,\mu}^a\left(x,s\right)\overline{\Psi}\left(x,s\right)P_R\lambda^a\Psi\left(x,s+1\right) - \overline{\Psi}\left(x,s+1\right)P_L\lambda^a\Psi\left(x,s\right). \tag{2.62}$$

The conserved four dimensional vector current is given as

$$J_\mu^{a,Shamir} = \sum_s j_{4,\mu}^a\left(x,s\right). \tag{2.63}$$

In order to construct the axial current the following five dimensional fermion field rotation is considered

$$\Psi\left(x,s\right) \to \begin{cases} e^{i\Gamma(s)}\Psi\left(x,s\right) & : x = x_0 \\ \Psi\left(x,s\right) & : x \neq x_0 \end{cases} \tag{2.64}$$

where

$$\Gamma\left(s\right) = \begin{cases} -1 & : 0 \leq s < \frac{L_s}{2} \\ +1 & : \frac{L_s}{2} \leq s \end{cases} \tag{2.65}$$

which gives the axial current for the Möbius action as [19]

$$A_\mu^{Mob} = \left(1 + T^{-L_s}\right)^{-1}\left[\sum_{s=0}^{L_s-1} T^{-s}\Gamma\left(s\right)\delta\left(T^{-1}\right)T^{-(L_s-s-1)}\right]\left(T^{-L_s}+1\right)^{-1}. \tag{2.66}$$

In the Shamir case this simplifies to

$$A_\mu^{a,Shamir} = \Gamma\left(s\right)j_{4,\mu}^a. \tag{2.67}$$

For both the Möbius and Shamir constructions the axial current leads to a lattice PCAC relation of the form

$$a\left\langle \partial^{\mu} A_{\mu}^{a}\left(x\right)\right\rangle = 2ma\left\langle P^{a}\left(x\right)\right\rangle + 2\left\langle P_{J5}^{a}\right\rangle , \tag{2.68}$$

where P^a is the pseudoscalar density, defined in Equation (1.31) and P^a_{J5} is known as the midpoint term and is given by

$$P_{J5}^{a}\left(x\right) = \overline{\Psi}\left(x, \frac{L_s}{2} - 1\right) P_R \lambda^a \Psi\left(x, \frac{L_s}{2} - 1\right) + \overline{\Psi}\left(x, \frac{L_s}{2}\right) P_L \lambda^a \Psi\left(x, \frac{L_s}{2}\right). \tag{2.69}$$

As we expect to recover the continuum PCAC, Equation (1.32), as we take $a \to \infty$ we see that the midpoint term is a deviation that does not disappear. If we dived across Equation (2.68) by $a\left\langle P^a\left(x\right)\right\rangle$ this gives

$$\frac{1}{2} = \frac{\left\langle \partial^{\mu} A_{\mu}^{a}\left(x\right)\right\rangle}{\left\langle P^{a}\left(x\right)\right\rangle} = m + m_{res} \tag{2.70}$$

where we have defined $am_{res} \equiv \frac{\left\langle P^a_{J5}\right\rangle}{\left\langle P^a(x)\right\rangle}$ as the residual mass. This residual mass represents the extent to which the finite L_s leads to mixing of the left- and right-handed fermions, leading to residual chiral symmetry breaking. For the lighter quarks, the up, down, and strange, m_{res} has been studied for the ensembles used in this thesis and the L_s extent is long enough the m_{res} is small. For the charm quark that is needed to study the rare kaon decays, however, more consideration is needed. This is discussed further in Section (4.1).

2.2 Simulation and Measurement

2.2.1 Gauge Configuration Generation

In order to calculate correlation functions, as in Equation (2.1) after performing a Wick rotation, for a given gauge and fermion action the number of degrees of freedom in the path integral must be reduced, as it would be too computationally expensive to perform the calculation directly. The fermions are typically integrated out for this reason, and instead are represented in terms of bosonic

"pseudofermion" fields, ϕ, as

$$\int D\psi D\overline{\psi} e^{-\overline{\psi} D\psi} = det\left(D\right) = \frac{1}{det\left(D^{-1}\right)} = \int D\phi D\phi^{\dagger} e^{-\phi^{\dagger} D^{-1} \phi}. \tag{2.71}$$

The correlation function now takes the form

$$\left\langle 0|\mathcal{O}_1\left(x_1\right)\ldots\mathcal{O}_n\left(x_n\right)|0\right\rangle = \frac{1}{Z}\int D\left[A,\phi,\phi^{\dagger}\right]\mathcal{O}_1\left(x_1\right)\ldots\mathcal{O}_n e^{iS\left[A,\phi,\phi^{\dagger}\right]}. \tag{2.72}$$

Integrating over the space of all ensembles is still prohibitively expensive and instead a statistical approach is taken to evaluated $\left\langle 0|\mathcal{O}_1\left(x_1\right)\ldots\mathcal{O}_n\left(x_n\right)|0\right\rangle$. A sequence of N gauge field configurations, U_i, are generated with probability weighted appropriately, such that

$$\left\langle 0|\mathcal{O}_1\left(x_1\right)\ldots\mathcal{O}_n\left(x_n\right)|0\right\rangle \approx \frac{1}{N}\sum_{i=1}^{N}\mathcal{O}_1\left(x_1\right)\ldots\mathcal{O}_n e^{[U_i]} \tag{2.73}$$

which hold true up to $O\left(\frac{1}{\sqrt{N}}\right)$ statistical errors. The method with which the gauge configurations used in this project were generated was a hybrid Monte Carlo algorithm [19, 42].

2.2.2 Construction of Correlators

As a simple example of how to construct such a correlation function as in Equation (2.73) let us consider the pion two point function

$$\left\langle \phi_{\pi^+}\left(y\right)\phi^{\dagger}_{\pi^+}\left(x\right)\right\rangle \tag{2.74}$$

where $\phi^{\dagger}_{\pi^+}\left(x\right)$ is the pseudoscalar interpolator that creates a state with the same quantum numbers of a π^+ meson at position $\left(t_x,\vec{x}\right)$ and $\phi\left(y\right)$ is the equivalent annihilation operator. For the π^+ these interpolators are given by

$$\begin{aligned}\phi_{\pi^+}\left(y\right) &= \overline{d}\left(y\right)^{\alpha}_{a}\left(\gamma_5\right)^{\alpha\beta} u\left(y\right)^{\beta}_{b} \\ \phi^{\dagger}_{\pi^+}\left(x\right) &= \left(\overline{d}\left(x\right)^{\alpha}_{a}\left(\gamma_5\right)^{\alpha\beta} u\left(x\right)^{\beta}_{b}\right)^{\dagger} = -\overline{u}\left(x\right)^{\beta}_{b}\left(\gamma_5\right)^{\beta\alpha} d\left(x\right)^{\alpha}_{a}\end{aligned} \tag{2.75}$$

where the minus sign comes from the interchange of the Grassman variables, the Greek indices give spin and the Roman indices color. Using these interpolators

we get

$$\begin{aligned}\left\langle \phi_{\pi^+}(y)\,\phi^{\dagger}_{\pi^+}(x)\right\rangle &= -\left\langle \overline{d}(y)^{\alpha}_{a}(\gamma_5)^{\alpha\beta}u(y)^{\beta}_{b}\,\overline{u}(x)^{\gamma}_{c}(\gamma_5)^{\gamma\delta}d(x)^{\delta}_{d}\right\rangle \\ &= \left\langle [u(y)\,\overline{u}(x)]^{\beta\gamma}_{bc}(\gamma_5)^{\gamma\delta}\left[d(x)\,\overline{d}(y)\right]^{\delta\alpha}_{da}(\gamma_5)^{\alpha\beta}\right\rangle \\ &= \langle Tr\left[S_u(y,x)\,\gamma_5 S_d(x,y)\,\gamma_5\right]\rangle \\ &= \left\langle Tr\left[S^{\dagger}_{u}(x,y)\,S_d(x,y)\right]\right\rangle\end{aligned} \tag{2.76}$$

where we have performed a Wick contraction, used the definition of the propagator

$$S_q(x,y)^{\alpha\beta}_{ab} = [q(x)\,\overline{q}(y)]^{\alpha\beta}_{ab}\,, \tag{2.77}$$

and used the γ_5 hermiticity property of the propagator:

$$\gamma_5 S_q(x,y)\,\gamma_5 = S^{\dagger}_{q}(y,x)\,. \tag{2.78}$$

In order to compute the pion two point function for a specific momentum, $\vec{p}$, such that is couples to the corresponding eigenstates of the Hamiltonian, we consider the Fourier transform of the interpolator

$$\tilde{\phi}_{\pi^+}(t,\vec{p}) = \frac{1}{V}\sum_{\vec{x}}\phi_{\pi^+}(y)\,e^{-i\vec{p}\cdot\vec{x}}. \tag{2.79}$$

Since the Fourier transform is over the spatial part of the lattice the creation and annihilation operators are projected to the momentum, $\vec{p}$, at source and sink times, t_0 and t_s. The two pion correlator is then given as

$$\left\langle \tilde{\phi}_{\pi^+}(t_s,\vec{p})\,\tilde{\phi}^{\dagger}_{\pi^+}(t_0,\vec{p})\right\rangle = \sum_{\vec{x},\vec{y}}\left\langle \phi_{\pi^+}(y)\,\phi^{\dagger}_{\pi^+}(x)\right\rangle e^{-i\vec{p}\cdot(\vec{y}-\vec{x})}. \tag{2.80}$$

2.2.3 Extracting Observables

To study the vacuum expectation value of the pion 2-point function we consider its time dependence. If we take Equation (2.80) and insert a complete set of eigenstates for the Hamiltonian

$$\mathbb{1} = \sum_{n}\frac{1}{2E_n(\vec{p})}\,|n\rangle\langle n|\,, \tag{2.81}$$

and use the Euclidean time evolution for operators

$$\mathcal{O}(t) = e^{t\hat{H}} \mathcal{O} e^{-t\hat{H}}, \tag{2.82}$$

where $\hat{H}$ is the Hamiltonian operator, we get

$$\begin{aligned}
\Gamma^{(2)}(t_s, t_0, \vec{p}) &= \sum_n \frac{1}{2E_n(\vec{p})} \langle 0| e^{(t_s - T)\hat{H}} \tilde{\phi}_{\pi^+}(0, \vec{p}) e^{-t_s \hat{H}} |n\rangle \langle n| e^{t_0 \hat{H}} \tilde{\phi}^\dagger_{\pi^+}(0, \vec{p}) e^{-t_0 \hat{H}} |0\rangle \\
&= \sum_n \frac{1}{2E_n(\vec{p})} \langle 0| e^{(t_s - T)E_0} \tilde{\phi}_{\pi^+}(0, \vec{p}) e^{-t_s E_n} |n\rangle \langle n| e^{t_0 E_n} \tilde{\phi}^\dagger_{\pi^+}(0, \vec{p}) e^{-t_0 E_0} |0\rangle \\
&= \sum_n \frac{Z_n^2(\vec{p})}{2E_n(\vec{p})} e^{-E_n(t_s - t_0)}
\end{aligned} \tag{2.83}$$

where T is the time extent of the lattice, the energy of the vacuum is $E_0 = 0$ and $Z_n(\vec{p})$, defined as

$$Z_n^2(\vec{p}) = \left| \left\langle n | \tilde{\phi}^\dagger_{\pi^+}(0, \vec{p}) |0 \right\rangle \right|^2, \tag{2.84}$$

represents the probability of the interpolator, $\tilde{\phi}^\dagger_{\pi^+}(0, \vec{p})$, to create the meson state $|n>$ from the vacuum. We can see that this 2-point function does not only the pion meson state, but also includes contributions from excited states. However, due to the exponentially decaying behavior of the correlator, in the $t >> t_s$ limit we have

$$\Gamma^{(2)}(t_s, t_0, \vec{p}) \xrightarrow{t_s >> t_0} \frac{Z_\pi^2(\vec{p})}{2E_\pi(\vec{p})} e^{-E_\pi(\vec{p})(t_s - t_0)} \tag{2.85}$$

as the pion is the ground state of the interpolator. In practice, as we have a finite volume on the lattice, we do not compute the VEV of the 2-point function, but instead

$$\Gamma^{(2)}(t_s, t_0, \vec{p}) = \sum_m \langle m| \tilde{\phi}_{\pi^+}(t_s, \vec{p}) \tilde{\phi}^\dagger_{\pi^+}(t_0, \vec{p}) |m\rangle, \tag{2.86}$$

which becomes the VEV in the infinite limit. Periodic boundary conditions are also used on the lattice, and these result in "round-the-world" effects that are due to the fact that the meson states also propagate in the negative time direction. If we perform the same procedure of evolving the interpolators of (2.86) in time, and combine those results with forward propagating equivalent, (2.83), we get

$$\begin{aligned}
\Gamma^{(2)}(t_s, t_0, \vec{p}) &\xrightarrow{T >> t_s >> t_0} \frac{Z_\pi^2(\vec{p})}{2E_\pi(\vec{p})} \left(e^{-E_\pi(\vec{p})(t_s - t_0)} + e^{-E_\pi(\vec{p})(T - (t_s - t_0))} \right) \\
&= \frac{Z_\pi^2(\vec{p})}{E_\pi(\vec{p})} e^{\frac{T}{2} E_\pi(\vec{p})} \cosh\left(E_\pi(\vec{p}) \left[t_s - t_0 - \frac{T}{2} \right] \right)
\end{aligned} \tag{2.87}$$

which takes these "round-the-world" into account. We use Equation (2.87) as a model to fit our lattice data for $Z_\pi^2(\vec{p})$ and $E_\pi(\vec{p})$, in the appropriate fit range $T >> t_s >> t_0$. For the zero momentum case fitting for $E_\pi\left(\vec{0}\right)$ is equivalent to fitting for the pion mass, and a useful quantity that can be used to determine an appropriate fit range is the effective mass

$$aM_{eff}(t_s) = ln\left(\frac{\Gamma^{(2)}\left(t_s, t_0, \vec{0}\right)}{\Gamma^{(2)}\left(t_s+1, t_0, \vec{0}\right)}\right), \tag{2.88}$$

which gives a clear plateau when excited states no longer contribute. A similar approach of inserting a complete set of states and using the Euclidean time evolution for interpolators is used to create the 3- and 4-point functions that are presented in Section (3.2.1), which we wish to fit for the matrix elements and energies we need to describe the rare kaon decays we are interested in.

2.2.4 Bootstrap Resampling

After calculating a distribution of some correlation function,

$$C = \{C_i\}; \quad 1 \leq i \leq N_C, \tag{2.89}$$

on N_C gauge configurations, we estimate the VEV of some observable, $\mathcal{O}$, by taking the average of each observable, $\mathcal{O}$, extracted from C_i

$$\langle\mathcal{O}\rangle \approx \bar{\mathcal{O}} = \frac{1}{N_C}\sum_{i=1}^{N_C}\mathcal{O}_i. \tag{2.90}$$

In the $N_C \to \infty$ limit this will coverage to the "true" VEV of the theory we are working in, but for finite N_C we can only calculate an estimator of the true value. A statistical error on the average must in order to consider the result meaningful. The distribution of observables is expected to follow a Gaussian distribution, so for large number of independent measurements we may calculate the variance on the observables as as

$$\sigma_{\mathcal{O}}^2 = \frac{1}{N_C - 1}\sum_{i=1}^{N_C}\left(\mathcal{O}_i - \bar{\mathcal{O}}\right)^2. \tag{2.91}$$

In practice it is too computationally costly to compute a large enough distribution for Equation (2.91) to hold true, and in any case our measurements are not always independent. The gauge configurations are generated as a Markov chain, using Monte Carlo methods, and so suffer from auto-correlation. To compensate for this we can either calculate observables on gauge configurations that are sufficiently separated in the Markov chain that the correlation contributes less than the statistical error would, or bin our data such that the binned data is sufficiently independent. To compensate for the low statistics in the distribution we may employ bootstrap resampling. This procedure involves creating a new distribution, C_j^B, called a bootstrap sample, that is given as [48]

$$C_j^B = \left\{C_i^b\right\}; \quad 1 \leq i \leq N_C; \quad C_i^b = \text{rand}\left(C_i\right), \tag{2.92}$$

that has the same number of elements as the the original distributions, but each element is chosen randomly from the original. This is repeated N_b times and a distribution of the mean of the bootstrap sample is created

$$C^B = \left\{\bar{C}_i^B\right\}; \quad 1 \leq j \leq N_b, \tag{2.93}$$

with corresponding observables being extracted, $\mathcal{O}^B$ and $\bar{\mathcal{O}}_i^B$. From this we can define the standard deviation as

$$\sigma_B = \frac{1}{N_b}\sum_{i=1}^{B_b}\left(\bar{\mathcal{O}}^B - \bar{\mathcal{O}}_i^B\right)^2 \tag{2.94}$$

or by finding the values, a and b, of $\bar{\mathcal{O}}_i^B$, that bound the 68% confidence interval

$$\frac{\#\left\{\bar{\mathcal{O}}_i^B < a\right\}}{N_b} = 0.16, \qquad \frac{\#\left\{\bar{\mathcal{O}}_i^B < b\right\}}{N_b} = 0.84, \tag{2.95}$$

and defining the bootstrap estimate of the standard deviation to be half the length of this interval

$$\sigma_B = \frac{b-a}{2}. \tag{2.96}$$

2.2.5 Fitting

When fitting some ensemble average lattice data, $\left\{\bar{Y}_i\right\}$, $\bar{Y}_i = \frac{1}{N_C}\sum_{i=1}^{N_C} Y_{ij}$, we want to test how well this data agrees with some model, $F\left(X, \alpha_1, \alpha_2, \ldots\right)$, where X is some variable associated with the lattice (usually time, but it may also be

quark mass or lattice spacing) and the α's are fit parameters of the model we wish to determine. If the data are independent then we find the fit parameters by comparing the data to the model on an appropriate set of data points, β, and look for the α's that minimize the χ^2 function, defined as

$$\chi^2 = \sum_{i\in\beta} \frac{\left[\bar{Y}_i - F\left(X, \alpha_1, \alpha_2, \ldots\right)\right]}{\sigma_i^2}. \tag{2.97}$$

The degrees of freedom (dof) in this fit are given by $N_\beta - N_\alpha$, and χ^2/dof gives an indication of the goodness of fit, with a smaller χ^2/dof corresponding to a good agreement between the data and model over a number of fit points. To be confident in our fit result we must also investigate the probability that randomly selected data would have the same χ^2. This probability is known as the p-value, and for this thesis the two-sided p-value is used, and is given by

$$p = 2\min\left\{P\left(X > \chi^2\right), P\left(X < \chi^2\right)\right\}, \tag{2.98}$$

where X is a random variable that has a χ^2-distribution. Our lattice data is not expected to be independent. As our observables may depend on multiple quantities that are measured using the same gauge fields they will be correlated with each other. Even within one correlator, $C(t)$, there may be significant correlation between adjacent time slices. Due to this we instead seek to minimize the correlated χ^2:

$$\chi^2 = \sum_{i,j\in\beta} \left(\bar{Y}_i - F\left(X, \alpha_1, \alpha_2, \ldots\right)\right) C_{ij}^{-1} \left(\bar{Y}_j - F\left(X, \alpha_1, \alpha_2, \ldots\right)\right) \tag{2.99}$$

where C_{ij} is the covariant matrix that describes the correlation between different data points, and is given by

$$C_{ij}^{-1} = \frac{1}{N_C\left(N_C - 1\right)} \sum_{k=1}^{N_C} \left(Y_{ik} - \bar{Y}_i\right)\left(Y_{jk} - \bar{Y}_j\right). \tag{2.100}$$

If the number of configurations used to create the ensemble average data is not large enough to give a good signal the the covariance matrix may become singular, or close to singular, making it impossible, or difficult, to invert. In these cases it is necessary to depend only on the uncorrelated χ^2 to determine goodness of fit.

2.3 Lattice Propagator

To compute a lattice propagator, as in Equation (2.77), needed to construct the correlation functions, we need to invert the Dirac matrix

$$S_q(x,y) = D^{-1}(x,y,m=m_q). \tag{2.101}$$

This describes the propagation amplitude of a quark from every point x on the lattice to every other point y, for each other $4 \times 3 = 12$ spin-color combinations. In the thesis we have made use of Dirac operators for gauge configurations with spacetime volume $N_L^3 \times N_T = 48^3 \times 96$ with $L_s = 10$ for the zMöbius action and $L_s = 24$ for the Möbius action. This leads to a Dirac matrix with $\sim 10^{16}$ elements in 4 dimensions and $\sim 10^{18}$ elements in 5 dimensions. These are prohibitively expensive to invert exactly and, although there are methods that can be employed to reduce the computational cost of inversion, some approximation is made. Typically the approximation is done by solving

$$D^{-1}(x,y) = \eta(x,z) = S(x,z) \tag{2.102}$$

where $\eta(x,z)$ is a source field that only has a subset of elements on the lattice. This matrix problem, where $S(x,z)$ is our solution, can be solved with various methods and for various source, $\eta(x,z)$. For this thesis the conjugate gradient (CG) algorithm, a Krylov subspace method, was used [84]. The remainder of this section is spent discussing ways to improve the convergence of this algorithm, reduction its computational cost with even-odd preconditioning in Section (2.3.1) and "deflating" the solves by constructing guess vectors using eigenvectors of the Dirac matrix in Section (2.3.2). Following that the "all-to-all" method of approximating the Dirac matrix will be introduced in Section (2.3.3) and the various $\eta(x,z)$ sources that are used in this thesis are introduced in Section (2.4).

2.3.1 Even-Odd Preconditioning

Consider the matrix problem

$$M\psi(x) = \eta(x) \tag{2.103}$$

where M is the massive lattice Dirac operator, $\eta(x)$ is a given source quark field, and $\psi(x)$ is the solution we are looking for. If we wish to solve the matrix problem though some conjugate gradient algorithm then the convergence of this algorithm depends on the condition number, $\kappa(M)$, of the matrix $M^\dagger M$, given by [73]

$$\kappa(M) = \left(\frac{\lambda_{max}}{\lambda_{min}}\right)^{1/2} \propto (am)^{-1} \tag{2.104}$$

where the λ's are the extremal eigenvalues of the matrix $M^\dagger M$, a is the lattice spacing and m is the quark mass. For small quark masses and lattice spacings the Dirac operator is said to be "ill-conditioned."

The problem can be rearranged in such a way that a different matrix with a better condition number must be inverted in order to find a solution. This procedure is called preconditioning and a common method used is called "even-odd preconditioning." A lattice point x is considered even or odd depending on whether the sum of its coordinates x_μ is even or odd. This allows for a Schur decomposition of M into LDU form:

$$\begin{aligned} M &= \begin{pmatrix} M_{ee} & M_{eo} \\ M_{oe} & M_{oo} \end{pmatrix} \\ &= \begin{pmatrix} 1 & 0 \\ M_{oe}M_{ee}^{-1} & 1 \end{pmatrix} \begin{pmatrix} M_{ee} & 0 \\ 0 & D_{oo} \end{pmatrix} \begin{pmatrix} 1 & M_{ee}^{-1}M_{eo} \\ 0 & M_{oo} \end{pmatrix} \\ &= LDU \end{aligned} \tag{2.105}$$

where $D_{oo} = 1 - M_{oe}M_{ee}^{-1}M_{eo}M_{oo}^{-1}$ and M_{eo}, for example, stands for the hopping terms that go from the odd to the even sites. M_{ee} and M_{oo} include mass terms (and possibly a Pauli term if the theory is $\mathcal{O}(a)$-improved). They can easily be inverted as they do not couple to different lattice points. Using this decomposition we can rewrite equation (2.103) as

$$LDU\psi = \eta. \tag{2.106}$$

Therefore we can write

$$\begin{aligned} DU\psi &= L^{-1}\eta \\ \begin{pmatrix} M_{ee} & M_{eo} \\ 0 & D_{oo}M_{oo} \end{pmatrix} \psi &= \begin{pmatrix} 1 & 0 \\ -M_{oe}M_{ee}^{-1} & 1 \end{pmatrix} \eta. \end{aligned} \tag{2.107}$$

This can be decomposed into odd and even subspaces

$$\begin{pmatrix} M_{ee} & M_{eo} \\ 0 & D_{oo}M_{oo} \end{pmatrix} \begin{pmatrix} \psi_e \\ \psi_o \end{pmatrix} = \begin{pmatrix} 1 & 0 \\ -M_{oe}M_{ee}^{-1} & 1 \end{pmatrix} \begin{pmatrix} \eta_e \\ \eta_o \end{pmatrix}$$
$$\begin{pmatrix} M_{ee}\psi_e + M_{eo}\psi_o \\ D_{oo}M_{oo}\psi_o \end{pmatrix} = \begin{pmatrix} \eta_e \\ \eta_o - M_{oe}M_{ee}^{-1}\eta_e \end{pmatrix} = \begin{pmatrix} \eta_e \\ \eta'_o \end{pmatrix} \tag{2.108}$$

By solving the equation

$$D_{oo}^{\dagger}D_{oo}M_{oo}\psi_o = D_{oo}^{\dagger}\eta'_o \tag{2.109}$$

for ψ_o we can find

$$\psi_e = M_{ee}^{-1}\left(\eta_e - M_{eo}\psi_o\right) \tag{2.110}$$

and obtain the full solution. $D_{oo}^{\dagger}D_{oo}$ is a Hermitian, positive definite matrix, so we can use the CG algorithm to find its inverse. The condition number of $D_{oo}^{\dagger}D_{oo}$ is smaller than that of $M^{\dagger}M$, and so the cost of the CG algorithm is reduced.

2.3.2 Deflation

If we had the N_l lowest eigenvectors and eigenvalues of $D_{oo}^{\dagger}D_{oo}$

$$D_{oo}^{\dagger}D_{oo}\phi_i = \lambda_i\phi_i \tag{2.111}$$

then this knowledge could be used to improve the condition number of and create a denser eigenvalue spectrum for the CG algorithm, both of which would improve convergence. To do this we first consider that for a matrix with M eigenvectors

$$D_{oo}^{-1} = \left(D_{oo}^{\dagger}D_{oo}\right)^{-1}D_{oo}^{\dagger} = \sum_{i=1}^{i=M}\frac{\phi_i\phi_i^{\dagger}}{\lambda_i}D_{oo}^{\dagger}. \tag{2.112}$$

and then rewrite $\left(D_{oo}^{\dagger}D_{oo}\right)^{-1}$ in terms of low and high mode parts

$$\begin{aligned} \left(D_{oo}^{\dagger}D_{oo}\right)^{-1} &= \sum_{i=1}^{i=M}\frac{\phi_i\phi_i^{\dagger}}{\lambda_i} \\ &= \sum_{i=1}^{i=N_l}\frac{\phi_i\phi_i^{\dagger}}{\lambda_i} + \sum_{i=N_l+1}^{i=M}\frac{\phi_i\phi_i^{\dagger}}{\lambda_i} \\ &= \left(D_{oo}^{\dagger}D_{oo}\right)^{-1(l)} + \left(D_{oo}^{\dagger}D_{oo}\right)^{-1(h)}. \end{aligned} \tag{2.113}$$

Similarly the source $D^{\dagger}_{oo}\eta'_o$ can be split into high and low mode parts

$$\begin{aligned} D^{\dagger}_{oo}\eta'_o &= \sum_{i=1}^{i=N_l} \phi_i \phi_i^{\dagger} D^{\dagger}_{oo}\eta'_o + \sum_{i=N_l+1}^{i=M} \phi_i \phi_i^{\dagger} D^{\dagger}_{oo}\eta'_o \\ &= \left(D^{\dagger}_{oo}\eta'_o\right)^{(l)} + \left(D^{\dagger}_{oo}\eta'_o\right)^{(h)}, \end{aligned} \tag{2.114}$$

as can ψ. The orthogonality of the eigenvectors means that we can write the solution as

$$\psi^{(l)} + \psi^{(h)} = \left(D^{\dagger}_{oo}D_{oo}\right)^{-1(l)} \left(D^{\dagger}_{oo}\eta'_o\right)^{(l)} + \left(D^{\dagger}_{oo}D_{oo}\right)^{-1(h)} \left(D^{\dagger}_{oo}\eta'_o\right)^{(h)} \tag{2.115}$$

The low mode part of the solution can be constructed using the known eigenvalues and eigenvectors and the high mode part is better conditioned. If the low mode part of the source is explicitly removed from $\left(D^{\dagger}_{oo}\eta'_o\right)^{(h)}$ and the conjugate gradient algorithm is started with a guess vector that is orthogonal to the space of low modes then the solution will remain orthogonal to the low modes also.
For this thesis, the Implicitly Restarted Lanczos method was employed to compute the eigenvectors that were used to deflate the Dirac matrix. A discussion on how to compute these eigenvectors is given in A .

2.3.3 All-to-All Propagators

General Case

All-to-all propagators are an approximation to the quark propagators $S(x,y) = D^{-1}(x,y)$ for any x and y that can be found without inverting the Dirac operator for each choice of y [50]. In general we write

$$D^{-1}_{A2A} = \sum_{i=1}^{i=N_l} \frac{\phi_i \phi_i^{\dagger}}{\lambda_i} + \sum_{h=1}^{h=N_h} D^{-1}_{defl}\eta_h \eta_h \tag{2.116}$$

where

$$D^{-1}_{defl} = D^{-1} - \sum_{j=1}^{j=N_l} \frac{\phi_j \phi_j^{\dagger}}{\lambda_j} \tag{2.117}$$

and η_h are N_h sets of 'source' vectors that have the property

$$\lim_{N_h \to \infty} \eta_h \eta_h = \mathbb{1} \tag{2.118}$$

and so

$$\lim_{N_h \to \infty} D^{-1}_{A2A} = D^{-1}. \tag{2.119}$$

The 'All-to-all Vectors' are defined as

$$v_i = \begin{cases} \frac{1}{\lambda_i}\phi_i : & 1 \leq i < N_l \\ D^{-1}_{defl}\eta_i : & N_l \leq i < N_l + N_h \end{cases} \tag{2.120}$$

$$w_i = \begin{cases} \phi_i : & 1 \leq i < N_l \\ \eta_i : & N_l \leq i < N_l + N_h \end{cases} \tag{2.121}$$

such that

$$D^{-1}_{A2A} = \sum_i v_i w_i \tag{2.122}$$

Preconditioned DWF Case

The inverse of the even-odd preconditioned Dirac operator given in Equation (2.105) is:

$$\begin{aligned} D^{-1}_{DWF} &= U^{-1} D^{-1} L^{-1} \\ &= \begin{pmatrix} 1 & -M^{-1}_{ee} M_{eo} M^{-1}_{oo} \\ 0 & M^{-1}_{oo} \end{pmatrix} \begin{pmatrix} M^{-1}_{ee} & 0 \\ 0 & D^{-1}_{oo} \end{pmatrix} \begin{pmatrix} 1 & 0 \\ -M_{oe} M^{-1}_{ee} & 1 \end{pmatrix} \\ &= U^{-1} \begin{pmatrix} M^{-1}_{ee} & 0 \\ 0 & (D^{\dagger}_{oo} D_{oo})^{-1} \end{pmatrix} \begin{pmatrix} 1 & 0 \\ 0 & D^{\dagger}_{oo} \end{pmatrix} L^{-1} \end{aligned} \tag{2.123}$$

This can be written in two parts by separating the low-mode parts of $D^{\dagger}_{oo} D_{oo}$:

$$\begin{aligned} D^{-1}_{DWF} &= A + B \\ A &= U^{-1} \begin{pmatrix} 0 & 0 \\ 0 & \sum \frac{1}{\lambda_i} \phi_i \phi_i^{\dagger} \end{pmatrix} \begin{pmatrix} 1 & 0 \\ 0 & D^{\dagger}_{oo} \end{pmatrix} L^{-1} \\ B &= U^{-1} \begin{pmatrix} M^{-1}_{ee} & 0 \\ 0 & D^{-1}_{ooDefl} \end{pmatrix} \begin{pmatrix} 1 & 0 \\ 0 & D^{\dagger}_{oo} \end{pmatrix} L^{-1} \end{aligned} \tag{2.124}$$

where $D^{-1}_{ooDefl} = (D^{\dagger}_{oo}D_{oo})^{-1} - \sum \frac{1}{\lambda_i}\phi_i\phi_i^{\dagger}$. The all-to-all vectors are then given as

$$\begin{aligned} v_i &= U^{-1}\begin{pmatrix} 0 \\ \frac{1}{\lambda_i}\phi_i \end{pmatrix} \\ w_i &= L^{-1\dagger}\begin{pmatrix} 1 & 0 \\ 0 & D_{oo} \end{pmatrix}\begin{pmatrix} 0 \\ \phi_i \end{pmatrix} \end{aligned} \tag{2.125}$$

for $1 \leq i < N_l$ and

$$\begin{aligned} v_i &= U^{-1}\begin{pmatrix} M^{-1}_{ee} & 0 \\ 0 & D^{-1}_{ooDefl} \end{pmatrix}\begin{pmatrix} 1 & 0 \\ 0 & D^{\dagger}_{oo} \end{pmatrix} L^{-1}\eta_i \\ w_i &= \eta_i \end{aligned} \tag{2.126}$$

for $N_l \leq i < N_l + N_h$.
Decomposing the v and w vectors into odd and even subspaces for the low-modes gives:

$$\begin{aligned} v_{ie} &= -\frac{1}{\lambda_i}M^{-1}_{ee}M_{eo}M^{-1}_{oo}\phi_i \\ v_{io} &= \frac{1}{\lambda_i}M^{-1}_{oo}\phi_i \end{aligned} \tag{2.127}$$

and

$$\begin{aligned} w_{ie} &= -M^{-1\dagger}_{ee}M^{\dagger}_{oe}D_{oo}\phi_i \\ w_{io} &= D_{oo}\phi_i. \end{aligned} \tag{2.128}$$

For the high-modes we note that we can rewrite the v_i part of equation 2.126 as:

$$\begin{aligned} \begin{pmatrix} M_{ee} & 0 \\ 0 & D^{-1\dagger}_{oo}D_{ooDefl} \end{pmatrix} U v_i &= L^{-1}\eta_i \\ \begin{pmatrix} M_{ee} & M_{eo} \\ 0 & D^{-1\dagger}_{oo}D_{ooDefl}M_{oo} \end{pmatrix} v_i &= \begin{pmatrix} 1 & 0 \\ -M_{oe}M^{-1}_{ee} & 1 \end{pmatrix}\eta_i \end{aligned} \tag{2.129}$$

This is almost equivalent to what we had in equation 2.107, and if we proceed with a similar even odd decomposition we find:

$$\begin{pmatrix} M_{ee} & M_{eo} \\ 0 & D_{oo}^{-1\dagger} D_{ooDefl} M_{oo} \end{pmatrix} \begin{pmatrix} v_e \\ v_o \end{pmatrix} = \begin{pmatrix} 1 & 0 \\ -M_{oe} M_{ee}^{-1} & 1 \end{pmatrix} \begin{pmatrix} \eta_e \\ \eta_o \end{pmatrix}$$
$$\begin{pmatrix} M_{ee} v_e + M_{eo} v_o \\ D_{oo}^{-1\dagger} D_{ooDefl} M_{oo} v_o \end{pmatrix} = \begin{pmatrix} \eta_e \\ \eta_o - M_{oe} M_{ee}^{-1} \eta_e \end{pmatrix} = \begin{pmatrix} \eta_e \\ \eta'_o \end{pmatrix} \tag{2.130}$$

Now we must solve the equation

$$D_{ooDefl} M_{oo} v_o = D_{oo}^{\dagger} \eta'_o \tag{2.131}$$

which is almost equivalent to equation 2.109. By finding v_o

$$\begin{aligned} v_o &= M_{oo}^{-1} (D_{ooDefl})^{-1} D_{oo}^{\dagger} \eta'_o \\ &= M_{oo}^{-1} \left((D_{oo}^{\dagger} D_{oo})^{-1} - \sum \frac{1}{\lambda_i} \phi_i \phi_i^{\dagger} \right) D_{oo}^{\dagger} \eta'_o \end{aligned} \tag{2.132}$$

we can compute

$$v_e = M_{ee}^{-1} \left(\eta_e - M_{eo} v_o \right) \tag{2.133}$$

The even and odd decomposition of w_i is trivially:

$$\begin{aligned} w_{ie} &= \eta_{ie} \\ w_{io} &= \eta_{io}. \end{aligned} \tag{2.134}$$

When using a 5-D Domain Wall Fermion action the 4-D propagator is given by:

$$\begin{aligned} S(x,y) = & P_R D_{DWF}^{-1} (x, L_s - 1; y, 0) P_R \\ & + P_R D_{DWF}^{-1} (x, L_s - 1; y, L_s - 1) P_L \\ & + P_L D_{DWF}^{-1} (x, 0; y0) P_R \\ & + P_L D_{DWF}^{-1} (x, 0; y, L_s - 1) P_L. \end{aligned} \tag{2.135}$$

Similarly for a 5-D All-to-All propagator:

$$D_{A2A}^{-1}(x, s; y, t) = \sum_i v_i(x, s) w_i(y, t) \tag{2.136}$$

the 4-D v and w vectors are given by

$$\begin{aligned} v_i(x) &= P_L v_i(x,0) + P_R v_i(x, L_s - 1) \\ w_i(y) &= w_i(x, L_s - 1) P_L + w_i(x,0) P_R \end{aligned} \tag{2.137}$$

which is the same projection to the walls of the fifth dimension that would be done to find the physical 4-D quark fields.

Meson Correlation Function

We can now write the meson correlator functions

$$C(t) = \sum_{\mathbf{x},\mathbf{y}} \mathrm{Tr}\left[S^{(q)}(x,y) \Gamma_1 S^{(q')}(y,x) \Gamma_2 \right] \tag{2.138}$$

as

$$\begin{aligned} C(t) &= \sum_{\mathbf{x},\mathbf{y},i,j} \mathrm{Tr}\left[v_i^{(q)}(x) w_i^{(q)}(y) \Gamma_1 v_j^{(q')}(y) w_j^{(q')}(x) \Gamma_2 \right] \\ &= \sum_{i,j} \sum_{\mathbf{x}} w_j^{(q')}(x) \Gamma_2 v_i^{(q)}(x) \sum_{\mathbf{y}} w_i^{(q)}(y) \Gamma_1 v_j^{(q')}(y) \\ &= \sum_{i,j} \Pi_{ji}^{(q',q)}(t_x; \Gamma_2) \Pi_{ij}^{(q,q')}(t_y; \Gamma_1) \end{aligned} \tag{2.139}$$

where the $\Pi_{ij}^{(q,q')}(t_x;\Gamma) = \sum_{\mathbf{x}} w_i^{(q)}(x) \Gamma v_j^{(q')}(x)$ are known as "Meson Fields." A description of how to construct the 3- and 4-point functions that are relevant to the rare kaon decays we are interested in are given in (B).

2.4 Lattice Sources

Lattice propagators, $S(x,z)$, are constructed by solving the matrix problem given in Equation (2.101) using some source field $\eta(y,z)$. $S(x,z)$ here may be the full lattice propagator or it may the high-mode portion of an A2A propagator. The source field typically consists of a subset of the available parameter space, and the solutions of the corresponding matrix problems are combined to approximate the full results. For example, all the sources in this thesis are said to be "spin-color"

diluted, that is

$$\eta\left(y,z\right)_{ab}^{\alpha\beta}=\kappa\left(y,z\right)\delta_{\alpha\beta}\delta_{ab}, \tag{2.140}$$

where $\kappa\left(y,z\right)$ is a source field that describes only the spacetime structure of $\eta\left(y,z\right)$. This means that we perform have to perform 12 inversions, one for each spin-color combination, which can then be combined to give a propagator that describes the full spin-color space.
The most basic of the spacetime sources, $\kappa\left(y,z\right)$ is the point source, that corresponds to a single lattice site, z_0,

$$\kappa\left(y,z_0\right)=\delta\left(\vec{y}-\vec{z}_0\right)\delta\left(t_y-t_{z_0}\right). \tag{2.141}$$

The propagator obtained using the point source describes the propagation amplitude from z_0 to all other sites, y. Several such propagators can be computed with point sources defined at different lattice sites and these can be combined in average when constructing correlators. When these correlators are analyzed to extract physical observables, as discussed in Section (2.2.3), the spatial distribution of the source vector can change the regions where the ground state of the interpolators dominates. This means that some spatial distributions in the source vector can results in larger regions of ground state domination over which we can fit, leading to more precise results for no additional computational cost.
For this thesis wall sources are used to compute the propagators used in studying the rare kaon decays, these are given as [51]

$$\kappa\left(y,z,\vec{p}\right)=\delta\left(t_y-t_W\right)e^{i\vec{p}\cdot\vec{z}}, \tag{2.142}$$

which is the sum of all spatial point sources for a given time, t_W. This choice of source is not gauge invariant and so gauge fixing must be performed in order to make use of them.

Gauge Fixing

Lattice "links" transcribe the gauge field via the matrix exponential given in Equation (2.13). We use the Coulomb gauge

$$\partial^i A_i=0,\quad i=1,2,3 \tag{2.143}$$

to fix the gauge in order to use wall sources. On the lattice this is the equivalent of minimizing the functional

$$F\left[A\left(x\right)\right]=\frac{1}{\left(N_d-1\right)N_cV}\sum_x\sum_{i=0}^{N_d-1}Tr\left[\left(ag_0A_i\left(x+\frac{1}{2}a\hat{i}\right)\right)^2\right] \tag{2.144}$$

which is done using a Fourier accelerated conjugate gradient algorithm [61]. This algorithm iteratively produces a gauge transformation matrix, $g^{(n)}\left(x\right)$, such that the gauge is transformed as

$$g^{(n)}\left(x\right)=e^{-\alpha a\Delta_i ag_0A_i^n(x)} \tag{2.145}$$

$$U_i^{(n+1)}\left(x+\frac{1}{2}a\hat{i}\right)=g^{(n)}\left(x\right)U_i^{(n)}\left(x+\frac{1}{2}a\hat{i}\right)g^{\dagger(n)}\left(x+a\hat{i}\right) \tag{2.146}$$

where α is a tuning parameter, chosen to be 0.1 for Coulomb gauge fixing. This procedure s performed iteratively, until after N iterations the criteria $F\left[A\left(x\right)\right]<\theta$, for some θ chosen to be small, is met.

This procedure minimizes $g_0A_i^n\left(x\right)$ while retaining the gauge invariance of the action, and so the gauge is transformed as in (2.146) with $g^{(N)}\left(x\right)$ and can be used for wall sources.

If eigenvectors are being used to deflate solved with a fixed gauge, but have been generated on the unfixed gauge, then the gauge transformation matrix must also be applied to them

$$\lambda_i\rightarrow g^{(N)}\left(x\right)\lambda_i \tag{2.147}$$

in order to achieve the same speed-up in inversion.

2.4.1 Stochastic Sources

The spacetime distribution of a source may also be treated stochastically, which decreases the effects of local fluctuations in the gauge fields. This is important for constructing lattice propagators of the form $S\left(x,x\right)$, which may be needed to calculate a disconnected diagram or a single-propagator trace contribution to a correlation function. To create the propagators we depend on N stochastic source

that fulfill the properties

$$\begin{aligned} \lim_{N\to\infty} \frac{1}{N} \sum_{i=1}^{N} \kappa_i(x) = 0, \\ \lim_{N\to\infty} \frac{1}{N} \sum_{i=1}^{N} \kappa_i(x)\, \kappa_i^{\dagger}(y) = \delta_{xy}. \end{aligned} \tag{2.148}$$

One appropriate choice is the Z_2 source [41], where each element is randomly chosen from

$$Z_2 \otimes Z_2 = \left\{ \frac{1}{\sqrt{2}} (\pm 1 \pm i) \right\}. \tag{2.149}$$

Using these as a fermion field source, we can solve

$$D^{-1}(x,y)\, \kappa_i(y) = \psi_i(x), \tag{2.150}$$

and create N propagators that have the form

$$S_i(x,x) = \psi_i(x)\, \kappa_i^{\dagger}(x). \tag{2.151}$$

We can see, by right-multiplying Equation (2.150) with $\kappa_i^{\dagger}$, that

$$\lim_{N\to\infty} \sum_{i=1}^{N} S_i(x,x) = D^{-1}(x,x). \tag{2.152}$$

It is expected that the statistical error introduced from using stochastic sources scales as $\frac{1}{\sqrt{N}}$. This Z_2 noise structure was used in our investigation of A2A propagators, with the spatial components being given by Z_2 noise with spin-color-time dilution. For the 48^3 gauge ensemble the high mode noise in Equation (2.116) was given by

$$\eta_i(x)_{ab}^{\alpha\beta} = \kappa_{Z_2}(\vec{x})\, \delta_{t,t_i} \delta_{\alpha\beta} \delta_{ab}, \tag{2.153}$$

for a total of $N = 96 \times 12 = 1152$ high modes.

Each stochastic source here covers the the full volume but we can also create "sparse sources" to improve the $\frac{1}{\sqrt{N}}$ scaling of the statistical error. In d-dimensional spacetime we we create $N = n^d$ sparse sources where

$$\kappa_{sparse}(x) = \begin{cases} \kappa_{Z_2}(x) : x_\mu \bmod n = 0, \quad \mu = 0,1,2,3 \\ 0 : \text{otherwise} \end{cases} \tag{2.154}$$

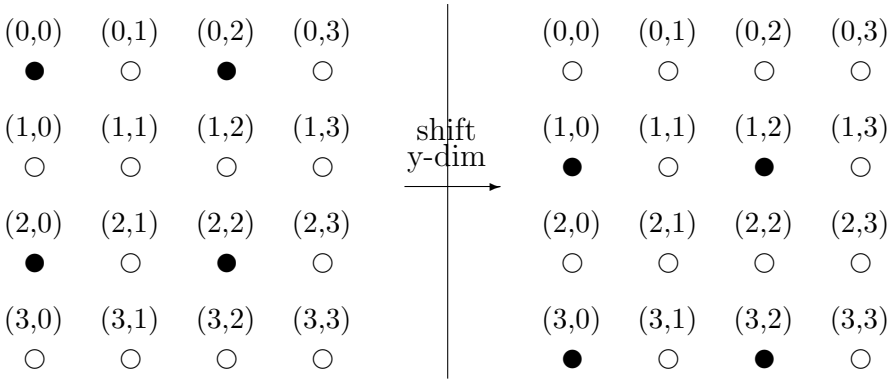

Figure 2.1 *An example of sparse noises for $d = 2$, $n = 2$. The filled circles represent a site with Z_2 noise, the empty circles represent a site that has been set to zero. Two further shifts are needed to cover the full volume, giving $2^2 = 4$ sparse sources.*

for the first source and we shift in each dimension to ensure that the N sources cover the entire volume with no overlap when combined, see Figure (2.1) for a $d = 2$, $n = 2$ example. When investigating rare kaon decays we use $N = 2^4 = 16$ sparse sources for each hit of a propagator, $S(x, x)$ that we compute.

2.4.2 Sequential Sources

For the study of rare kaon decays we will be interested in correlators that have a vector current inserted between two meson interpolators. The simplest of these correlators is the 3-point function

$$C^{\mu}_{J,\pi^+}(t_\pi, t_J, t, \vec{p_1}, \vec{p_2}) = \sum_z \left\langle \tilde{\phi}_{\pi^+}(t, \vec{p_2})\, J^{\mu}(t_J, \vec{z})\, \tilde{\phi}^{\dagger}_{\pi^+}(t_\pi, \vec{p_1}) \right\rangle e^{-i\vec{q}\cdot\vec{z}}, \tag{2.155}$$

where $q = p_1 - p_2$ and J^μ is the conserved vector current, as described in Section (2.1.5). These correlators can be constructed using a sequential source [76], which is given by

$$\Sigma_\mu(z, y) = J_\mu(t_J, z)\, S(z, y)\, e^{-i\vec{q}\cdot\vec{z}}. \tag{2.156}$$

Using this source in a Dirac operator matrix problem gives

$$D^{-1}(x, z)\, \Sigma_\mu(z, y) = S_\sigma(x, y) \tag{2.157}$$

which gives the propagator

$$S_{\Sigma}(x,y) = \sum_{z} S(x,y)\, J_{\mu}(t_J, z)\, S(z,x)\, e^{-i\vec{q}\cdot\vec{z}}. \tag{2.158}$$

When working with 5 dimensional Dirac actions that have conserved currents that depend on the fifth dimension it is important to include this dimension in the sequential source. This is done by introducing the "surface-to-bulk" propagator [36]

$$S_{SB}(x,s;y) = \left\langle \Psi(x,s)\, \overline{\psi}(y) \right\rangle, \tag{2.159}$$

and defining the 5-dimensional sequential sources as

$$\Sigma^{5}_{\mu}(z,y) = J_{\mu}(t_J, z)\, S_{SB}(z,s;y)\, e^{-i\vec{q}\cdot\vec{z}}. \tag{2.160}$$

Using this source in a Dirac operator matrix problem returns a 5-dimensional propagator, which must be converted to the physical 4-dimensional, using Equation (2.135).

The γ_5 hermiticity of the sequential propagator for a general operator $\mathcal{O}$ has the property

$$S_{\Sigma}(x,y,\mathcal{O}) = \gamma_5 S^{\dagger}_{\Sigma}\left(x,y,\mathcal{O}^{\dagger}\right)\gamma_5. \tag{2.161}$$

In the case of the vector current this means

$$S_{\Sigma}(x,y) = -\gamma_5 S^{\dagger}_{\Sigma_{\mu}}(x,y)\,\gamma_5. \tag{2.162}$$

Chapter 3

The Rare Kaon Decay $K \to \pi\ell^+\ell^-$

3.1 Phenomenology of the $K \to \pi\ell^+\ell^-$ decay

The $K \to \pi\ell^+\ell^-$ ($\ell = e, \mu$) decays are flavor changing neutral current (FCNC) processes that are suppressed in the standard model (SM) from which insights into new physics (NP) may be gleaned. This process is dominated by a single virtual-photon exchange ($K \to \pi\gamma^*$), whose amplitude is predominantly described by long-distance, non-perturbative physics. The branching rations for these decays, taken from the latest PDG average [92], are $\mathrm{Br}\left[K^+ \to \pi^+e^+e^-\right] = (3.00 \pm 0.09) \times 10^{-7}$ and $\mathrm{Br}\left[K^+ \to \pi^+\mu^+\mu^-\right] = (9.4 \pm 0.6) \times 10^{-8}$. With tensions between the measurement of the R_K ratio from LHCb and SM predictions [2] creating increased interest in lepton-flavor universality violations (LFUV), these equivalent rare kaon decays could also be suitable candidates to study LFU in the kaon sector.

The relevant long-distance Minkowski amplitude for the $j = +, S$ decays are [39]

$$\mathcal{A}_\mu^j = \int d^4x, \left\langle \pi^j\left(\vec{p}\right) \middle| T\left[J_\mu\left(0\right) H_W^{\Delta S=1}\left(x\right)\right] \middle| K^j\left(\vec{k}\right) \right\rangle, \tag{3.1}$$

where $z = q^2/M_K^2$, $q = k - p$, and k and p indicate the momenta of the K and π respectively. Here J_μ is the conserved current operator and $H_W^{\Delta S=1}$ is an effective weak Hamiltonian.

The contraction of this amplitude is performed using the Fermi effective theory, for which the weak bosons have been integrated out. This process allows us to separate the long-distance, hadron contributions, which we seek to study on the

lattice, from the short-distance contributions, which can be investigated using perturbation theory. The short-distance dominated processes that contribute to the full amplitude of the decay are described by local $\Delta S = 1$ operators that are also involved in $K^+\pi^0\ell^+\nu$ ($K_{\ell 3}$) decays, that are known accurately from experiment and previous lattice results [4, 78].

In Section (3.1.1) the relevant effective weak Hamiltonian will be presented with a discussion on how it will be applied to the $K \to \pi\ell^+\ell^-$ decay. Section (3.1.2) will introduce the electromagnetic form factor that we seek to extract from the amplitude that we calculate on the lattice, with experimental and theoretical predictions for this form factor presented for comparison.

3.1.1 The $\Delta S = 1$ Weak Hamiltonian

The $K \to \pi\ell^+\ell^-$ decay requires an effective weak Hamiltonian to describe the four-quark interaction that results in a $s \to d$ transition. This $\Delta S = 1$ weak Hamiltonian is given by [28]

$$H_W^{\Delta S=1} = \frac{G_F}{\sqrt{2}} V_{us}^* V_{ud} \left(\sum_{i=1}^{2} C_i(\mu) \left(Q_i^u(\mu) - Q_i^c(\mu) \right) + \sum_{i=3}^{10} C_i(\mu) Q_i(\mu) \right). \quad (3.2)$$

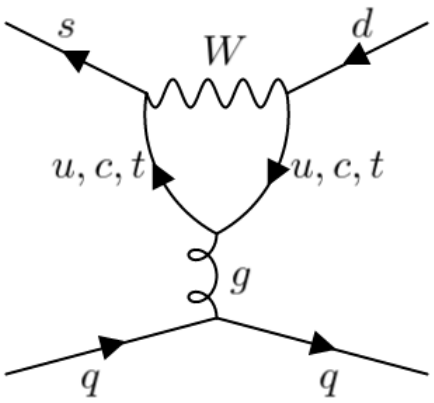

Figure 3.1 *The diagram from which the operators $Q_{3,\ldots,6}$ originate.*

As we wish to consider the four-flavor theory the renormalization scale is taken to be $m_c < \mu < m_b$. The operators of $H_W^{\Delta S=1}$ are [28]

$$Q_1^q = \left(\bar{s}_i \gamma^{L,\mu} q_j\right) \left(\bar{q}_j \gamma_\mu^L d_i\right), \tag{3.3}$$

$$Q_2^q = \left(\bar{s}_i \gamma^{L,\mu} q_i\right) \left(\bar{q}_j \gamma_\mu^L d_j\right), \tag{3.4}$$

$$Q_3 = \left(\bar{s}_i \gamma^{L,\mu} d_i\right) \sum_q \left(\bar{q}_j \gamma_\mu^L q_j\right), \tag{3.5}$$

$$Q_4 = \left(\bar{s}_i \gamma^{L,\mu} d_j\right) \sum_q \left(\bar{q}_j \gamma_\mu^L q_i\right), \tag{3.6}$$

$$Q_5 = \left(\bar{s}_i \gamma^{L,\mu} d_i\right) \sum_q \left(\bar{q}_j \gamma_\mu^R q_j\right), \tag{3.7}$$

$$Q_6 = \left(\bar{s}_i \gamma^{L,\mu} d_j\right) \sum_q \left(\bar{q}_j \gamma_\mu^R q_i\right), \tag{3.8}$$

$$Q_7 = \frac{3}{2} \left(\bar{s}_i \gamma^{L,\mu} d_i\right) \sum_q e_q \left(\bar{q}_j \gamma_\mu^R q_j\right), \tag{3.9}$$

$$Q_8 = \frac{3}{2} \left(\bar{s}_i \gamma^{L,\mu} d_j\right) \sum_q e_q \left(\bar{q}_j \gamma_\mu^R q_i\right), \tag{3.10}$$

$$Q_9 = \frac{3}{2} \left(\bar{s}_i \gamma^{L,\mu} d_i\right) \sum_q e_q \left(\bar{q}_j \gamma_\mu^L q_j\right), \tag{3.11}$$

$$Q_{10} = \frac{3}{2} \left(\bar{s}_i \gamma^{L,\mu} d_j\right) \sum_q e_q \left(\bar{q}_j \gamma_\mu^L q_i\right). \tag{3.12}$$

where $\gamma_\mu^{L/R} = \gamma_\mu \left(1 \pm \gamma_5\right)$, e_q are quark charges, and i, j are summed color indices. For $Q_{1,2}^q$ the quark is $q = u, c$ whereas for the remaining operators $Q_{3,\ldots,10}$ the quark q runs over all active quark flavors.

The $Q_{1,2}^q$ operators are the result of the current-current diagrams in Figure

(1.4). The $Q_{3,\ldots,6}$ operators are the result of QCD-penguin diagrams, as shown in Figure (3.1), and the $Q_{7,\ldots,10}$ operators come from electroweak-penguin diagrams, as shown in Figure (3.2).
The Wilson coefficients for these operators have been calculated in the $\overline{MS}$ scheme at two-loop order in [29] and regularization-independent symmetric momentum-subtraction (RI/SMOM) schemes for the operators have been defined in [71] along with one-loop matching factors to the $\overline{MS}$ scheme in naive dimensional regularization. In order to run the Wilson coefficients down to the four-flavor theory it is convenient to express them in terms of 10-dimensional vectors

$$\vec{C}\,(\mu) = \vec{z}\,(\mu) + \tau\vec{y}\,(\mu)\,, \tag{3.13}$$

where [92]

$$\tau = -\frac{\lambda_t}{\lambda_u}, \quad |\tau| \simeq 1.3 \times 10^{-3} \tag{3.14}$$

is the ratio of CKM matrix elements, $\lambda_q = V_{qd}V_{qs}^*$. The $\vec{y}\,(\mu)$ vector, containing up, charm, and top quark contributions, can be written as

$$\vec{y}\,(\mu) = \vec{v}\,(\mu) - \vec{z}\,(\mu) \tag{3.15}$$

where $\vec{z}\,(\mu)$ contains only up and charm quark contributions. Running the Wilson coefficients down to the four-flavor theory thus requires taking

$$\vec{v}^{\,4}\,(\mu) = U^4\,(m_c, m_b, \mu)\,M\,(m_b)\,U^5\,(m_b, m_W, \mu)\,\vec{v}\,(m_W)\,, \tag{3.16}$$

where the superscripts indicate the number of active quarks, $U^f\,(m_1, m_2, \mu)$ are the evolution matrices, and $M\,(m_b)$ is the quark threshold matching matrix.

In the four flavor theory we see that the Wilson coefficients for the $Q_{1,2}^q$ operators are significantly larger than the Wilson coefficients for the $Q_{3,\ldots,10}$ operators. For the QCD- and photon-penguin diagrams this is due to a logarithmic GIM mechanism that occurs occurs when computing the Wilson coefficients. Due to the logarithm the heavier quark mass enhancement is diminished, and are thus comparable to the light quark contributions. The top quark contributions are also suppressed by CKM matrix elements. For the Z-penguin diagram there is a quadratic GIM mechanism, as well as top quark contributions that are enhanced due to compared to the lighter quarks. However the weak coupling of the Z boson suppresses these contributions. The study of rare kaon decays with four quark flavors can then be confined to the Q_1^q and Q_2^q operators.

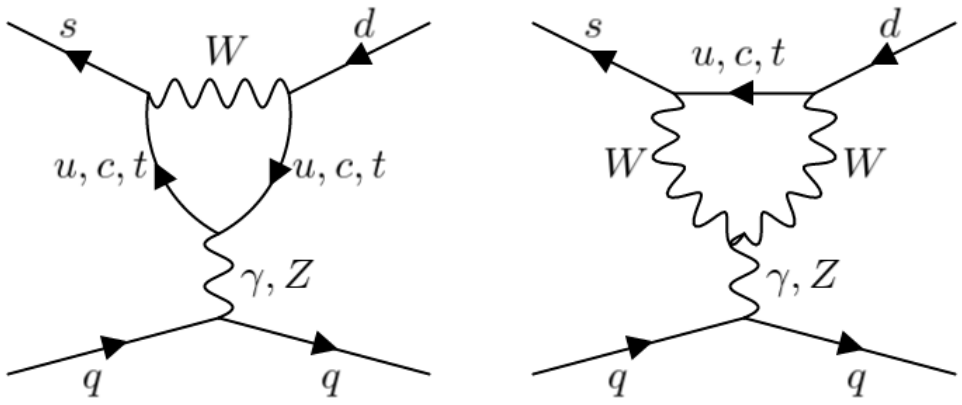

(a) (b)

Figure 3.2 *The diagrams from which the operators $Q_{7,\ldots,10}$ originate.*

There are additional short distance processes that can contribute to the $K \to \pi\ell^+\ell^-$ Hamiltonian that should be considered. For example the penguin diagrams in Figure (3.3) contribute to the $K_L \to \pi^0\ell^+\ell^-$ decay and are described by the operators [28]

$$Q_{7V} = \left(\bar{s}_i\gamma^{L,\mu}d_i\right)\sum_q e_q\left(\bar{q}_j\gamma_\mu q_j\right), \tag{3.17}$$

$$Q_{7A} = \left(\bar{s}_i\gamma^{L,\mu}d_i\right)\sum_q e_q\left(\bar{q}_j\gamma_\mu\gamma_5 q_i\right). \tag{3.18}$$

This contribution is, again suppressed by the GIM mechanism and CKM suppression for the top quark contribution. The effective weak Hamiltonian we use for our four-flavor study of the $K \to \pi\ell^+\ell^-$ is

$$H_W = \frac{G_F}{\sqrt{2}}V_{us}^*V_{ud}\sum_{i=1}^{2}C_i\left(\mu\right)\left(Q_i^u\left(\mu\right) - Q_i^c\left(\mu\right)\right). \tag{3.19}$$

In the three-flavor theory we would not be able to take advantage of the GIM suppression and so several other operators would still have to be considered. The effective weak Hamiltonian in such a case is

$$H_W^3 = \frac{G_F}{\sqrt{2}}V_{us}^*V_{ud}\left(\sum_{i=1}^{2}C_i\left(\mu\right)Q_i^u\left(\mu\right) + \sum_{i=3}^{6}C_i\left(\mu\right)Q_i\left(\mu\right) + C_{7V}\left(\mu\right)Q_{7V}\left(\mu\right)\right). \tag{3.20}$$

An extensive description of this effective weak Hamiltonian is given in [69].

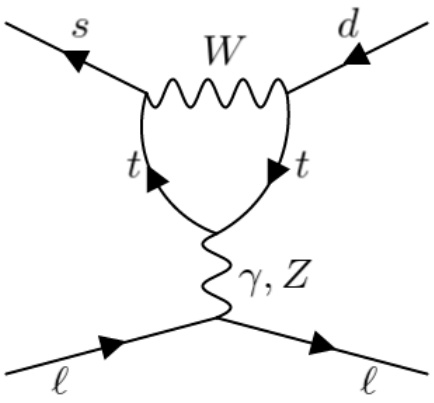

Figure 3.3 *The diagram from which the operators Q_{7A} and Q_{7V} originate.*

3.1.2 Form Factor

The amplitude in Equation (3.1) can be written in terms of the form factor $V^i(z)$ as [39, 47]

$$\mathcal{A}^j = -iG_F \frac{V^i(z)}{(4\pi)^2} \left(q^2 (k+p)_\mu - \left(M_K^2 - M_\pi^2 \right) q_\mu \right). \tag{3.21}$$

This form factor has been analyzed in χPT [39] and can parameterized as

$$V_i(z) = a_i + b_i z + V_i^{\pi\pi}(z), \tag{3.22}$$

where a_i and b_i are free real parameters and $V^{\pi\pi}(z)$ describes the contribution from a $\pi\pi\pi$ intermediate state with a $\pi^+\pi^- \to \gamma^*$ transition. A detailed description of $V^{\pi\pi}(z)$ is given in [39] and the free parameters have, until recently, only been obtained by fitting experimental data. Having previously measured the K^+ decay channel for electrons and muons at the NA48 experiment at the CERN SPS [11], the follow-up NA62 experiment made measurements of the $K^+ \to \pi^+\mu^+\mu^-$ decay during the 2016-2018 Run 1 [17], with prospects for further measurements during the 2021-2024 Run 2 [70]. From the NA48 data the free parameters have been determined to be $a_+ = -0.578 \pm 0.016$ and $b_+ = -0.779 \pm 0.066$ for the electron [11], and from the available NA62 data values of $a_+ = -0.592 \pm 0.015$ and $b_+ = 0.699 \pm 0.058$ have been obtained for the muon [17].

In parallel there is work being done to improve the theoretical understanding of these processes. The authors of [43, 44] have constructed a theoretical prediction

of a_+ and b_+ by considering a two-loop, low energy, expansion of the form factor in three flavor QCD, with a phenomenological determination of quantities that are unknown at vanishing momentum transfer. For the electron and muon they find $a_+ = -1.59 \pm 0.08$ and $b_+ = -0.82 \pm 0.06$.

The non-perturbative ab initio approach of lattice QCD is well suited to study the dominant long-distance contribution to the matrix element of the $K \to \pi\gamma^*$ decay and obtaining a lattice prediction for a and b by investigating the $K \to \pi\gamma^* \to \pi\ell^+\ell^-$ decay will complement the experimental and theoretical results. Methods with which such a lattice calculation could be performed were first proposed in [62] and additional details of how the $K \to \pi\ell^+\ell^-$ matrix elements could be extracted using renormalized operators, in order to have full control of ultraviolet divergences, were introduced in [36]. Following these an exploratory lattice calculation was performed in [34], using unphysical masses, in order to demonstrate how the results in [36, 62] could be applied. This calculation led to predictions of $a_+ = 1.6 \pm 0.7$ and $b_+ = 0.7 \pm 0.8$ for the free parameters.

For the K_S decays the dilepton invariant-mass spectra are unavailable, due to the low number of observations of the decay in experiment. By assuming vector meson dominance, i.e. that

$$\frac{a_S}{b_S} = \frac{1}{r_V^2}, \quad r_V = \frac{M_\rho}{M_K}, \tag{3.23}$$

the magnitude of a_S has been estimated to be $|a_S| = 1.06^{+0.26}_{-0.21}$ for the electron and $|a_S| = 1.54^{+0.40}_{-0.32}$ for the muon [39].

3.2 $K \to \pi\ell^+\ell^-$ on the Lattice

In order to study the rare kaon decays discussed in Section 3.1 on the lattice we must relate the amplitudes of the decays in Euclidean space to 4-point correlation functions that we can compute. In practice this means that we calculate the single photon exchange amplitude of the $K^+ \to \pi^+\gamma^*$ decay, in place of the $K^+ \to \pi^+\ell^+\ell^-$ amplitude on the lattice.
The correlators needed for the lattice study, made of bilocal operators inserted between meson states, will be presented in Section (3.2.1) with the Euclidean formulation given in Section (3.2.2). A description of these correlators on a discrete, finite volume, lattice is given in Section (3.2.3) along with a description of the unphysical intermediate states that the Euclidean formulation introduces. Finally in Section (3.2.4) the renormalization of the lattice operator will be discussed.

3.2.1 Operators and Correlators

For the $K^+ \to \pi^+\gamma^*$ decay the long-distance amplitude we wish to compute is given in Equation (3.1). In this expression the the electromagnetic current operator is given by the standard flavor-diagonal operator

$$J_\mu = \frac{1}{3}\left(2V_\mu^u - V_\mu^d - V_\mu^s + 2V_\mu^c\right), \tag{3.24}$$

where V_μ^q id the local or conserved vector current, as described in Section (2.1.5), for quark q. The weak Hamiltonian operator that we use for our calculation is

$$H_W = \sum_{i=1}^{2} C_i \left(Q_i^u - Q_i^c\right), \tag{3.25}$$

a repetition of the operator given in Equation (3.19) with the prefactor $G_F V_{us}^* V_{ud}/\sqrt{2}$ excluded for simplicity, as it can be reintroduced at a later stage. It is useful to consider the 3-point function given by the weak Hamiltonian operator inserted between pion and kaon interpolators

$$\Gamma_H^{(3)}\left(t_H, \vec{p}\right) = \int d^3\vec{x} \left\langle \phi_\pi\left(t_{\pi,\vec{p}}\right) H_W\left(t_H, \vec{x}\right) \phi^\dagger\left(t_H, \vec{p}\right)\right\rangle, \tag{3.26}$$

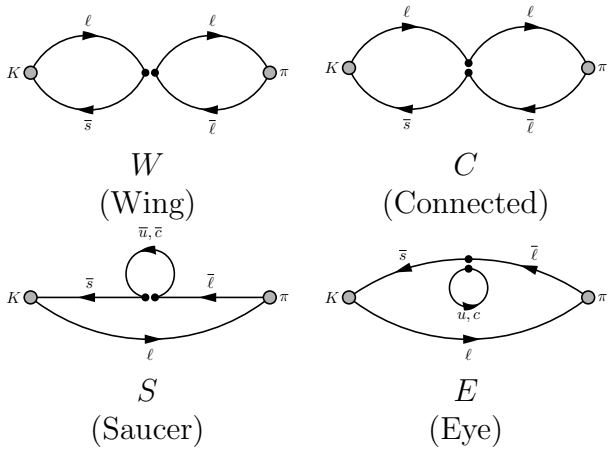

Figure 3.4 *The four classes of diagrams obtained after performing the Wick contractions of the charged pion and kaon interpolating operators with the H_W operator. ℓ denotes a light (u or d) quark propagator. The two black circles represent the currents in the four-quark operators $Q^q_{1,2}$ defined in (3.25). The Connected and Eye diagrams contain an insertion of Q^q_1 and the Wing and Saucer diagrams contain an insertion of Q^q_2.*

where $t_k < t_H < t_\pi$. The four classes of diagrams that are obtained from the resulting Wick contractions are shown in Figure (3.4). These diagrams primarily serve as the foundation on which the 4-point functions are built upon, but in our analysis we are also interested in extracting the weak Hamiltonian matrix elements from these 3-point functions. Using the same procedure as outlined in Section (2.2.3) we can see that for $t_k \ll t_H \ll t_\pi$ $\Gamma^{(3)}_H(t_H, \vec{p})$ has the following behavior

$$\Gamma^{(3)}_H(t_H, \vec{p}) = \frac{Z_\pi(\vec{p})\, Z_K(\vec{p})\, \mathcal{M}_H(\vec{p})}{4E_\pi(\vec{p})\, E_K(\vec{p})} e^{-E_\pi(\vec{p})t_\pi} e^{-[E_K(\vec{p})-E_\pi(\vec{p})]t_H}, \tag{3.27}$$

where $\mathcal{M}_H(\vec{p}) = \langle \pi(\vec{p}) | H_W(0) | K(\vec{p}) \rangle$ is the matrix element we wish to fit for.

In our analysis we are also interested in the 3-point function of the electromagnetic current

$$\Gamma^{(3),P}_{J_\mu}\left(t, t_J, \vec{p}, \vec{k}\right) = \int d^3\vec{x} e^{-i\vec{q}\cdot\vec{x}} \left\langle \phi_P(t, \vec{p})\, J_\mu(t_J, \vec{x})\, \phi^\dagger_P\left(0, \vec{k}\right) \right\rangle, \tag{3.28}$$

where $P = \pi, K$ denotes the pseudoscalar meson. For $0 \ll t_J \ll t$ $\Gamma^{(3),P}_{J_\mu}$ has the following behavior

$$\Gamma^{(3),P}_{J_\mu}(t, t_J, \vec{p}, \vec{k}) = \frac{Z_P(\vec{p})\, Z_P\left(\vec{k}\right) \mathcal{M}^P_{J_\mu}\left(\vec{p}, \vec{k}\right)}{4E_P(\vec{p})\, E_P\left(\vec{k}\right)} e^{-(t-t_J)E_P\left(\vec{k}\right)} e^{-t_J E_P(\vec{p})}, \tag{3.29}$$

where $\mathcal{M}^P_{J_\mu}\left(\vec{p},\vec{k}\right) = \left\langle P(E_P(\vec{p}),\vec{p})\right| J_\mu(0) \left|P\left(E_P\left(\vec{k}\right),\vec{k}\right)\right\rangle$.

3.2.2 Euclidean Rare Kaon Decay Amplitude

To construct the 4-point correlators that we need, the conserved current is inserted on each of the quark legs in the four classes of diagrams in Figure (3.4), along with a disconnected self-contracted current contribution, resulting in 20 total diagrams to be completed. Examples of the resulting diagrams are given for the "Connected" class in Figure (3.5). The combination of all these diagrams make up the 4-point correlation function

$$\Gamma^{(4)}_\mu\left(t_H,t_J,\vec{k},\vec{p}\right) = \int d^3\vec{x}\int d^3\vec{y}\left\langle \phi_\pi\left(t_\pi\vec{p}\right) T\left[J_\mu\left(t_J,\vec{x}\right) H_W\left(t_H,\vec{y}\right)\right]\phi^\dagger_K\left(0,\vec{k}\right)\right\rangle, \tag{3.30}$$

where $0 < t_J, t_H < t_\pi$. In order to compute the final amplitude without including source/sink factors and normalizations that should not contribute, it is convenient to define the factor

$$Z_{K\pi} = \frac{Z_\pi\left(\vec{p}\right) Z^\dagger_K\left(\vec{k}\right) L^3}{4E_\pi\left(\vec{p}\right) E_K\left(\vec{k}\right)} e^{-E_{\pi(\vec{p})}t_\pi}, \tag{3.31}$$

and use this to define the "reduced" correlator

$$\tilde{\Gamma}^{(4)}_\mu = \frac{\Gamma^{(4)}_\mu}{Z_{K\pi}}. \tag{3.32}$$

Obtaining the amplitude requires us to integrate this reduced 4-point correlator as

$$I_\mu\left(T_a,T_b,\vec{k},\vec{p}\right) = e^{-\left[E_\pi(\vec{p})-E_K\left(\vec{k}\right)\right]t_J}\int_{t_J-T_a}^{t_J+T_b} dt_H \tilde{\Gamma}^{(4)}_\mu\left(t_H,t_J,\vec{k},\vec{p}\right), \tag{3.33}$$

in the limit $T_a, T_b \to \infty$. The exponential factor in front of the integral allows us to omit any t_J dependence on the decay by translating to $t_J = 0$.

The spectral decomposition of the unintegrated 4-point correlator can be written as

$$\tilde{\Gamma}^{(4)}_\mu\left(t_H,\vec{k},\vec{p}\right) = \begin{cases} \int_0^\infty dE \frac{\rho(E)}{2E}\left\langle \pi\left(\vec{p}\right)\right| J_\mu\left|E,\vec{k}\right\rangle\left\langle E,\vec{k}\right| H_W\left|K\left(\vec{k}\right)\right\rangle e^{-\left(E_K\left(\vec{k}\right)-E\right)t_H}, & t_H < 0, \\ \int_0^\infty dE \frac{\rho_S(E)}{2E}\left\langle \pi\left(\vec{p}\right)\right| H_W\left|E,\vec{p}\right\rangle\left\langle E,\vec{p}\right| J_\mu\left|K\left(\vec{k}\right)\right\rangle e^{-(E-E_\pi(\vec{p}))t_H}, & t_H > 0, \end{cases} \tag{3.34}$$

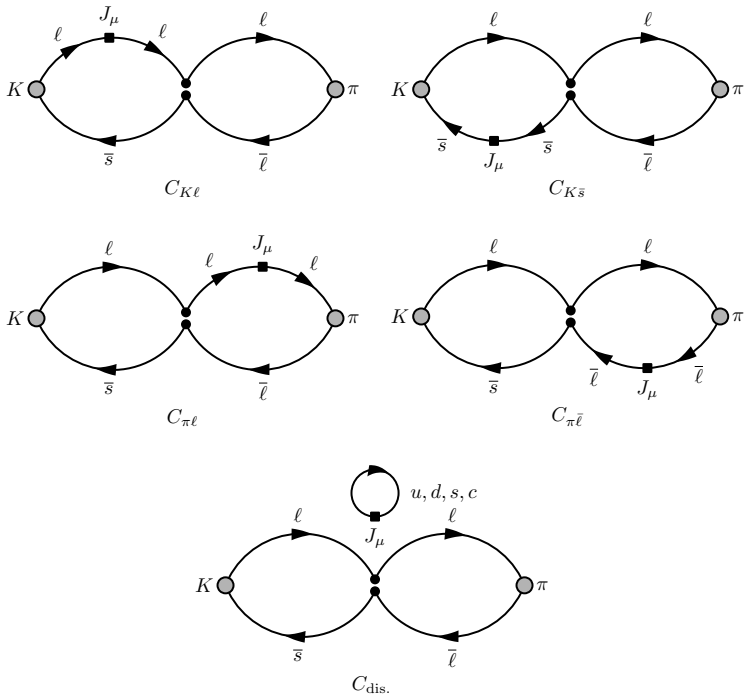

Figure 3.5 *The five possible current insertions for the C class of diagrams, contributing to the rare kaon decay correlator (3.30). The diagramtic conventions are the same as in Fig. 3.4*

where $\rho(E)$ and $\rho_S(E)$ are spectral density functions that select states with strangeness $s = 0$ and $s = 1$ respectively. The integral in Equation (3.33) can thus be written as

$$I_\mu\left(T_a, T_b, \vec{k}, \vec{p}\right) = -\int_0^\infty dE \frac{\rho(E)}{2E} \frac{\left\langle \pi(\vec{p}) \right| J_\mu \left| E, \vec{k} \right\rangle \left\langle E, \vec{k} \right| H_W \left| K\left(\vec{k}\right) \right\rangle}{E_K\left(\vec{k}\right) - E} \left(1 - e^{\left(E_K\left(\vec{k}\right) - E\right)T_a}\right)$$
$$+ \int_0^\infty dE \frac{\rho_S(E)}{2E} \frac{\left\langle \pi(\vec{p}) \right| H_W \left| E, \vec{p} \right\rangle \left\langle E, \vec{p} \right| J_\mu \left| K\left(\vec{k}\right) \right\rangle}{E - E_\pi(\vec{p})} \left(1 - e^{-(E - E_\pi(\vec{p}))T_b}\right). \tag{3.35}$$

The states $\left|E, \vec{k}\right\rangle$, in the $\rho(E)$ term of the integral, have strangeness $S = 0$, and so have the quantum numbers of a pion. For physical pion and kaon masses there are three intermediate states that could exists with $E < E_K\left(\vec{k}\right)$ which would cause the exponential T_a term to diverge, namely the π, $\pi\pi$, and $\pi\pi\pi$ states. For the $\rho_S(E)$ term the states $|E, \vec{p}\rangle$ have the quantum numbers of the kaon. Thus all the states will have $E > E_{\pi(\vec{p})}$ and this term of the integral converges to the appropriate value for $0 \ll T_b$.

The rare kaon decay amplitude is given by the constant terms in the integral in

Equation (3.35), i.e. the terms that have no T_a or T_b dependence. Extracting this amplitude requires the subtraction of the exponentially growing terms related to T_a. If we define $\tilde{I}_\mu\left(T_a, T_b, \vec{k}, \vec{p}\right)$ to be the integrated 4-point function where this subtraction has been performed the the Minkowski amplitude for the $K^+ \to \pi^+\gamma^*$ decay is given by

$$\mathcal{A}_\mu\left(q^2\right) = -i\frac{G_F}{\sqrt{2}}V_{us}^* V_{ud} \lim_{T_a, T_b \to \infty} \tilde{I}_\mu\left(T_a, T_b, \vec{k}, \vec{p}\right), \tag{3.36}$$

where we have reintroduced the $G_F/\sqrt{2}V_{us}^* V_{ud}$ prefactor that we dropped in Equation (3.25). From this we can use Equation (3.21) relate the form factor we wish to study to the integrated 4-point function as

$$V\left(z\right)\left(q^2\left(k+p\right)_\mu - \left(M_K^2 - M_\pi^2\right)q_\mu\right) = \frac{(4\pi)^2}{\sqrt{2}}V_{us}^* V_{ud} \lim_{T_a, T_b \to \infty} \tilde{I}_\mu\left(T_a, T_b, \vec{k}, \vec{p}\right). \tag{3.37}$$

3.2.3 Lattice Implementation

We now seek to express the correlators that described the rare kaon decay amplitude in a discrete, finite volume, fashion, such that they can be related to the lattice results we obtain. This involves using the fundamental concepts of discretization discussed in Section (2.1.1), primarily the replacement of the continuous integrals in Equations (3.33) and (3.35) with Riemann sums, along with the finite volume spectral density being given as $\rho\left(E\right) = \sum_n E_n \delta\left(E - E_n\right)$. It was first noted in [34] that the discretization of the exponential terms with T_a and T_b dependence, in Equation (3.35) should be considered with care. Instead of a simple summation of the exponential contributions we evaluate the sums that correspond to the integral of Equation (3.34) as a geometric series. To do so we first introduce the notation

$$\Delta_n^a = E_K\left(\vec{k}\right) - E_n, \quad \Delta_m^b = E_m - E_\pi\left(\vec{p}\right), \tag{3.38}$$

where n and m label the states contained in the finite volume spectral densities, $\rho\left(E\right)$ and $\rho_S\left(E\right)$ respectively, and a and b label the contributions associated with T_a and T_b respectively. The geometric series that we are interested in are given

by

$$a\sum_{t_H=-T_a}^{0} e^{-\Delta_n^a t_H} = a\frac{1+e^{a\Delta_n^a}\left(1-2e^{\Delta_n^a T_a}\right)}{2\left(1-e^{a\Delta_n^a}\right)}, \tag{3.39}$$

$$a\sum_{t_H=0}^{T_b} e^{-\Delta_m^b t_H} = a\frac{1+e^{-a\Delta_m^b}\left(1-2e^{-\Delta_m^b T_b}\right)}{2\left(1-e^{-a\Delta_m^b}\right)}. \tag{3.40}$$

The unphysical intermediate states are contained by the terms that depend in T_a and T_b in Equations (3.39) and (3.40) Expanding these terms in powers of the lattice spacing gives

$$-a\frac{e^{a\Delta_n^a}}{1-e^{a\Delta_n^a}}e^{\Delta_n^a T_a} = \left(1+\frac{a\Delta_n^a}{2}+\frac{\left(a\Delta_n^a\right)^2}{12}+\mathcal{O}\left(a^3\right)\right)\frac{e^{\Delta_n^a T_a}}{\Delta_n^a}, \tag{3.41}$$

$$-a\frac{e^{-a\Delta_m^b}}{1-e^{-a\Delta_m^b}}e^{-\Delta_m^b T_b} = \left(-1+\frac{a\Delta_m^b}{2}-\frac{\left(a\Delta_m^b\right)^2}{12}+\mathcal{O}\left(a^3\right)\right)\frac{e^{-\Delta_m^b T_b}}{\Delta_m^b}. \tag{3.42}$$

Here we can see that the continuum result is reproduced with $\mathcal{O}(a)$ discretization effects. A key observation from [34] is that neglecting these discretization effects results in an incorrect subtraction of the exponentially growing intermediate state contribution, and so the geometric series treatment of the integral reduces the systematic effect of discretization.

The integrated 4-point correlation function on a discrete, finite lattice is then given by

$$\begin{aligned} I_\mu\left(T_a,T_b,\vec{k},\vec{p}\right) = a\sum_n \frac{1}{2E_n}\frac{\mathcal{M}_\mu^{J,n\to\pi}\left(\vec{k},\vec{p}\right)\mathcal{M}_H^{K\to n}\left(\vec{k}\right)}{2\left(1-e^{a\Delta_n^a}\right)}\left[1+e^{a\Delta_n^a}\left(1-2e^{\Delta_n^a T_a}\right)\right]+ \\ a\sum_m \frac{1}{2E_m}\frac{\mathcal{M}_H^{\pi\to m}\left(\vec{p}\right)\mathcal{M}_\mu^{J,K\to m}\left(\vec{k},\vec{p}\right)}{2\left(1-e^{-a\Delta_m^b}\right)}\left[1+e^{-a\Delta_m^b}\left(1-2e^{-\Delta_m^b T_b}\right)\right], \end{aligned} \tag{3.43}$$

where $\mathcal{M}_H^{P_1\to P_2}\left(\vec{p}\right) = \left\langle P_2,\vec{p}\right| H_W \left|P_1,\vec{p}\right\rangle$ and $\mathcal{M}_\mu^{J,P_1\to P_2}\left(\vec{k},\vec{p}\right) = \left\langle P_2,\vec{p}\right| J_\mu \left|P_1,\vec{k}\right\rangle$ are equivalent to the 3-point matrix elements given in Equations (3.27) and (3.29) respectively. In this study we perform the calculation with approximately physical pion and kaon masses, satisfying $E_K\left(\vec{k}\right) < 3M_\pi$, and so we must consider the contributions of the single-, two-, and three-pion intermediate states.

Single-Pion Intermediate State: Explicit Subtraction

The unphysical term caused by the single-pion state in Equation (3.43) is given by

$$D_\mu^\pi\left(T_a,\vec{k},\vec{p}\right)=\frac{a}{2E_\pi\left(\vec{k}\right)}\frac{\mathcal{M}_\mu^{J,\pi\to\pi}\left(\vec{k},\vec{p}\right)\mathcal{M}_H^{K\to\pi}\left(\vec{k}\right)}{1-e^{-a\Delta_\pi^a}}e^{\Delta_\pi^a T_a}. \tag{3.44}$$

This term can either be fit from the integrated correlator or $D_\mu^\pi\left(T_a,\vec{k},\vec{p}\right)$ can be reconstructed using 2- and 3-point fit results of correlators discussed in Sections (2.2.3) and (3.2.1).

In practice we not only have to remove the exponential term that grows with T_a, but also the exponential term that shrinks with T_b. This term is an unphysical single-kaon contribution, which may not converge in our finite T_b range. We can treat the unphysical single-kaon state as we have the single-pion state, and express the integrated 4-point correlator as

$$\begin{aligned}I_\mu\left(T_a,T_b,\vec{k},\vec{p}\right)=&A_\mu\left(\vec{k},\vec{p}\right)+c_\mu^1\left(\vec{k},\vec{p}\right)e^{\Delta_\pi^a T_a}\left[\frac{\Delta_\pi^a}{1-e^{-\Delta_\pi^a}}\right]\\&+c_\mu^2\left(\vec{k},\vec{p}\right)e^{-\Delta_K^b T_b}\left[\frac{\Delta_K^b}{e^{\Delta_K^b}-1}\right],\end{aligned} \tag{3.45}$$

where A_μ is the amplitude we wish to extract, up to the factors given in Equation (3.36), and c_μ^1 and c_μ^2 can be written in terms of 3-point matrix elements and meson energies as

$$c_\mu^1\left(\vec{k},\vec{p}\right)=\frac{\mathcal{M}_\mu^{J,\pi}\left(\vec{k},\vec{p}\right)\mathcal{M}_H\left(\vec{k}\right)}{2E_\pi\left(\vec{k}\right)\Delta_\pi^a},\quad c_\mu^2\left(\vec{k},\vec{p}\right)=-\frac{\mathcal{M}_\mu^{J,K}\left(\vec{k},\vec{p}\right)\mathcal{M}_H\left(\vec{p}\right)}{2E_K\left(\vec{p}\right)\Delta_K^b}. \tag{3.46}$$

There are several approaches that can be taken to extract the amplitude using this strategy. The first is to simply fit the integrated correlator for A_μ, c_μ^1, and c_μ^2. We can also use a zero-momentum transfer approximation, and take $c_\mu^2=-c_\mu^1$, which is exactly true when $\vec{k}=\vec{p}$, and fit for A_μ and c_μ^1. Beyond this we can reconstruct c_μ^1 and c_μ^2 using results of 2- and 3-point fits. Typically the matrix element $\mathcal{M}_H\left(\vec{p}\right)$ is difficult to fit as the weak Hamiltonian 3-point function with non-zero momentum has a poor signal. This introduces a significant amount of statistical error to the reconstruction of c_μ^2. As a result an $SU\left(3\right)$ flavor symmetry approximation can be used, where we take $\mathcal{M}_H\left(\vec{k}\right)=\mathcal{M}_H\left(\vec{p}\right)$, which is exact when $M_\pi=M_K$. The proof of both of the approximations discussed here can be

found in the appendix of [34].

Single-Pion Intermediate State: Weak Hamiltonian Shift

A second method to remove the single-pion divergence is based on an additive shift to the weak Hamiltonian by the scalar density $\bar{s}d$ [8, 33] where a parameter $c_s(k)$ is chosen such that

$$\left\langle \pi\left(\vec{k}\right)\right| H'_W \left|K\left(\vec{k}\right)\right\rangle = \left\langle \pi\left(\vec{k}\right)\right| H_W - c_s\bar{s}d \left|K\left(\vec{k}\right)\right\rangle = 0. \tag{3.47}$$

By replacing H_w with H'_w in Equation (3.43) the divergent contribution from the single-pion state is removed. This shift does not change the amplitude, as was shown in [36] using the vector Ward identity

$$i(m_s - m_d)\bar{s}d = \partial_\mu V_\mu^{\bar{s}d}. \tag{3.48}$$

The c_s parameter can be extracted from the the ratio of 3-point functions

$$c_s\left(\vec{k}\right) = \frac{\Gamma^{(3)}_{H_W}\left(\vec{k}\right)}{\Gamma^{(3)}_{\bar{s}d}\left(\vec{k}\right)}, \tag{3.49}$$

by fitting the region $t_K \ll t_\mathcal{O} \ll t_\pi$, for $\mathcal{O} = H_w, \bar{s}d$. Similarly c_s can be obtained by fitting ratios of the equivalent 4-point functions, when $t_K \ll t_\mathcal{O} \ll t_J$.

Two- and Three-Pion States

In principle the two-pion intermediate state can contribute to the exponentially growing unphysical term, with the matrix elements of the contributions being given by

$$\mathcal{M}^{\pi\pi}_H = \langle \pi(p_1)\,\pi(p_2)|\, H_W\, |K(p_3)\rangle \tag{3.50}$$

$$\mathcal{M}^{\pi\pi}_{V_\mu} = \langle \pi(p_1)|\, V_\mu\, |\pi(p_2)\,\pi(p_3)\rangle\,. \tag{3.51}$$

In the continuum the vector current matrix element has the following for factor decomposition

$$\mathcal{M}^{\pi\pi}_{V_\mu} = \epsilon_{\mu\nu\rho\sigma} p_1^\nu p_2^\rho p_3^\sigma F(s,t,u)\,, \tag{3.52}$$

where $s = (p_1 + p_2)^2$, $t = (p_1 - p_3)^2$, and $u = (p_2 - p_3)^2$ are Mandelstam variables. As a result of four-momentum conservation p_1 is a linear combination of p_2 and p_3, and so the vector current contribution vanishes once the Levi-Civita contraction is performed. On the lattice, cubic symmetry allows for the same vanishing behavior, with lattice artifact corrections that shrink as $a \to 0$. Previous lattice studies of the $K_L - K_S$ mass difference with $a^{-1} = 1.73\text{GeV}$ and unphysical pion and kaon masses have found that the on-shell two-pion contributions are just a few per-cent and that the artifacts are of $O(3\%)$ of these [8, 32]. The calculation that was performed for this thesis has the same inverse lattice spacing, though with physical pion and kaon masses and a larger volume than theses ΔM_K studies. As such we do not expect the two-pion state contribution to be significant at the precision we hope to achieve.

The measured widths of the $K_{+,S} \to \pi\pi\pi$ decays are suppressed relative to the $K_{+,S} \to \pi\pi$, and the relative phase-space suppressions have been estimate to be a factor of $O(1/500)$ or smaller. As the two-pion contribution is expected to be small the three-pion contribution should then be negligible, and only of interest for a calculation that wishes to achieve percent-level precision. Removing the $\pi\pi\pi$ states would involve computing the $K \to \pi\pi\pi$ states and reconstructing a term similar to the single-pion state in Equation (3.44) that could be subtracted explicitly. In the future the construction of a three-particle quantization condition that relates finite-volume energies to infinite volume scattering amplitudes could lead to lattice calculations that would extract the intermediate states we are interested in [57, 58].

Multi-hadron states also suffer from finite volume effects in lattice calculations. In practice these would only come into play for the $\pi\pi$ intermediate states. Two-pion finite volume corrections have been studied in the context of $K \to \pi\pi$ decays and the ΔM_K lattice studies. If the results of our study of rare kaon decays were ever to reach a high enough precision then finite volume effects could be investigated using a similar approach.

3.2.4 Renormalization of Lattice Operators

The current and weak Hamiltonian operators in Equation (3.30) must be renormalized, both individually and in order to remove any UV divergences that occur when the two operators make contact. The renormalization of the currents J_μ are not needed if conserved currents are used, as conserved vector currents have $Z_V = 1$. If we use local currents, however, then Z_V must be determined. To

$C_1^{\overline{MS}}$	$C_2^{\overline{MS}}$	$\Delta r_{11} = r_{22}$	$\Delta r_{12} = r_{21}$	$Z_{11} = Z_{22}$	$Z_{12} = Z_{21}$
-0.2967	1.1385	-6.562×10^{-2}	7.521×10^{-3}	0.5916	-0.05901

Table 3.1 *The Wilson coefficients in the $\overline{MS}$ scheme, the RI $\rightarrow$ $\overline{MS}$ matching matrix entries, and the non-perturbative lat $\rightarrow$ RI operator renormalization matrix entries.*

do so we can calculate the pion electromagnetic form factor $f_{ll}^{+}\left(q^2\right)$, defined by the matrix element given in Equation (3.28) for the pion by

$$\left\langle \pi\left(p_1\right)\right| V_\mu \left|\pi\left(p_2\right)\right\rangle = f_{ll}^{+}\left(q^2\right)\left(p_1+p_2\right)_\mu \tag{3.53}$$

where $q = p_2 - p_1$ is the momentum transfer. For two pions at rest $f_{ll}^{+}\left(0\right) = 1$, and Z_V can be fit using the temporal component of Equation (3.53), using a ratio of correlators

$$Z_V \overset{1\ll t,|t_{src}-t_{snk}|}{=} \frac{\Gamma_\pi^2\left(t_{snk}\right)}{\Gamma_{J_\mu}^{3,\pi}\left(t_{src,t,t_{snk}}\right)}, \tag{3.54}$$

where Γ_π^2 is the pion two-point function with the around-the-world state removed.

The renormalization of the Q_1 and Q_2 operators that make up H_W requires a matching procedure to relate the bare lattice operators to those in continuum perturbation theory in the $\overline{MS}$ scheme, where the Wilson coefficients are known at NLO. This involves renormalizing the bare lattice operators non-perturbatively using the regularization independent symmetric momentum-subtraction renormalization (RI-SMOM) scheme [89] and using the matching formula [33]

$$\sum_{i=1,2} C_i^{lat}\left(\mu\right) Q_i^{lat}\left(\mu\right) = \sum_{i=1,2} C_i^{\overline{MS}}\left(\mu\right)\left(1+\Delta r^{RI\rightarrow\overline{MS}}\right)_{ij}\left(Z^{lat\rightarrow RI}\right)_{jk} Q_k^{lat}\left(\mu\right) \tag{3.55}$$

where $Z^{lat\rightarrow RI}$ is the RI-SMOM renormalization matrix for the bare lattice operators and $\Delta r^{RI\rightarrow\overline{MS}}$ is the matching matrix from the RI-SMOM scheme to the $\overline{MS}$ scheme. In the four flavor theory case this is a 2×2 matrix given by [71]

$$\Delta r^{RI\rightarrow\overline{MS}} = \frac{\alpha_S\left(\mu\right)}{4\pi}\begin{pmatrix} -4ln\left(2\right) & -8+12ln\left(2\right) \\ -8+12ln\left(2\right) & -4ln\left(2\right)\end{pmatrix}. \tag{3.56}$$

This renormalization procedure was performed in [33] at the scale $\mu = 2.15$GeV, the entries of the matching matrices $Z^{lat\rightarrow RI}$ and $\Delta r^{RI\rightarrow\overline{MS}}$ that were used are given in Table (3.1), along with the Wilson coefficients in the $\overline{MS}$ scheme. The lattice Wilson coefficients were found to be $C_1^{lat} = -0.2216$ and $C_2^{lat} = 0.6439$.

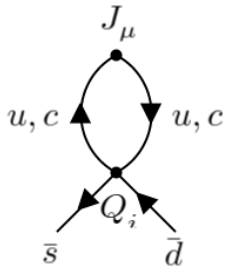

Figure 3.6 *The subdiagram of the Saucer and Eye class of diagrams that could lead to UV divergences.*

Having renormalized the J_μ and H_W operators individually, it is important to consider additional divergences that occur as the two operators approach each other. This is possible for one of the 4-point Saucer and Eye diagrams where the current is inserted on the loop [62]. The relevant part of these diagrams is shown in Figure (3.6), and we can see that this subdiagram is analogous to the one-loop contribution to the vacuum polarization in QED and QCD which, with naive power counting, is quadratically divergent. If the conserved vector current is used then electromagnetic gauge invariance gives a transversality factor of $q^\mu q^\nu - q^2 g^{\mu\nu}$, reducing the order of the divergence to a logarithmic one.

This logarithmic divergence is independent of mass, resulting in an exact cancellation of the divergence when the GIM subtraction of the up and charm quark loops is performed. This would not be the case if the process was described in a 3-flavor theory, or if local currents were used. In the three-flavor theory gauge invariance still reduces the quadratic divergence and with local currents in the four-flavor theory there is still some form of GIM suppression. In either case the remaining divergences would have to be removed using non-perturbative renormalization techniques [75].

Chapter 4

$K \to \pi\ell^+\ell^-$ Numerical Results

In this chapter I will present the results of the lattice calculation of the long distance contributions to the $K \to \pi\gamma^*$ decay, along with my analysis of the results. It was first shown in [62] that a lattice calculation of this kind was possible in principle. The approach was further refined in [36], where the operators required to control the ultraviolet divergences were introduced, and a lattice calculation using unphysical masses was performed in [34] to demonstrate the feasibility of extracting the amplitude of the decay. This calculation is the first of its kind to be performed using physical light quark masses.
In Section (4.1) I will introduce details of the gauge configurations used and I will give details of the setup of the calculations in Section (4.2). Following that I will present a justification of this choice of setup, over that of an all-to-all approach. I will then present numerical results for 2-, 3-, and 4-point correlation functions in Sections (4.4.1) and (4.4.2), with the application of methods to remove intermediate states being given in Section (4.4.3). I will then present the final result, the form factor extracted from the amplitude, in Section (4.4.4).

4.1 Details of the Simulation

This study was performed on a lattice ensemble generated with the Iwasaki gauge action and 2+1 flavors of Möbius DWF [19]. The spacetime volume of the ensemble is $48^3 \times 96$ and the inverse lattice spacing is $a^{-1} = 1.730\,(4)$GeV.

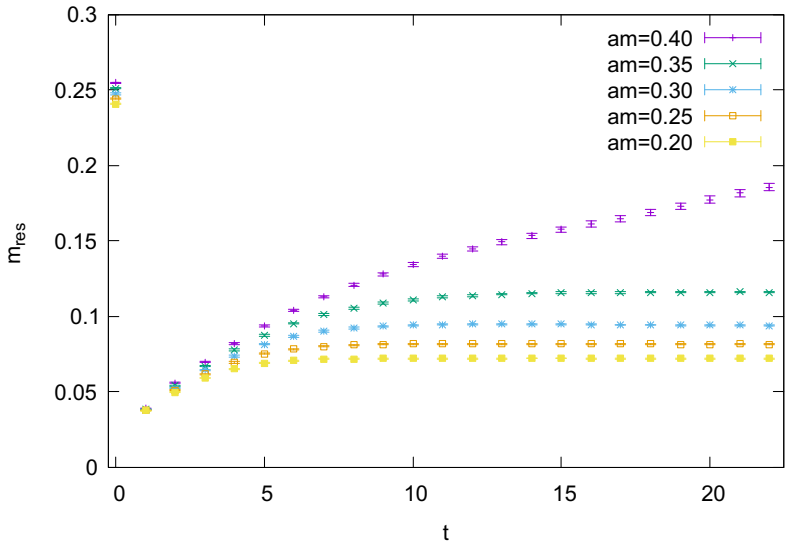

Figure 4.1 *The residual mass of various heavy quarks on the* 48^3 *gauge configuration. These were calculated using 60 gauge ensembles, with 4 times translations per ensemble. We see that the DWF theory breaks down for heavy quark masses, as the residual mass diverges for* $am = 0.40$.

The fifth-dimensional extent is $L_s = 24$ and the residual mass is $m_{\text{res}} = 6.102\,(40) \times 10^{-4}$ in lattice units. The light and strange sea quark masses are $m_l = 0.00078$ and $m_s = 0.0362$ respectively, corresponding to pion and kaon masses of $M_\pi = 139.2(4)$MeV and $M_K = 499(1)$MeV.

The Möbius action was used to simulate the light quarks in the ensemble, with a rational approximation being used to simulate the strange quarks. In our calculation the valence quarks use zMöbius for the light quarks for which 2000 low mode eigenvectors per configuration were generated in order to deflate the low mode inversions. In order to perform the GIM subtraction unphysical charm quark masses were used. With the choice of zMöbius parameters for the light quark it would be impossible to use a physical charm quark mass, as the DWF theory breaks down for heavy quarks. This can be seen in Figure (4.1) where we plot the residual mass for various heavy quark masses. As the quark masses increase the residual mass increases, and additional time is needed for m_{res} to plateau, until reach $am = 0.40$ where the result diverges. Whilst it may have been possible to use another action, this would have interfered with the the GIM subtraction, where the difference between the light and charm quarks depend strongly on the very low modes that the actions are sensitive to.

Instead we simulate 3 unphysical charm quarks and use these to extrapolate our results to the physical point. The quark masses were taken to be $am_{c_1} = 0.25$,

$am_{c_2} = 0.30$, $am_{c_3} = 0.35$. The calculations of the η_c mesons used for the extrapolation were performed with a sample of 13 configurations, each separated by 20 time units. The results for the amplitude were calculated with a sample of 87 configurations with the same separation.
For the investigation into using the A2A method to calculate the decay amplitude another lattice ensemble was used, this one generated with the Iwasaki gauge action and 2+1 flavors of Shamir DWF [5]. The spacetime volume of the ensemble is $24^3 \times 64$ and the inverse lattice spacing is $a^{-1} = 1.73\,(3)$GeV. The fifth-dimensional extent is $L_s = 16$ and the residual mass is $m_{\text{res}} = 3.08\,(6) \times 10^{-3}$ in lattice units. The light and strange sea quark masses are $m_l = 0.005$ and $m_s = 0.04$ respectively, corresponding to pion and kaon masses of $M_\pi = 340(1)$MeV and $M_K = 594(2)$MeV.

4.2 Calculation Setup

In order to calculate the 2-, 3- and 4-point correlators that were outlined in Section (3.2.1), the C++ library "Grid" [24] and the framework based on Grid, "Hadrons" [82], were used. The correlators are constructed with a kaon at time $t_K = 0$, at rest, decaying to a pion at time $t_\pi = 32$, with momentum $\vec{p}_\pi = \frac{2\pi}{L}(1, 0, 0)$. The time separation between between the mesons is chosen to be as small as possible such that the signal we achieve is clear, but as large as possible such that the integral around the current insertion is can be extended to give a wider fit range for the rare kaon decay amplitude. There have been studies of kaon semileptonic form factors [25] that have used similar time separations and we have also investigated other time separations for the 4-point correlation function ourselves, as in Figure (4.2). The current is inserted midway between the kaon and the pion such that excited states from the interpolators can be avoided, following the precedent set by [34] . Coulomb gauge-fixed wall sources are used as they give good overlap with the kaon and pion ground states, helping us reduce excited state contamination. The Möbius conserved vector current is used, and is implemented using sequential solves and using only the time extent, $\mu = 0$. This allows us to extract the form factor from the amplitude, as in Equation (3.1). The loops in the Saucer and Eye diagrams, shown in Figure (3.4), were calculated using spin-color diluted sparse sources, as described in Section (2.4.1). It is these single quark propagator traces that introduce the largest contributions of statistical noise in

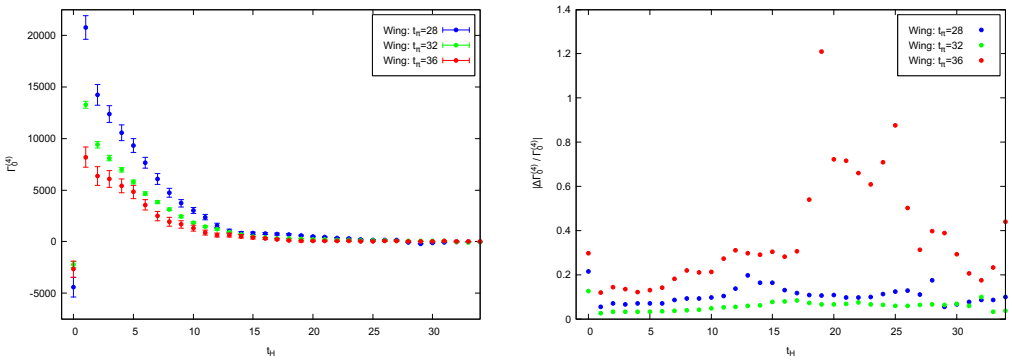

(a) (b)

Figure 4.2 *(a) The Wing diagram contribution to the rare kaon 4-point correlator for different sink times. The kaon is always at $t_K = 0$ and the current is always inserted midway between the pion and the kaon. (b) The relative error of the Wing diagram contributions.*

the diagrams we compute. The strategy to reduce this noise is to compute the correlators with multiple hits for the loop and to employ all-mode-averaging [20], as shown in Equation (2.50). This entails performing the inversions required for the loop propagators on a given source with an "exact" solver residual and using the same source to perform inversions using an "inexact" solver residual. The difference between the exact and inexact results are used to compute an AMA correction that are applied to a further 9 inexact hits. For the light quark the exact solver residual is 10^{-8}, for the heavier quarks a more precise residual must must be used in order to accurately describe large time behavior, as can be seen in Figure (4.3). For this reason the charm residuals are taken to be 10^{-10}, 10^{-12}, and 10^{-14} for c_1, c_2, and c_3 respectively. The inexact residuals were taken to be 10^{-4} for all quarks. For this calculation we do not include disconnected diagrams, as in "C_{dis}" in Figure (3.5), where the electromagnetic current is self-contracted. These diagrams are very noisy, the statistics needed such that the signal from these diagrams would be comparable to the rest of the calculation would be prohibitively expensive. We also expect that the disconnected contribution is suppressed by a factor of $1/N_C$ and approximate $SU(3)$ flavor symmetry [40], giving $\sim 10\%$ of the connected contributions in the continuum. We have not reached a statistical precision where including the disconnected diagrams are necessary, but the disconnected light and charm loops have been contracted and saved as part of our calculation. The strange loops could be computed at a later date, along with further light and charm statistics, and combined with the connected diagrams in order to compute the disconnected contribution.

Table (4.1) shows the number of quark propagators needed for one config-

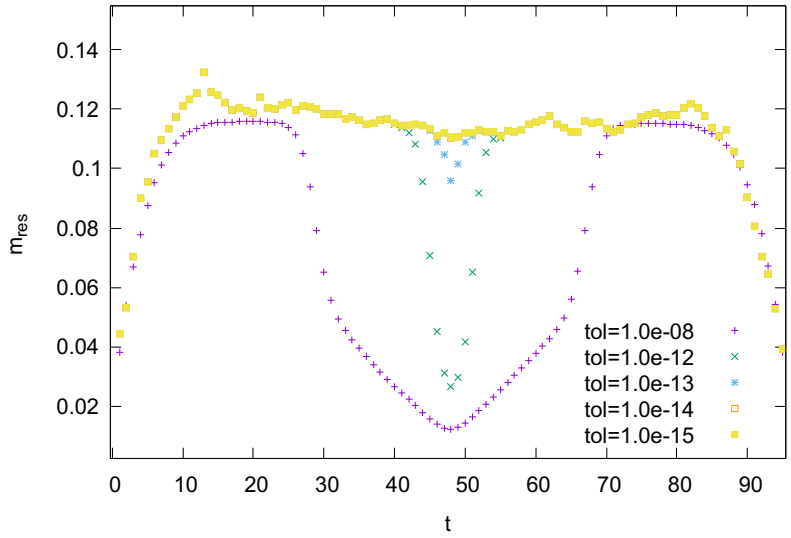

Figure 4.3 *The residual mass of a heavy quark with mass* $am = 0.35$ *on the* 48^3 *gauge configuration, calculated with several solver precision tolerances. The* $tol = 10^{-08}$ *result was calculated using the same statistics as shown in Figure (4.1) and the remaining results were computed using a significantly smaller set of statistics. Error bars are omitted.*

uration. If we were to include disconnected this would require a further $16\,(N_\eta + 1)\,(N_t + 1)$ strange propagators. The motivation for the use of the zMöbius action, to reduce the L_s dimension, can be seen in the large number of light inversions to be computed, as well as the application of deflation, discussed in Section (2.3.2). In order to compute the bias correction for the zMöbius action, as discussed in Section (2.1.4), the same set of diagrams were computed using the Möbius action for $N_t = 1$ times translations on 62 configurations. The Möbius inversions were computed using the Möbius-accelerated DWF solver [91], that uses the zMöbius approximation to compute a guess that is close to the solution of the Möbius Dirac matrix problem.

4.3 All-to-All Approach

The setup of the calculation outlined in the previous section is similar to the approach taken in the exploratory calculation with unphysical masses, with the significant change being the use of sparse noise and three unphysical charm quark masses for the loop. The decision to take this approach was taken after an investigation of the application of the A2A method to study the rare kaon decays.

Description	Source Type	Number of Inversions		
		Light	Strange	Charm
C and W propagators	Gauge-fixed wall	$3N_t$	N_t	0
S and E loops: Exact	Sparse random volume	16	0	48
S and E loops: Inexact	Sparse random volume	$16N_\eta$	0	$48N_\eta$
Current insertions: Exact	Sequential	$19N_t$	N_t	$48N_t$
Current insertions: Inexact	Sequential	$16N_\eta N_t$	0	$48N_\eta N_t$
Scalar density	Gauge-fixed wall	0	N_t	0
Total: $N_\eta = 10$, $N_t = 6$	-	1268	18	3696

Table 4.1 *Number of propagators needed to be computed for a single configuration of our calculation. N_η is the number of on noise sources used for the quark loops and N_t is the number of time translations per configuration.*

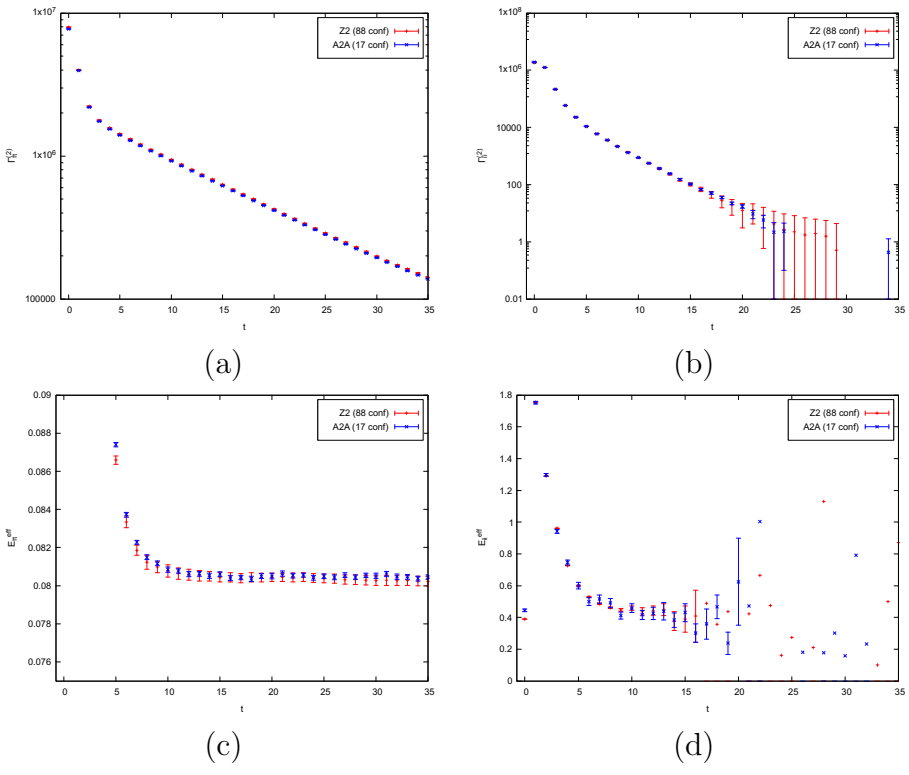

Figure 4.4 *The light-light 2-point correlators for the (a) pseudoscalar-pseudoscalar and (b) vector-vector cases, found using the A2A method and Z2 wall sources. The effective masses of the (c) pseudoscalar-pseudoscalar and (d) vector-vector correlators are given, as in Equation (2.87)*

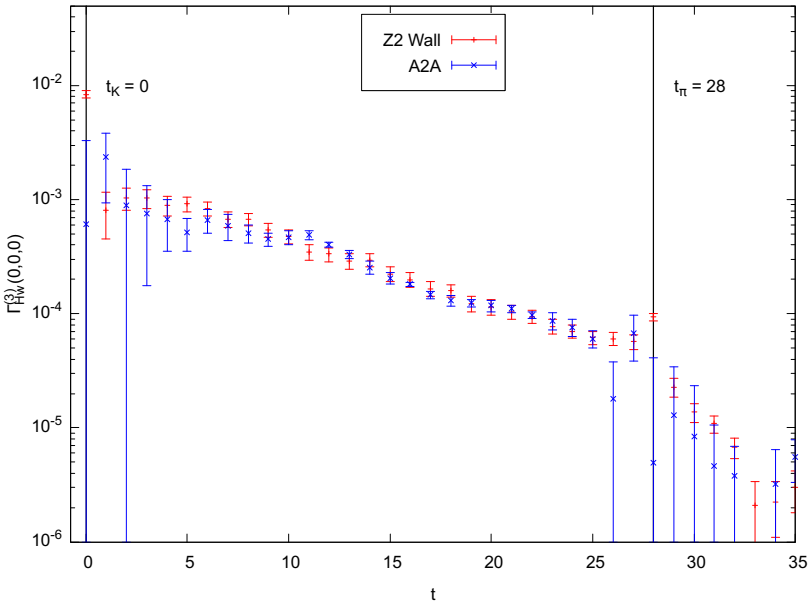

Figure 4.5 *The zero-momentum Wing diagram contribution to the 3-point weak Hamiltonian correlation function, computed using A2A vectors and Z2 wall sources.*

On the same $48^3 \times 96$ gauge configuration a number of A2A vectors were computed for the light and strange quarks. These were spin-color-time diluted vectors, with 2000 low modes. Two sets of of A2A vectors were constructed using two separate noises in order to avoid introducing bias when performing contractions. Meson fields were constructed using these vectors, from which correlation functions could be created. Figures (4.4) (a) through (d) show the correlators and effective masses of light-light pseudoscalar-pseudoscalar and vector-vector 2-point functions, created using 17 configurations worth of A2A vectors, using the method given in Equation (2.139). These are compared to results found using $Z2$ wall source, with 88 configurations and a source at each time slice. We can see that the results between the two methods are consistent and that the A2A results have a signal that extends further in time for the vector-vector case.

The non-eye 3-point H_W correlators were constructed using the $24^3 \times 64$ DWF action, with 600 low modes for the light quark. Figure (4.5) shows the Wing diagram, with zero-momentum, created using the A2A approach, as detailed in Appendix (B), compared to using Z2 wall sources. The A2A results were constructed using 20 configurations, and the Z2 wall results were constructed using 24 configuration with a wall source at every 4th timeslice. We see here that we have good agreement between the methods. When performing the 4-quark contraction it is empirically known that placing all the"v-vectors," those

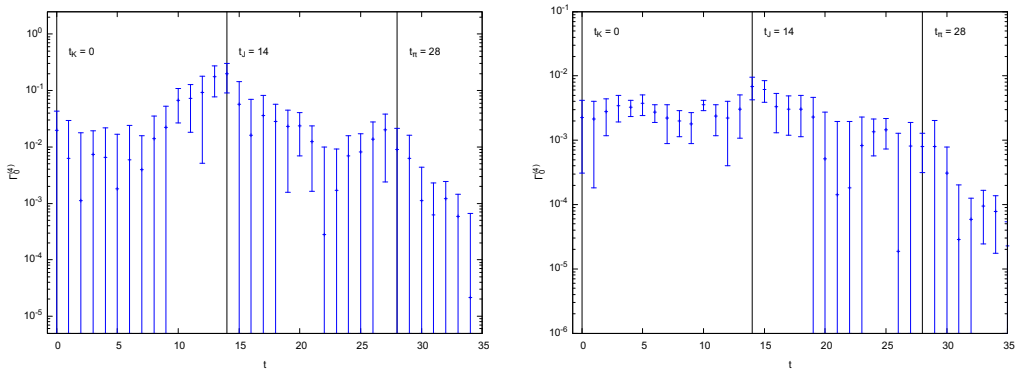

(a) (b)

Figure 4.6 *The 4-point Wing diagram computed using the A2A method with the current inserted (a) stochastically and (b) sequentially on the kaon's light quark.*

for which the solves have been performed, at the vertex leads to the best signal, and so including the "w-vector" noise at the vertex should be avoided.

For the the 4-point rare kaon correlators two approaches were taken, the first was to treat all propagators in the A2A fashion. With this method it is impossible to avoid creating a contraction that places the w-vector noise on either the 4-quark vertex or on the current insertion, leading to noisy results. Figure (4.6) (a) shows the result for this method when constructing the wing diagram with a local current inserted on the kaon's light quark, with 15 $24^3 \times 64$ gauge configurations used in the bootstrap resampling of the result.

The second method is to perform a set of sequential solves, such as those described in Section (2.4.2), in order to remove the noise at the current insertion. Figure (4.6) (b) shows the result of this approach for the same diagram as (a), computed using 8 $24^3 \times 64$ gauge configurations. This method results in a loss of the translation of the current insertion time t_J, requiring that a sequential solve be performed for a number of time translations, similar to the wall source approach. However, this involves performing inversions on all of the low modes, which become prohibitively expensive for the 2000 low modes on the $48^3 \times 96$ gauge configuration.

Due to the inability to escape the noise of the current when computing all propagators in the A2A fashion and the cost of treating the current sequentially using A2A vectors we decided to investigate a hybrid approach to calculate the rare kaon decay amplitude. The non-loop propagators would be be computed with Coulomb gauge-fixed wall sources and the loops would be calculated using A2A vectors. The results of the method were compared to correlation functions computed using full volume and sparse noises on the $48^3 \times 96$ gauge configuration.

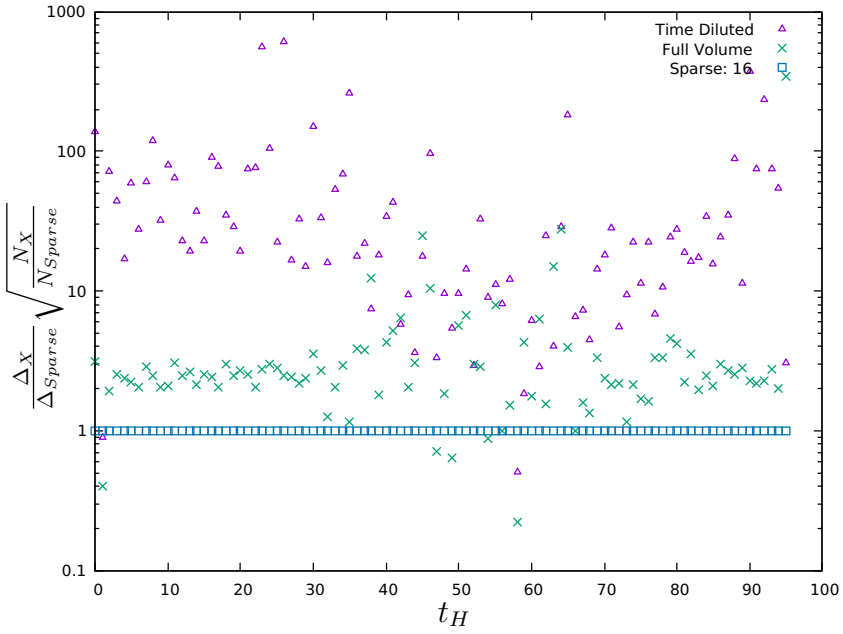

Figure 4.7 *The relative error, weighted by the cost of inversions, of the zero-momentum Saucer diagram contribution to the 3-point weak Hamiltonian correlation function, computed using different noise strategies for the single quark propagator loop.*

A cost benefit analysis was performed using the quantity $\frac{\Delta X}{\Delta Sparse}\sqrt{\frac{N_X}{N_{Sparse}}}$, where ΔX is the statistical error of the result from method X and the root of the number of inversions N_X tracks the computational cost of using method X. Figure (4.7) shows the results of this cost-benefit analysis for the 3-point Saucer diagram with zero momentum. It can clearly be seen that the sparse noise approach is the most successful. It is also worth repeating that the current insertion for the 4-point functions here were performed using a local current insertion. The Möbius action conserved current requires information from the fifth dimension of the source to construct a sequential source as described in Equation (2.160), but saving the A2A vectors to disk in their full five dimensions is too costly. Instead the four dimensional vectors are saved and local currents are used, which leads to a quadratic divergence when the current is in inserted on the loop of the Eye and Saucer diagrams, as discussed in Section (3.2.4).

After these investigations into applying the A2A approach we came to the conclusion that Coulomb gauge-fixed wall sources are the the best way to we have to calculate the rare kaon decay amplitude. Constructing all diagrams using entirely A2A propagators leaves noise at the current insertion, performing sequential A2A solves is prohibitively expensive, time diluted A2A vectors are beaten by sparse volume random noise sources when computing loop propagators,

and the A2A method does not practically allow for the use of conserved vector currents.

Another reason to abandon the A2A approach is a lack of compatibility with other projects. The main strength of the A2A method is that the A2A vectors and meson fields only need to be computed once. They can be saved to disk and reused to construct a variety of diagrams. However in the UKQCD collaboration there are no projects where the A2A method was deemed useful. The calculation of isospin-breaking corrections to $K_{\ell 2}$ and $\pi_{\ell 2}$ decays found a similar need for A2A sequential solves when dealing with $\not{A}$ insertions, and though they did not lose translations of the insertion with their method, it was found to return a disappointing signal given the cost. Other projects, such as the calculation of $K\pi$ scattering at the physical point, have been looking towards distillation, and the study of rare hyperon decays must overcome all the same problems as the rare kaon decays A2A approach, with the additional struggle of controlling the noise that comes with a lattice calculation of baryon decays.

4.4 Numerical Results

The goal of this calculation is to determine the amplitude of the $K^+ \to \pi^+\gamma^*$ decay using physical light quark masses. In this Section I will present the results of our calculation and discuss various methods of analyzing the results. All results presented are in lattice units, unless otherwise stated.

In order to extract the decay amplitude we must integrate the reduced 4-point correlator given in Equation (3.32) and subtract intermediate states that appear in Equation (3.43). To calculate the source/sink factors needed to normalize the 4-point correlator we must fit 2-point pion and kaon correlators. In order to subtract the intermediate states we can either construct the single pion state using matrix elements and energies extracted from 2- and 3-point fits, as in Equation (3.45) or shift the weak Hamiltonian, as in Equation (3.47), requiring a fit of the scalar density and weak Hamiltonian 3-point ratio given in Equation (3.49). The final result we extract will come from an extrapolation to the physical charm quark mass, which requires fits to the unphysical 2-point η_c meson correlators. I will thus present the results of these 2- and 3-point correlators before discussing the 4-point correlators.

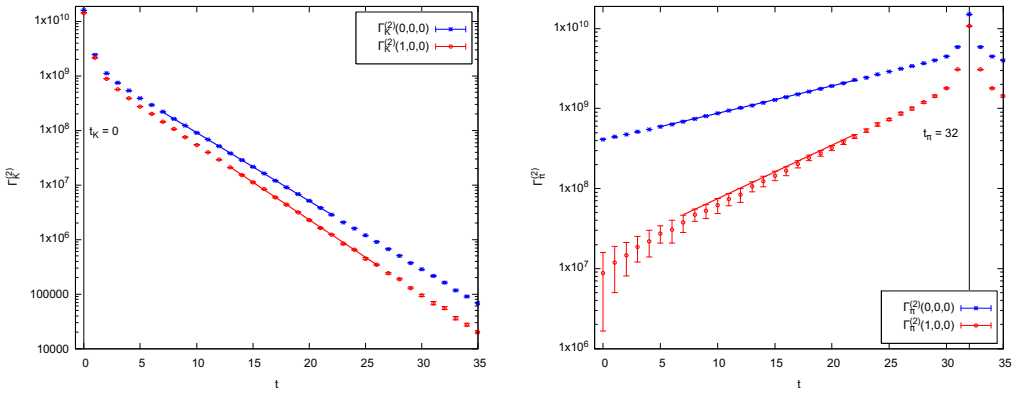

(a) (b)

Figure 4.8 *Fits to the 2-point wall sink (a) kaon and (b) pion correlators. The source time for each meson is shown.*

4.4.1 2- and 3-point Correlators

	$\vec{p}$	
	$(0,0,0)$	$\frac{2\pi}{L}(1,0,0)$
$E_K(\vec{p})$	0.28888(22)	0.31699(37)
$E_\pi(\vec{p})$	0.08015(18)	0.15402(30)
$Z_K(\vec{p})$	30812(60)	28760(150)
$Z_\pi(\vec{p})$	28341(89)	26098(153)
$\mathcal{M}^{J,K}_{\mu=3}(\vec{0},\vec{p})$	-	0.5676(30)
$\mathcal{M}^{J,\pi}_{\mu=3}(\vec{0},\vec{p})$	-	0.2323(19)

Table 4.2 *Fit results to 2- and 3-point correlators that do not depend on charm mass. The 2-point fits results are obtained with a fully-correlated simultaneous fit with point sink correlators for each meson and kinematic. The Z_m $(m = K, \pi)$ results contain a volume factor of $\sqrt{L^3}$ that is retained in order to aid the calculation of the renormalization factor in Equation (3.31). The 3-point fit results are obtained with a fully-correlated simultaneous fit to the relevant 2-point functions, that are outlined in Equation (3.29).*

When fitting the 2-point pion, kaon, and eta correlators we fit our data to Equation (2.87), seeking to extract Z_m for $m = K, \pi$ and E_m for $m = K, \pi, \eta_{1,2,3,}$. The matrix elements we need to calculate must be obtained using the same wall-source/sink-smearing setup as the 4-point functions. However, as we apply the sink smearing after our inversion we can compute the correlator with a point sink with only the cost of a contraction. The point sink produces a clearer signal and can be used as part of a simultaneous fit, allowing for a better fit of the energy. We compute four 2-point correlators for the pion and kaon, two for each momentum used in the calculation with either a wall or point sink. Results

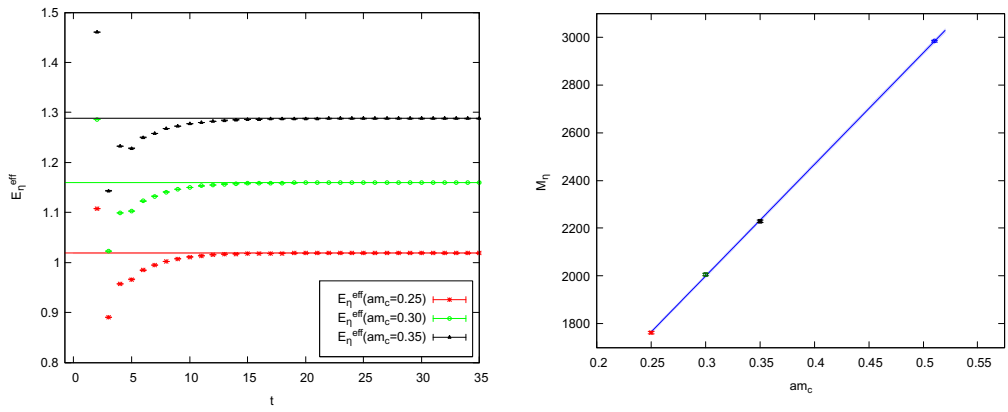

(a) (b)

Figure 4.9 *(a) The effective masses, as described in Equation (2.88), of the η_c mesons found using the unphysical charm quark masses and (b) the extrapolation to the physical η_c mass $M_\eta = 2983.8(4) MeV$. The result of the extrapolation gives $am_c = 0.510(1)$.*

	$am_{c_1} = 0.25$	$am_{c_2} = 0.30$	$am_{c_3} = 0.35$
aE_η	1.0187(2)	1.1598(2)	1.2881(2)
M_η	1762(4) MeV	2006(5)Mev	2228(5)

Table 4.3 *The masses of the η_c mesons found by fitting the 2-point correlators constructed using the unphysical charm quark masses, given in lattice and physical units. Extrapolation to the physical η_c mass $M_{\eta_c} = 2983.8(4) MeV$ gives $am_c = 0.510(1)$*

of fits to the wall sink correlators are shown in Table (4.2), along with plots of the correlators with the fits shown in Figure (4.8). For each of the unphysical charm quark masses we computed point-sink η_c 2-point correlators and fit for their masses, which are shown in Figure (4.9) (a) and given in Table (4.3). The extrapolation to the physical η_c mass is shown in Figure (4.9) (b).

The 3-point matrix element for the H_W operator is found by fitting the correlator given by Equation (3.26) to the model given in Equation (3.27). The matrix elements for the 3-point correlators with the vector current insertion are

	$am_{c_1} = 0.25$	$am_{c_2} = 0.30$	$am_{c_3} = 0.35$
$\mathcal{M}_H(\vec{k})$	-0.000378(19)	-0.000483(19)	-0.000580(19)
$\mathcal{M}_H(\vec{p})$	-0.000434(232)	-0.000512(235)	-0.000582(237)
c_s	-0.000163(10)	-0.000209(10)	-0.000250(10)

Table 4.4 *Fit results to 3-point function that depend on charm mass. The $\mathcal{M}_H$ fit results are obtained for $\vec{k} = (0,0,0)$ and $\vec{p} = \frac{2\pi}{L}(1,0,0)$ with a fully-correlated simultaneous fit to the relevant 2-point functions, that are outlined in Equation (3.27).*

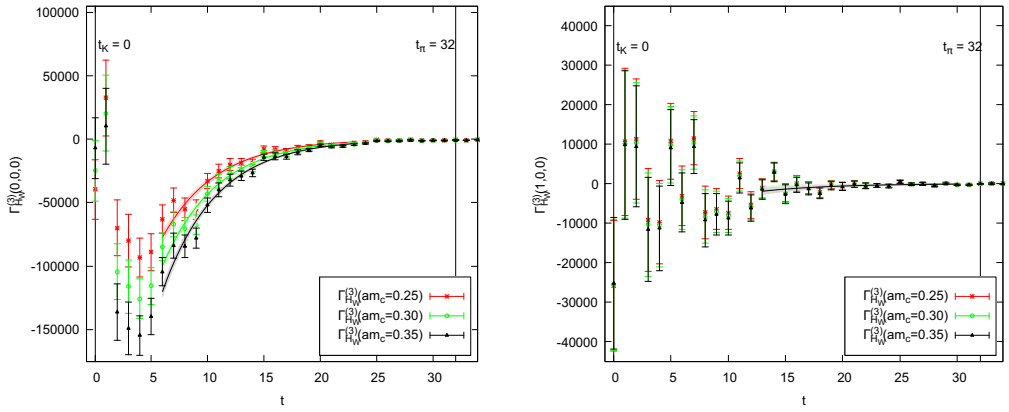

(a) (b)

Figure 4.10 *Fits to the 3-point correlators used to extract $\mathcal{M}_H(\vec{p})$ for (a) $\vec{p} = (0,0,0)$ and (b) $\vec{p} = \frac{2\pi}{L}(1,0,0)$.*

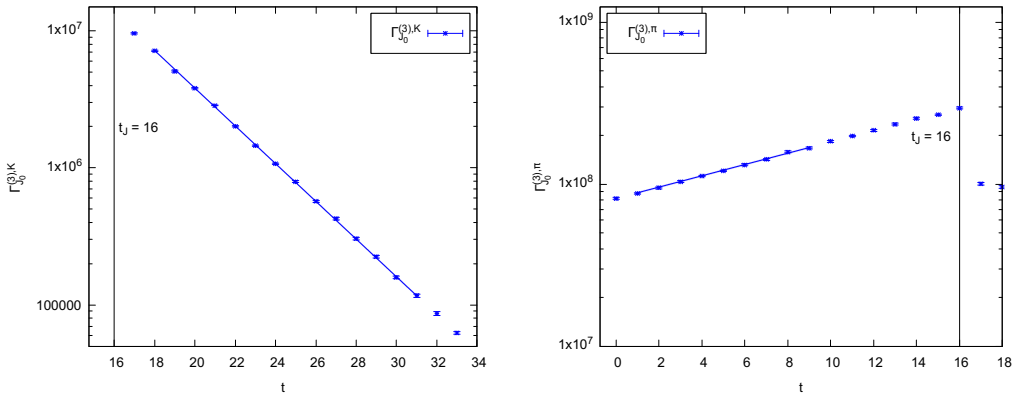

(a) (b)

Figure 4.11 *Fits to the 3-point (a) kaon and (b) pion correlators with a vector current insertion.*

found by fitting the correlator given by Equation (3.28), for mesons $m = K, \pi$, to the model given in Equation (3.29). Results for matrix elements extracted from these fits are given in Tables (4.2) and (4.4), with plots of the H_W 3-point correlator results given in Figure (4.10) and plots of the J_μ 3-point correlator results given in Figure (4.11). In order to shift the weak Hamiltonian, with the aim of removing the exponentially growing intermediate single pion state, the parameter c_s must be fit from the ratio of H_w and scalar-density correlators, as in Equation (3.49). The results of these ratios are shown in Figure (4.12) for the 3-point ratios for the 3 unphysical charm quark masses. A fit was performed for the 3-point ratio in the region $t_K \ll t_\mathcal{O} \ll t_\pi$, where $t_\mathcal{O}$ is the time position of the operator $\mathcal{O} = H_W, \bar{s}d$, and the results are given in Table (4.4).

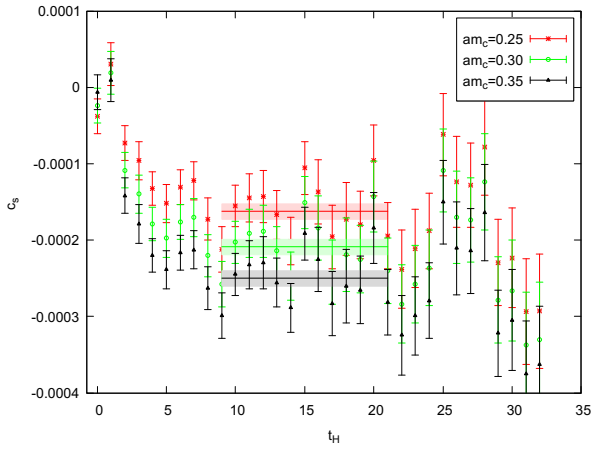

Figure 4.12 .

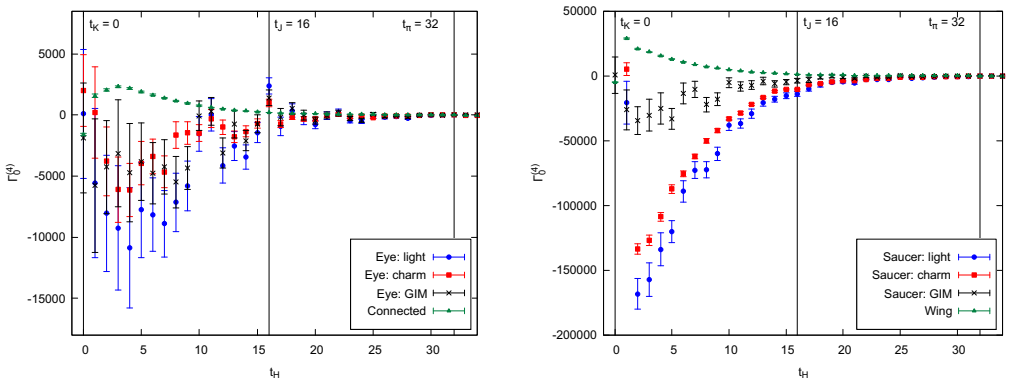

(a) (b)

Figure 4.13 *The (a) Q_1 and (b) Q_2 operator contributions to the rare kaon 4-point correlator, separated into the diagrams given in Figure (3.4) both before and after GIM subtraction, shown for the lightest unphysical charm quark mass, $am_{c_1} = 0.25$.*

4.4.2 4-point Correlators

Figures (4.13) (a) and (b) show the the contributions from the Q_1 and Q_2 diagrams, that make up the 4-point function in Equation (3.30), for the lightest charm quark mass. These diagrams have been constructed by applying the appropriate fractional quark charges and Wilson coefficients needed to match to the $\overline{MS}$ scheme. For the bare lattice operators Q_1 and Q_2, at the scale $\mu = 2.15$GeV, we use the Wilson coefficients $C_1^{lat} = -0.2216$ and $C_2^{lat} = 0.6439$ respectively. These were calculated in [33] on a 2+1 flavor, domain wall fermion, $16^3 \times 32$ gauge ensemble with a 421 MeV pion mass and the same lattice spacing that the gauge ensemble for this calculation used. The results are given without

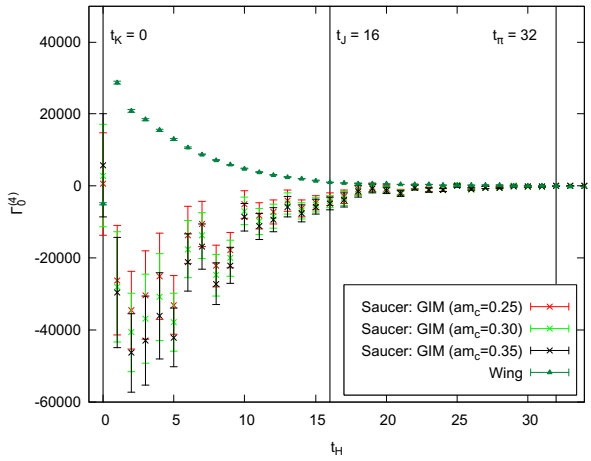

Figure 4.14 *The Q_2 operator contributions to the rare kaon 4-point correlator after GIM subtraction, shown for all three unphysical charm quark masses.*

error, though the systematic errors caused by the Wilson coefficients have been discussed for calculations of the $K \to \pi\pi$ decay amplitudes in [18], where they were estimated to be 12%. As we are currently dominated by statistical error for this project we neglect to calculate the equivalent systematic error for this decay. It can be seen that the diagrams in Figure (4.13) (b), associated with the Q_2 operator, contribute to the 4-point function more significantly than those associated with the Q_1 operator, and that these diagrams produce the cleaner signal. We also see that the Saucer and Eye contributions, given by the GIM subtractions, are more significant here than they were in [34], as the physical light quark mass reduces the severity of the GIM cancellation. This results in a larger degree of separation between the Saucer and Wing diagrams, as they add destructively when creating the rare kaon 4-point correlator. It is the Saucer diagram that has the largest contribution to the statistical error of our final result, as the GIM subtracted result has a magnitude that is comparable to the Wing diagram contribution, but with larger statistical error. Figure (4.14) shows the GIM subtracted Saucer diagram results for the three unphysical charm quark masses, with the Wing diagram for comparison. Figure (4.15) shows the 4-point function, as defined in Equation (3.30), for each of the unphysical charm quark masses. Figures (4.16) (a) and (b) show a slice of the T_a and T_b dependence of the normalized, integrated 4-point correlator. The exponential growth of the intermediate states that depend on T_a can clearly be seen, and we also see the smaller contribution of the shrinking intermediate states that depend on T_b. In order to extract the amplitude from these correlators we must remove these

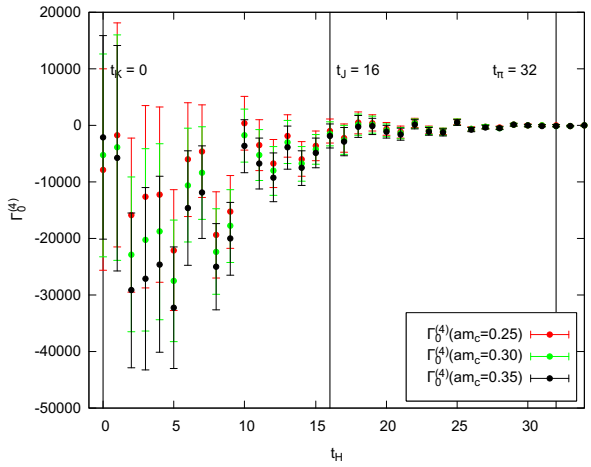

Figure 4.15 *The rare kaon 4-point correlator after GIM subtraction, shown for all three unphysical charm quark masses.*

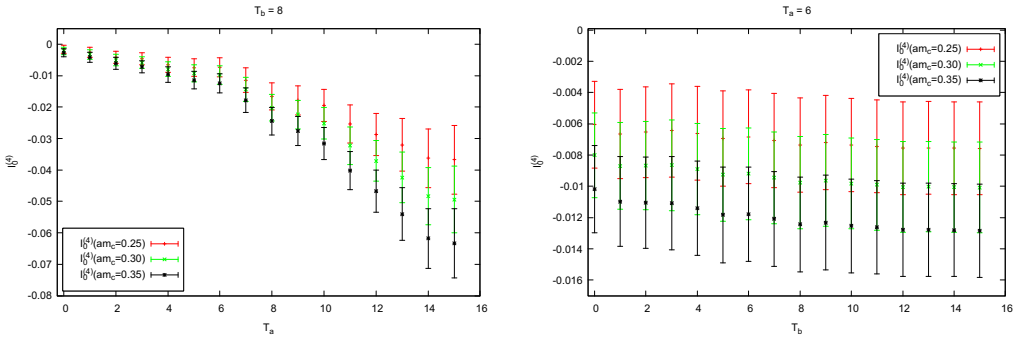

(a) (b)

Figure 4.16 *The normalized, integrated rare kaon 4-point correlator, shown for (a) $T_b = 8$ and (b) $T_a = 6$.*

intermediate states.

4.4.3 Extracting the Rare Kaon Amplitude

Construction and Removal of the Single Pion State

The first method we use to remove the intermediate pion state is to fit to the model given in Equation (3.45). We can do this by fitting the the A_0, c_0^1, and c_0^2 parameters explicitly, with a simultaneous fit to with the relevant 2-point functions needed to describe the exponential dependence on meson energies. We can also construct the c_0^1 and c_0^2 parameters, as they are given in Equation (3.46), performing a simultaneous fit with the relevant 2- and 3-point function to extract

Analysis	$A_0\,(m_{c_1})$	$A_0\,(m_{c_2})$	$A_0\,(m_{c_3})$
A_0, c_0^1, c_0^2	-0.00025(219)	-0.00017(220)	-0.00012(220)
$A_0, c_0^2 = -c_0^1$	-0.00033(167)	-0.00027(167)	-0.00024(167)
2pt/3pt	-0.00026(182)	-0.00002(183)	0.00018(183)
$\mathcal{M}_H(\vec{p}) = \mathcal{M}_H(\vec{k})$	-0.00027(176)	-0.00014(177)	-0.00003(177)
c_s shift	0.00027(237)	0.00031(239)	0.00035(239)
$c_s \times \bar{s}d$	-0.00002(5)	-0.00003(7)	-0.00003(9)

Table 4.5 *Fit results for the rare kaon amplitude using several different methods, as well as a sanity check that $c_s \times \bar{s}d$ does not contribute to the amplitude. These fits were performed with simultaneous fit to the relevant 2- and 3-point functions, with the 2- and 3-point fits being fully-correlated and the fit of the integrated 4-point function being uncorrelated.*

Coefficient	Fit Method	$am_{c_1} = 0.25$	$am_{c_2} = 0.30$	$am_{c_3} = 0.35$
c_0^1	A_0, c_0^1, c_0^2 fit	-0.0023(10)	-0.0031(10)	-0.0037(10)
	$A_0, c_0^2 = -c_0^2$ fit	-0.0023(10)	-0.0030(10)	-0.0037(10)
	2pt/3pt	-0.0023(4)	-0.0030(4)	-0.0037(4)
	$\mathcal{M}_H(\vec{p}) = \mathcal{M}_H(\vec{k})$	-0.0023(5)	-0.0031(5)	-0.0037(5)
c_0^2	A_0, c_0^1, c_0^2	0.0021(14)	0.0028(14)	0.0034(14)
	2pt/3pt	0.0016(7)	0.0020(7)	0.0023(7)
	$\mathcal{M}_H(\vec{p}) = \mathcal{M}_H(\vec{k})$	0.0019(4)	0.0026(4)	0.0031(4)

Table 4.6 *The c_0^1 and c_0^2 parameters of Equation (3.46) obtained via fitting the integrated 4-point correlator using different methods.*

the 3-point matrix elements and meson energies needed. As the 3-point weak Hamiltonian correlation function is noisy at non-zero momentum the c_0^2 parameter is less well resolved. In order to avoid this additional statistical error we can investigate two approximations that were introduced in [34] and described in Section (3.2.3), namely the zero-momentum transfer approximation: $c_0^2 = -c_0^1$, and the $SU\,(3)$ flavor symmetry approximation: $\mathcal{M}_H\left(\vec{k}\right) = \mathcal{M}_H\,(\vec{p})$. Table (4.6) shows values of the c_0^1 and c_0^2 parameters obtained using various methods. It can can be seen that the zero-momentum transfer approximation holds well, as we only have 1 unit of momentum difference between the pion and kaon. The $SU\,(3)$ flavor symmetry limit gives results that are consistent with others, which is unexpected as we work with physical light quark masses. Figures (4.18) through (4.21) show the T_a and T_b dependence of the integrated correlator with the intermediate states subtracted using the various methods described above. These are shown for the various charm quark masses, and the results of the fits to the plateaus are given in Table (4.5).

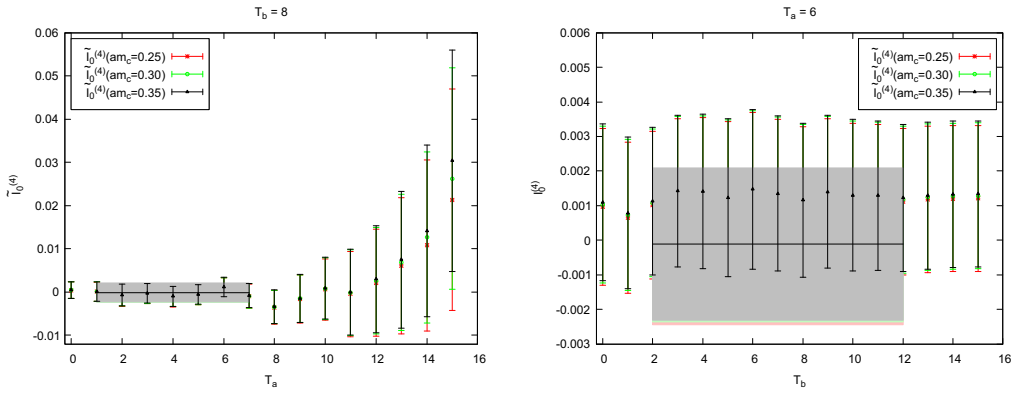

(a) (b)

Figure 4.17 *Fit of the normalized, integrated rare kaon 4-point correlator with the intermediate states removed, shown for (a) $T_b = 8$ and (b) $T_a = 6$. The results were obtained by fitting A_0, c_0^1, and c_0^2 directly. The fits to the plateaus correspond to $A_0\,(am_{c_1}) = -0.00025(219)$, $A_0\,(am_{c_2}) = -0.00017(220)$, and $A_0\,(am_{c_3}) = -0.00012(220)$.*

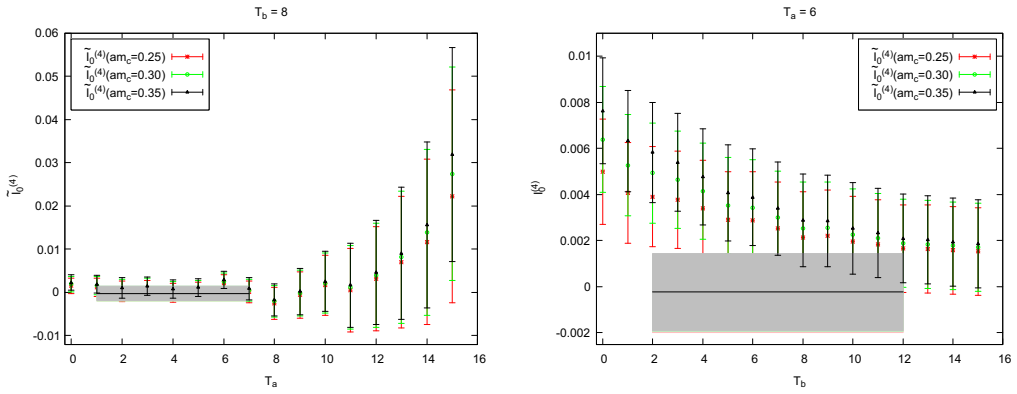

(a) (b)

Figure 4.18 *Fit of the normalized, integrated rare kaon 4-point correlator with the intermediate states removed, shown for (a) $T_b = 8$ and (b) $T_a = 6$. The results were obtained by fitting A_0 and c_0^1, with the zero-momentum transfer approximation that $c_0^2 = -c_0^1$. The fits to the plateaus correspond to $A_0\,(am_{c_1}) = -0.00033(167)$, $A_0\,(am_{c_2}) = -0.00027(167)$, and $A_0\,(am_{c_3}) = -0.00024(167)$.*

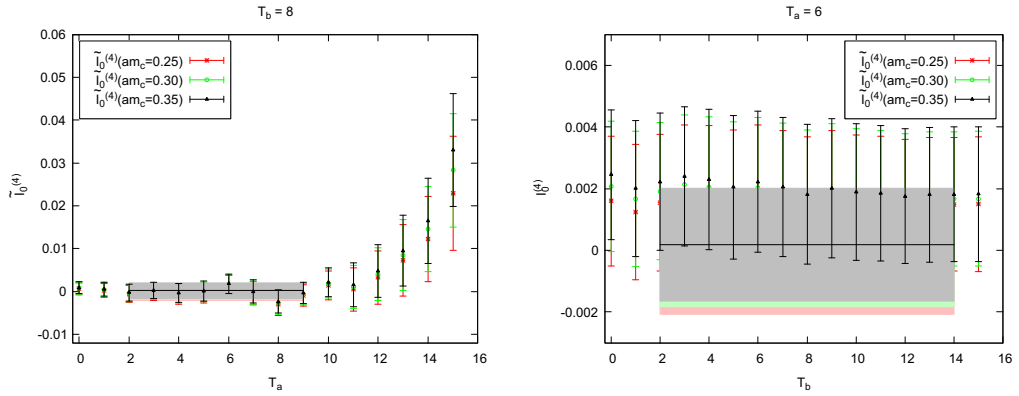

(a) (b)

Figure 4.19 *Fit of the normalized, integrated rare kaon 4-point correlator with the intermediate states removed, shown for (a) $T_b = 8$ and (b) $T_a = 6$. The results were obtained by fitting A_0 the 2- and 3-point parameters that make up c_0^1 and c_0^2, as in Equation (3.46). The fits to the plateaus correspond to $A_0\left(am_{c_1}\right) = -0.00026(182)$, $A_0\left(am_{c_2}\right) = -0.00002(183)$, and $A_0\left(am_{c_3}\right) = 0.00018(183)$.*

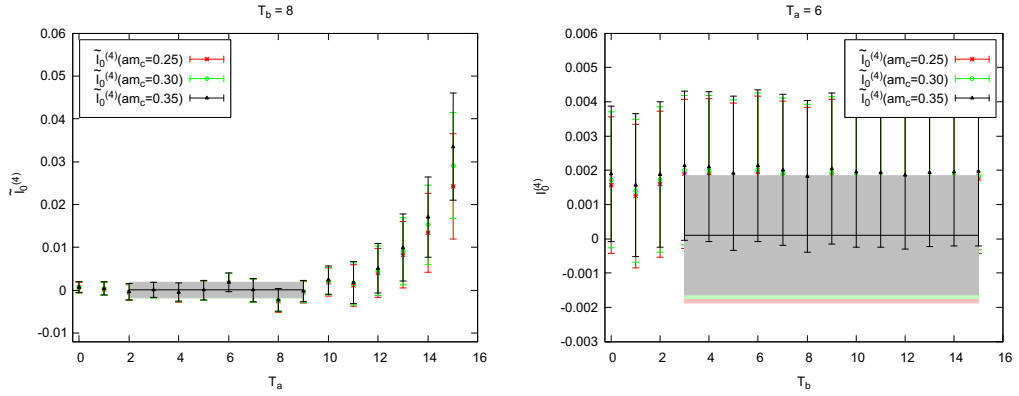

(a) (b)

Figure 4.20 *Fit of the normalized, integrated rare kaon 4-point correlator with the intermediate states removed, shown for (a) $T_b = 8$ and (b) $T_a = 6$. The results were obtained by fitting A_0 the 2- and 3-point parameters that make up c_0^1 and c_0^2, with the $SU(3)$ flavor symmetry approximation, where we take $\mathcal{M}_H\left(\vec{k}\right) = \mathcal{M}_H\left(\vec{p}\right)$ as discussed in Section (3.2.3). The fits to the plateaus correspond to $A_0\left(am_{c_1}\right) = -0.00027(176)$, $A_0\left(am_{c_2}\right) = -0.00014(177)$, and $A_0\left(am_{c_3}\right) = 0.00003(177)$.*

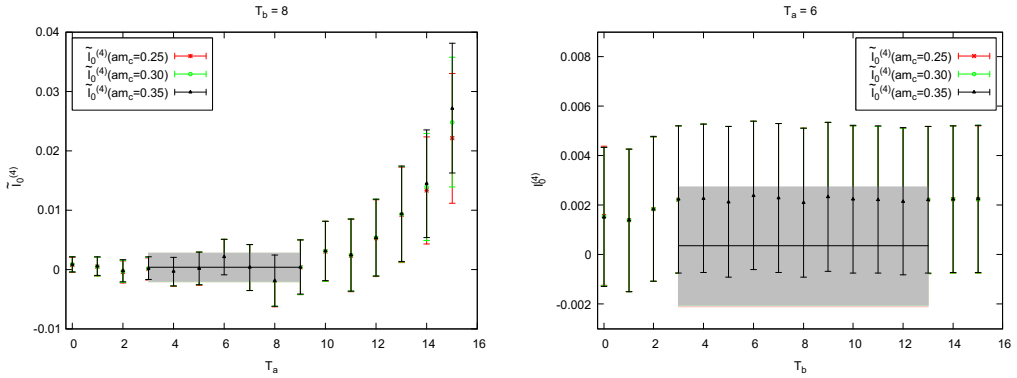

(a) (b)

Figure 4.21 *Fits to the the normalized, integrated rare kaon 4-point correlator with the with the intermediate states removed using a shift of the weak Hamiltonian, shown for (a) $T_b = 8$ and (b) $T_a = 6$. The fits to the plateaus correspond to $A_0\,(am_{c_1}) = 0.00027(237)$, $A_0\,(am_{c_2}) = 0.00031(239)$, and $A_0\,(am_{c_3}) = 0.00035(239)$.*

Shift the Weak Hamiltonian

After shifting the rare kaon 4-point correlator by $c_s\bar{s}d$, with the values of c_s given in Table (4.4) and shown in Figure (4.12), and performing the integration over T_a and T_b we obtain the results that are shown in Figures (4.21). The amplitude is extracted by fitting the integrated correlator in the regions where both sides of the integral plateau. Fit results for the amplitude are given in Table (4.5).
As the $c_s\bar{s}d$ correlator is supposed to describe solely the intermediate states a useful consistency check is to apply the fit methods described in Section (3.2.3) in order to verify that any contribution to the amplitude is compatible with zero. The results of this consistency check, performed with a direct fit to A_0, c_0^1, and c_0^2 are shown in Figures (4.22) and the result of the fits are given in Table (4.5).

4.4.4 Form Factor and Discussion

The results of extracting the amplitude from the 4-point rare kaon correlator are shown in Table (4.5). We can see that our results are still dominated by statistical error, as the noisy contribution from the GIM subtracted Saucer diagram proves to be too poorly resolved. Results between the different methods agree within errors, however this does not encourage much excitement, given the size of these errors. We are unable to confidently establish the sign of the amplitude, although we can place a bound on the value of A_0, and thus the form factor from Equation

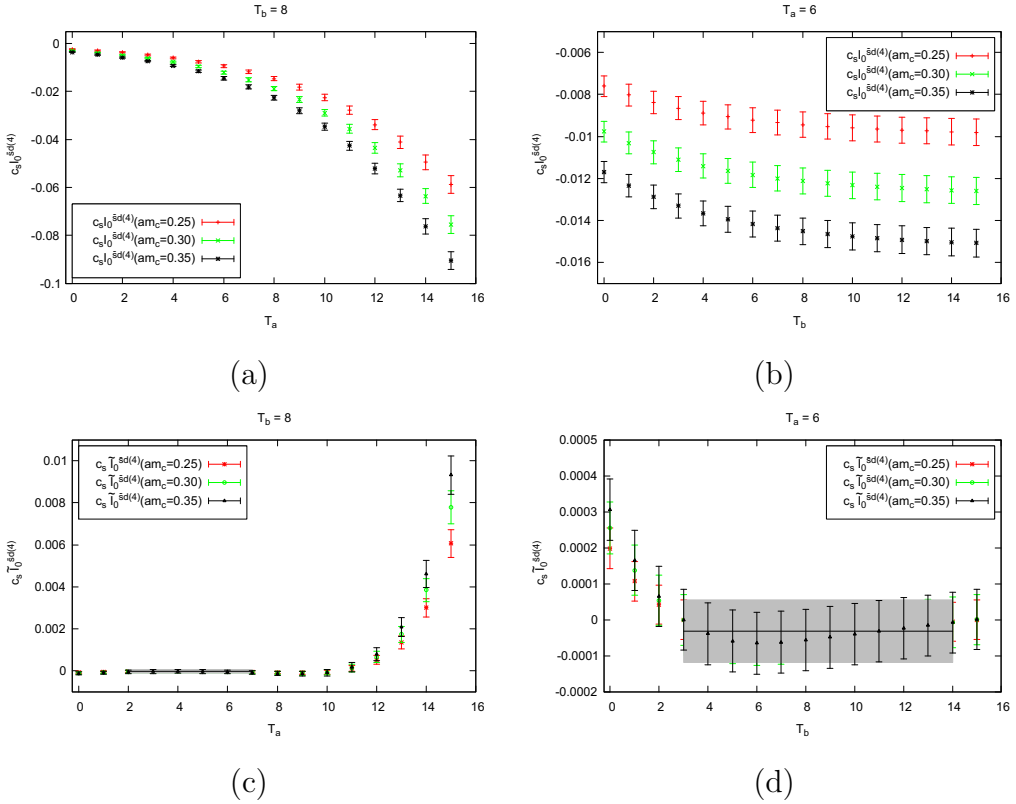

Figure 4.22 *A consistency check to ensure that the four-point scalar density correlator $c_s\bar{s}d$ does not contribute to the rare kaon amplitude when the weak Hamiltonian is shifted. The integrated 4-point correlator $\int_{t_J-T_a}^{t_J+T_b} c_s\tilde{\Gamma}_0^{\bar{s}d}dt_H$ is shown for (a) $T_a = 6$ and (b) $T_b = 8$. Performing the same fit analysis as in Figure (4.18) results in plateaus that correspond to $A_0\,(am_{c_1}) = -0.00002(5)$, $A_0\,(am_{c_2}) = -0.00003(7)$, and $A_0\,(am_{c_3}) = -0.00003(9)$, as shown for (c) $T_a = 6$ and (d) $T_b = 8$.*

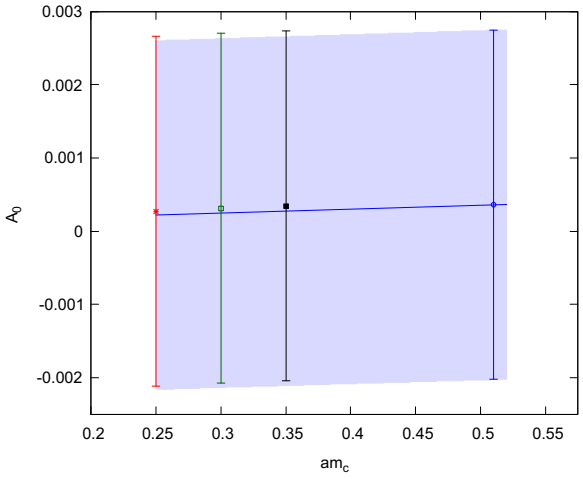

Figure 4.23 *The extrapolation of the amplitude, found using the weak Hamiltonian shift, to the physical charm quark mass. The result of the extrapolation is* $A_0 = 0.00036(239)$.

(3.21), given these results.

The intermediate pion state contribution that grows exponentially with T_a can be seen in Figure (4.16) (a) and it can be seen that the subtraction of this state for all the methods attempted was successful, as we have a clear plateau with which to fit A_0 in all cases. The exponentially shrinking kaon state with T_b dependence is seen to have be suppressed, which is to be expected as we work with a near-physical kaon mass. The subtraction of this state is successful for all methods, with the exception of the zero-momentum transfer approximation. As can be seen in Figure (4.18) (b) taking $c_0^2 = -c_0^1$ leads to a poor estimation of the intermediate kaon state.

Perhaps surprisingly, given the use of near physical pion and kaon masses, the $SU(3)$ symmetric limit approximation holds strong, giving reasonable values for the amplitude, as well as a reconstruction of the c_0^1 and c_0^2 parameters that agrees well with fits from other methods, as given in Table (4.6). The choice to neglect the 2π and 3π intermediate states appears to be justified for this calculation, given the reasonable fits to c_0^1 and c_0^2, with consistent results between methods, and the fact that we see plateaus when fitting for A_0. As the charm quark tends towards the physical point the central values of the fits to A_0 move to a positive result, while the errors remain consistent. Of the methods used the weak Hamiltonian shift is the only method that uses no approximations and it is the method that gives the largest errors, and so gives the most conservative estimate of A_0. It is for these reasons that the c_s shift result is taken to be extrapolated to the physical charm quark mass and used to compute the form factor as our final

result. Figure (4.23) shows the extrapolation of the amplitude to the physical charm quark mass, giving a value of $A_0 = 0.00035(239)$.
For our choice of kinematics we have $z = 0.0151(5)$, giving us a form factor of $V(z) = -0.8(5.9)$. This value approximates the a_+ parameter in Equation (3.22), as our low value of z brings us close to the intercept and suppresses the value of the slope b_+, which we expect to be of the same order at a_+. As discussed in Section (3.1.2), the value of a_+ extracted from experiment is $a_+^{exp} = -0.578(16)$ for the electron and $a_+^{exp} = -0.592(15)$ for the muon. The value extracted from the 3 flavor, 2 loop, QCD prediction is $a_+^{pheno} = -1.59(8)$, and the previous lattice calculation using unphysical pion and kaon masses found $a_+^{latt} = 1.6(7)$.

Chapter 5

Conclusions

The aim of this work was to study the long-distance contributions to the rare kaon decay $K^+ \to \pi^+\ell^+\ell^-$, using lattice QCD with physical light quark masses. This has been the first calculation of its kind to be performed with near-physical pion and kaon masses. The calculation was investigated using both all-to-all propagators and Coulomb gauge-fixed wall source propagators. The A2A approach struggled when confronted with the insertion of currents and was deemed inappropriate for this calculation, whereas computing wall source propagators with sequentially inserted currents proved to sufficient for all non-loop propagators. When using physical light quark masses, even with unphysically light charm quark masses, the GIM subtraction introduces an unsatisfactory amount of noise. Although sparse noises reduced the statistical error introduced by the single-propagator trace contribution to the Eye and Saucer diagrams, more needs to be done in order to reach a well resolved result. The form factor that encapsulates the behavior of the long-distance amplitude of the rare kaon decay was found to be $V\left(0.0151\left(5\right)\right) = -0.8\left(5.9\right)$. When this is compared to experimental results, $V^{exp}\left(0\right) \equiv a_+^{exp} = -0.578(16)$ for the electron and $a_+^{exp} = -0.592(15)$ for the muon, it can be seen that the error on our lattice result is ~ 10 times larger than the central value of the experimental result. Naïve square root scaling of the error tells us that 100 times the current statistics would need to be generated in order to have an error that is of the same order as the experimental central value, which would at least allow for a lattice determination of the sign of a_+, but this is computationally unfeasible at this time.

Approaches that may be developed to reduce the statistical error introduced but the loops in the Eye and Saucer diagrams will be closely coupled to studies of

disconnected diagrams, any improvements that can be made to the calculation of single-propagator traces will be crucial for the study of the decay process we are interested in. Further improvements to the analysis may come from integrating over the current insertion time, as well as the weak Hamiltonian time. Though this will not tackle the dominant source of noise for this decay, its use may be needed in conjunction with improvements to the loop noise in order to reduce the computational cost of a physical point calculation.

It is also possible to work in 3 flavor QCD, forgoing the calculation of the charm quark loop, further reducing computational costs. This would require a new renormalization procedure which would be analogous to that of the $K \to \pi\nu\bar{\nu}$ study that was performed by the RBC-UKQCD collaborations previously [9, 35]. This is particularly relevant for the study of this rare kaon decay on RBC-UKQCD's $48^3 \times 96$ DWF ensemble, on which physical charm quarks can not be simulated. RBC-UKQCD's $64^3 \times 96$ ensemble, with inverse lattice spacing $a^{-1} = 2.38\text{GeV}$, could be used to study the decay with a physical charm quark mass. If methods to control the statistical error introduced by single-propagator traces are formulated then such a calculation would be feasible, given improvements to computational capabilities of future computers.

Appendix A

Eigenvector Generation

The lattice Dirac operator is a large, sparse, near-singular, hermitian, matrix. Although it is unreasonable to expect to be able to compute any significant proportion of the Dirac matrix it is the low lying eigenvectors that couple to low energy physics, and so only the lowest few eigenvectors are important to us. We thus wish to find an algorithm that can find a small subset of eigenvectors of a large, sparse, hermitian matrix. It would also be beneficial to conserve the structure of the Dirac matrix in this process, as its sparsity can be used to our advantage when multiplication is carried out. We would also like a method that has low memory requirements, as the storage costs of these eigenvectors can be unwieldy. For example, the lowest 2000 eigenvectors of the preconditioned zMöius DWF Dirac operator for light quark masses on 48^3 and 64^3 Iwasaki ensembles at near physical pion mass take up 9.3TB and 36TB per configuration respectively. [37]

This section discusses the Symmetric Lanczos Algorithm, a Krylov Subspace method that is used to find a small subset of eigenvectors of a large, sparse, hermitian matrix. Improvements to the performance of this algorithm using implicit restarting and Chebyshev polynomials are also discussed, along with a compression method that can be used to reduce memory requirements.

A.1 Krylov Subspaces

Subspaces of the form

$$\mathcal{K}_m(A, x) \equiv span\left\{x, Ax, \ldots, A^{m-1}x\right\} \tag{A.1}$$

for a matrix A and vector x are called Krylov subspaces. Repeatedly applying A on the vector x brings x closer to the dominant eigendirection. So the Krylov space can be seen to be close to spanning the dominant eigenvectors.

Suppose the columns of the matrix, $V_m = [v_1, \ldots, v_m]$, form an orthonormal basis of $\mathcal{K}_m(A, x)$. Then if A is hermitian

$$T_m = V_m^\dagger A V_m \tag{A.2}$$

is tridiagonal. To see this we consider T_{ij} for $i < j + 1$. Note that $T_{ij} = v_i^\dagger A v_j$, and

$$\begin{aligned} Av_j &\in span\left\{x, Ax, \ldots, A^j x\right\} \\ &= span\left\{v_1, v_2, \ldots, v_{j+1}\right\}. \end{aligned} \tag{A.3}$$

Since $\{v_i\}_{i=1}^m$ form an orthonormal set, v_i is orthogonal to $span\{v_1, v_2, \ldots, v_{j+1}\}$ for $i > j+1$. This means that $v_i^\dagger A q_j = 0$, all the entries below the first subdiagonal are zero, so T_m has an upper Hessenberg form. However, as A is symmetric, $V_m^\dagger A V_m = T_m$ is also symmetric. Thus $T_{ij} = 0$ for $i < j - 1$ and T_m is tridiagonal. We write it is as

$$T_m = \begin{pmatrix} \alpha_1 & \beta_2 & & & \\ \beta_2 & \alpha_2 & \beta_3 & & \\ & . & . & . & \\ & & \beta_{m-1} & \alpha_{m-1} & \beta_m \\ & & & \beta_m & \alpha_m \end{pmatrix} \tag{A.4}$$

The next Krylov subspace is found by by orthogonalizing Av_j against $v_1, \ldots, v_j$,

instead of $A^j v$:

$$\begin{aligned} \mathcal{K}_{m+1}(A,x) &= span\left\{x, Ax, \ldots, A^j x\right\} \\ &= span\left\{v_1, v_2, \ldots, v_j, Av_j\right\}. \end{aligned} \tag{A.5}$$

Let

$$\begin{aligned} w_j &= Av_j - \sum_{k=1}^{j} v_k \left(v_k^\dagger A v_j\right) \\ &= Av_j - \alpha_j v_j - \beta_j v_{j-1} \end{aligned} \tag{A.6}$$

and

$$v_{j+1} = \frac{w_j}{\|w_j\|_2}. \tag{A.7}$$

By construction, $v_i^\dagger v_{j+1} = 0$ for $i = 1, 2, \ldots, j$, so

$$\mathcal{K}_{m+1}(A,x) = span\left\{v_1, v_2, \ldots, v_j, v_{j+1}\right\}. \tag{A.8}$$

Using the mutual orthogonality of the v_i's a recursion relation can be used to find the α_i's and the β_i's. We first examine the j^{th} column of $AV_m = V_m T_m$:

$$Av_j = \beta_j v_{j-1} + \alpha_j v_j + \beta_{j+1} v_{j+1}. \tag{A.9}$$

Thus we can find α_j as

$$v_j^\dagger A v_j = \alpha_j \tag{A.10}$$

and $\beta_{j+1} v_{j+1}$ can be found as

$$\beta_{j+1} v_{j+1} = Av_j - \alpha_j v_j - \beta_j v_{j-1} = w_j. \tag{A.11}$$

This gives

$$v_{j+1} = \frac{w_j}{\beta_{j+1}} \tag{A.12}$$

where $\beta_{j+1} = \|w_j\|_2$.

The algorithm that uses this recursion relation to find the α_i's and the β_i's is called the Lanczos Algorithm.

A.2 The Lanczos Algorithm

The Lanczos Algorithm is given as [84]

1. Choose an initial vector v_1 of norm unity. Set $\beta_1 \equiv 0, v_0 \equiv 0$
2. For $j = 1, 2, \ldots, m$ Do:
3. $\quad w_j = Av_j - \beta_j v_{j-1}$
4. $\quad \alpha_j = v_j^\dagger w_j$
5. $\quad w_j = w_j - \alpha_j v_j$
6. $\quad \beta_{j+1} = \|w_j\|_2$. If $\beta_{j+1} = 0$ then Stop
7. $\quad v_{j+1} = \frac{w_j}{\beta_{j+1}}$
8. EndDo

This algorithm produces a tridiagonal matrix T_m and m vectors $V_m = [v_1, \ldots, v_m]$ such that

$$AV_m = V_m T_m + w_m e_m^\dagger \tag{A.13}$$

and

$$V_M^\dagger w_m = 0. \tag{A.14}$$

An orthonormal matrix S_m that diagonalizes T_m can be found:

$$S_M^\dagger T_m S_m = \Theta_m = \begin{pmatrix} \theta_1 & & \\ & \ddots & \\ & & \theta_m \end{pmatrix}. \tag{A.15}$$

Letting $Y_m = V_m S_m$, the column vectors, y_i, of $Y_m = [y_1, \ldots, y_m]$ are said to be "close" to the eigenvectors of A and the θ_i's are said to be "close" to the eigenvalues of A. Specifically:

$$\|Ay_i - \theta_i y_i\|_2 = |\beta_{m+1}||(S_m)_{mi}|. \tag{A.16}$$

To see this we right-multiply (A.13) by S_m

$$AV_m S_m = V_m T_m S_m + w_m e_m^\dagger S_m \tag{A.17}$$

and using the definition of Y_m and the fact that S_m is orthonormal we get

$$\begin{aligned} AY_m &= V_m S_m S_m^\dagger T_m S_m + w_m e_m^\dagger S_m \\ &= Y_m \Theta_m + w_m e_m^\dagger S_m. \end{aligned} \tag{A.18}$$

Looking at the i^{th} column:

$$Ay_i = \theta_i y_i + w_m e_m^\dagger S_m e_i \tag{A.19}$$

implies that that $\|Ay_i - \theta_i y_i\|_2 = |\beta_{m+1}||(S_m)_{mi}|$ since $|\beta_{m+1}| = \|w_m\|_2$.

In exact arithmetic the Lanczos Algorithm guarantees that the vectors, v_i, are orthogonal. In practice the exact orthogonality of these vectors is lost rapidly. There is also no way to determine in advance how many steps it will take to find the eigenvalues of interest to a specified accuracy. Convergence is determined by the distribution of the eigenvalues and the choice of the starting vector, v_1. In many case convergence will not occur until m gets very large, and maintaining the orthogonality of the vectors, v_m, becomes costly.

Another way to converge to the required eigenvalues and maintain orthogonality s to limit the size of V_m and use restarting schemes. For each restart of the Lanczos Algorithm the starting vector, v_1, is replaced with an "improved" starting vector, $\tilde{v}_1$. The residual vector, w_m, vanishes if $\tilde{v}_1$ is a linear combination of m eigenvectors of A, and restarting schemes aim to have this happen. A scheme in which a new starting vector is produced by some process is called explicit restarting.

An implicit restart involves a combination of an implicitly shifted QR scheme and an m-step Lanczos factorization.

A.3 Implicitly Restarted Lanczos

Consider the case where the starting vector is a linear combination of two eigenvectors

$$v = c_1 v_1 + c_2 v_2. \tag{A.20}$$

If the eigenvalue associated with v_2, λ_1, is known an "improved" starting vector

could be given by

$$\tilde{v} = (A - \lambda_1)\, v = c_1 (\lambda_1 - \lambda_1)\, v_1 + c_2 (\lambda_2 - \lambda_1)\, v_2 \tag{A.21}$$

which removes the component n the known v_1 direction. By applying a polynomial with shifts, s_n,

$$p(A) = (A - s_1) \ldots (A - s_n) \tag{A.22}$$

to the starting vector we can remove or reduce components in some eigen direction and converge to a desired subspace. The spectrum of T_m, $\sigma(T_m) = \{\theta_1, \ldots, \theta_m\}$, can be divided into k wanted and p unwanted components, and the p unwanted components can be used as shifts. The polynomial, $p(A)$, is not applied directly, but instead through a QR transformation, as shown in the following algorithm [56].

1. For $m > k$, $p = m - k$, compute an m-step Lanczos factorization
   $AV_m = V_m T_m + w_m e_m^\dagger$
2. Repeat until convergence ($T_k = D_k$ diagonal)
3. Compute $\sigma(T_m)$ and select p shifts $\theta_1, \ldots, \theta_p$
4. $Q = I_m$
5. For $j = 1, 2, \ldots, p$ Do:
6. $Q_j R_j = T_m - \theta_j I_m$
7. $Q = QQ_j$
8. $T_m = Q_j^\dagger T_m Q_j$
9. EndDo
10. $\sigma_k = Q(m, k)$
11. $\beta_k = T_m(k, k-1)$
12. $w_k = v_{k+1}\beta_{k+1} + w_m \sigma_k$
13. $V_k = V_m Q(1 : m, 1 : k)$
14. $T_k = T_m(1 : k, 1 : k)$
15. Beginning with the k-step Lanczos factorization
    $AV_k = V_k T_k + w_k e_k^\dagger$
    apply p additional steps of the Lanczos process to obtain a new m-step Lanczos
    factorization
    $AV_m = V_m T_m + w_m e_m^\dagger$
16. EndRepeat

To see how the implicit restart works consider the QR decomposition after the m-step Lanczos factorization

$$QR = T_m - \theta I_m \tag{A.23}$$

that is constructed for a given shift θ. Using the fact that Q is orthonormal

$$AV_m = V_m T_m + w_m e_m^\dagger \tag{A.24}$$

$$AV_m Q_m = V_m T_m Q_m + w_m e_m^\dagger Q_m \tag{A.25}$$

$$AV'_m = V'_m T'_m + w_m e_m^\dagger Q_m. \tag{A.26}$$

It can be shown that

$$e_m^\dagger Q = \tilde{e} = (0, \ldots, 0, \tilde{e}_k, \ldots, \tilde{e}_m). \tag{A.27}$$

The first non-zero row of Q is the k^{th} one. Equating the first k columns above gives

$$AV_k = V_k T_k + w_k e_k^\dagger. \tag{A.28}$$

This is the k-step Lanczos factorization. This is the same factorization we would have obtained had we started with the vector $p(A)v$. To show this consider

$$\begin{aligned} AV_m &= V_m T_m + w_m e_m^\dagger \\ &= V_m(QR + \theta I_m) + w_m e_m^\dagger \end{aligned} \tag{A.29}$$

so

$$(A - \theta I_m)V_m = V'_m R + w_m e_m^\dagger. \tag{A.30}$$

Multiplying by e_1 gives the first column

$$(A - \theta I_m)V_m e_1 = V'_m R e_1. \tag{A.31}$$

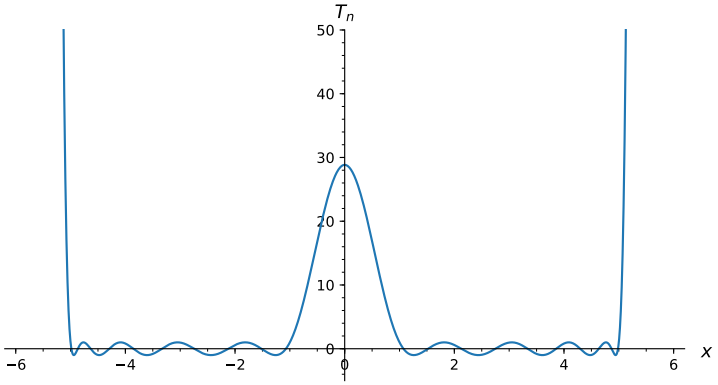

Figure A.1 *The polynomial* $T_{10}(q(x; \alpha = 5, \beta = 1))$

Since R is upper triangular

$$Re_1 = (\rho, 0, \ldots, 0) \tag{A.32}$$

we have

$$v_1' = \frac{1}{\rho}(A - \theta I_m)v_1. \tag{A.33}$$

The new factorization is equivalent to one started with $(A - \theta I_m)v_1$ instead of v_1 and repeating this process with the other shifts effectively multiplies this by the other factors of $p(A)$.

A.4 Chebyshev Filters

The matrix whose eigensystem is to be found may be replaced with a polynomial of the matrix $p(A)$ which has better spectral properties, namely that the wanted eigenvalues are large and well separated. The largest eigenvalues of $p(A)$

$$p(A) = p(\lambda_i)v_i \tag{A.34}$$

can be found in fewer iterations than the lowest eigenvalues of A. Since $p(A)$ and A have common eigenvectors the eigenvalues of A can be obtained from the Rayleigh quotient

$$\lambda_i = \frac{v_i^\dagger A v_i}{v_i^\dagger v_i} \tag{A.35}$$

once the eigenvectors have been found. The polynomial is applied explicitly and will be more expensive than doing a single multiplication by A, so there is a trade off between a smaller number of iterations and a larger cost for each one.

In order to compute the lowest eigenvalues of A we need a polynomial that is nearly zero for the high modes and rapidly increasing for the low ones, separating them from each other. First, consider the polynomial

$$q(A) = q(A; \alpha, \beta) = \frac{2A^2 - (\alpha^2 + \beta^2)}{\alpha^2 - \beta^2} \tag{A.36}$$

where α and β are some constants. Now consider the n^{th} order Chebyshev polynomial defined by

$$T_n(t) = \begin{cases} cos[ncos^{-1}(t)], & \text{if } -1 \leq t \leq 1 \\ cosh[ncosh^{-1}(t)], & \text{otherwise} \end{cases} \tag{A.37}$$

which can be given by the recursion relation

$$T_n(t) = 2tT_{n-1}(t) - T_{n-2}(t). \tag{A.38}$$

Note that $-1 \leq q(x) \leq 1$ for $\beta \leq x \leq \alpha$, and that the Chebyshev polynomials are small in the interval $[-1, 1]$ and rapidly rising outside. Thus $T_n(q(x))$ is large for $x > \alpha$ and $x < \beta$. If we choose α as the largest eigenvalue of the matrix A (or larger) and β as the largest eigenvalue we wish to compute then the wanted part of the spectrum is greatly enhanced and the spectrum in the interval $[\beta, \alpha]$ is damped.

A.5 Local Coherence Lanczos Solver

Little appears to be known about the space-time structure of the low quark modes, but numerical inspection suggests that they are locally coherent.[74] This property allows highly effective deflation subspaces to be built from only a few low modes using block projectors, which is utilized in the Local Coherence Lanczos solver. A spatially-blocked basis of the lowest N eigenmodes allows for the creation of a coarse-grid representation of the eigenmodes that can have a significantly reduced memory requirement than that of a fine-grid. The following steps are to be taken

Figure A.2 *When restricted to a small block of lattice points, the O(V) low modes of the Dirac operator tend to align to a relatively low-dimensional linear space, a property referred to as local coherence. [73]*

[37]:

1. Find N basis vectors using the Chebyshev-accelerated Implicitly Restarted Lanczos method
2. For each block use these N basis vectors to create a locally orthogonal basis to define a mapping between the coarse and the fine grid
3. Use the IRL method to find a full set of eigenvectors on the coarse grid
4. Reconstruct an approximation of the eigenvalues by locally inverting the Chebyshev polynomial of the Lanczos eigenvalues
5. Correct the eigenvalues outside of the basis with a smoothing procedure

Appendix B

A2A Formulation of the Weak Hamiltonian 3-point Functions

The contractions given by the diagrams in Figure (3.4) can be written in terms of A2A vectors and meson fields as follows.

B.1 Wing (W) Diagram

$$
\begin{aligned}
C(t) &= \sum_{\mathbf{x}_H,\mathbf{x}_\pi,\mathbf{x}_K} \mathrm{Tr}\left[\gamma_5 S^{(l)}(x_\pi,x_H)\gamma_\mu^L S^{(l)}(x_H,x_\pi)\right] \mathrm{Tr}\left[\gamma^{L\mu} S^{(l)}(x_H,x_K)\gamma_5 S^{(s)}(x_K,x_H)\right] \\
&= \sum_{\mathbf{x}_H,\mathbf{x}_\pi,\mathbf{x}_K} \sum_{i,j,m,n} \mathrm{Tr}\left[\gamma_5 v_i^{(l)}(x_\pi) w_i^{(l)}(x_H)\gamma_\mu^L v_j^{(l)}(x_H) w_j^{(l)}(x_\pi)\right] \\
&\qquad \times \mathrm{Tr}\left[\gamma^{L\mu} v_m^{(l)}(x_H) w_m^{(l)}(x_K)\gamma_5 v_n^{(s)}(x_K) w_n^{(s)}(x_H)\right] \\
&= \sum_{\mathbf{x}_H,\mathbf{x}_\pi,\mathbf{x}_K} \sum_{i,j,m,n} w_j^{(l)}(x_\pi)\gamma_5 v_i^{(l)}(x_\pi) w_i^{(l)}(x_H)\gamma_\mu^L v_j^{(l)}(x_H) \\
&\qquad \times w_n^{(s)}(x_H)\gamma^{L\mu} v_m^{(l)}(x_H) w_m^{(l)}(x_K)\gamma_5 v_n^{(s)}(x_K) \\
&= \sum_{i,j,m,n} \Pi_{ji}^{(l,l)}(t_\pi;\gamma_5)\Pi_{mn}^{(l,s)}(t_K;\gamma_5) \sum_{\mathbf{x}_H} \left[w_i^{(l)}(x_H)\gamma_\mu^L v_j^{(l)}(x_H) w_n^{(s)}(x_H)\gamma^{L\mu} v_m^{(l)}(x_H)\right]
\end{aligned}
\tag{B.1}
$$

B.2 Connected (C) Diagram

$$\begin{aligned} C(t) &= \sum_{\mathbf{x}_H,\mathbf{x}_\pi,\mathbf{x}_K} \mathrm{Tr}\left[\gamma_5 S^{(l)}(x_\pi,x_H)\gamma_\mu^L S^{(l)}(x_H,x_K)\gamma_5 S^{(l)}(x_K,x_H)\gamma^{L\mu} S^{(s)}(x_H,x_\pi)\right] \\ &= \sum_{\mathbf{x}_H}\sum_{i,j,m,n} \Pi_{ni}^{(l,l)}(t_\pi;\gamma_5) w_i^{(l)}(x_H)\gamma_\mu^L v_j^{(l)}(x_H) w_j^{(l)}(x_K)\gamma_5 v_m^{(s)}(x_K) w_m^{(s)}(x_H)\gamma^{L\mu} v_n^{(l)}(x_H) \\ &= \sum_{i,j,m,n} \Pi_{ni}^{(l,l)}(t_\pi;\gamma_5)\Pi_{jm}^{(l,s)}(t_K;\gamma_5) \sum_{\mathbf{x}_H}\left[w_i^{(l)}(x_H)\gamma_\mu^L v_j^{(l)}(x_H) w_m^{(s)}(x_H)\gamma^{L\mu} v_n^{(l)}(x_H)\right] \end{aligned} \tag{B.2}$$

B.3 Saucer (S) Diagram

For the charm quark case:

$$\begin{aligned} C(t) &= \sum_{\mathbf{x}_H,\mathbf{x}_\pi,\mathbf{x}_K} \mathrm{Tr}\left[\gamma_5 S^{(l)}(x_\pi,x_K)\gamma_5 S^{(s)}(x_K,x_H)\gamma_\mu^L S^{(c)}(x_H,x_H)\gamma^{L\mu} S^{(l)}(x_H,x_\pi)\right] \\ &= \sum_{i,j,m,n} \Pi_{ni}^{(l,l)}(t_\pi;\gamma_5)\Pi_{ij}^{(l,s)}(t_K;\gamma_5) \sum_{\mathbf{x}_H}\left[w_j^{(s)}(x_H)\gamma_\mu^L v_m^{(c)}(x_H) w_m^{(c)}(x_H)\gamma^{L\mu} v_n^{(l)}(x_H)\right] \end{aligned} \tag{B.3}$$

B.4 Eye (E) Diagram

For the charm quark case:

$$\begin{aligned} C(t) &= \sum_{\mathbf{x}_H,\mathbf{x}_\pi,\mathbf{x}_K} \mathrm{Tr}\left[\gamma_5 S^{(l)}(x_\pi,x_K)\gamma_5 S^{(s)}(x_K,x_H)\gamma_\mu^L S^{(l)}(x_H,x_\pi)\right] \mathrm{Tr}\left[\gamma^{L\mu} S^{(c)}(x_H,x_H)\right] \\ &= \sum_{i,j,m,n} \Pi_{mi}^{(l,l)}(t_\pi;\gamma_5)\Pi_{ij}^{(l,s)}(t_K;\gamma_5) \sum_{\mathbf{x}_H}\left[w_j^{(s)}(x_H)\gamma_\mu^L v_m^{(l)}(x_H) w_n^{(c)}(x_H)\gamma^{L\mu} v_n^{(c)}(x_H)\right] \end{aligned} \tag{B.4}$$

Bibliography

[1] R. Aaij et al. Observation of $j/\psi p$ resonances consistent with pentaquark states in $\Lambda_b^0 \to j/\psi K^- p$ decays. *Phys. Rev. Lett.*, 115:072001, Aug 2015.

[2] R. et al Aaij. Test of lepton universality in beauty-quark decays. *arXiv:2103.11769 [hep-ex]*, 2021.

[3] B. et al Abi. Measurement of the positive muon anomalous magnetic moment to 0.46 ppm. *Phys. Rev. Lett.*, 126:141801, Apr 2021.

[4] S. Aoki, Y. Aoki, D. Beirevi, T. Blum, G. Colangelo, S. Collins, M. Della Morte, P. Dimopoulos, S. Dürr, H. Fukaya, and et al. Flag review 2019. *The European Physical Journal C*, 80(2), Feb 2020.

[5] Y. Aoki, R. Arthur, T. Blum, P. A. Boyle, D. Broemmel, N. H. Christ, C. Dawson, J. M. Flynn, T. Izubuchi, X-Y. Jin, and et al. Continuum limit physics from2+1flavor domain wall qcd. *Physical Review D*, 83(7), Apr 2011.

[6] T. Aoyama et al. The anomalous magnetic moment of the muon in the Standard Model. *Physics Reports*, 887:1–166, 2020.

[7] Tatsumi Aoyama, Masashi Hayakawa, Toichiro Kinoshita, and Makiko Nio. Tenth-order electron anomalous magnetic moment: Contribution of diagrams without closed lepton loops. *Phys. Rev. D*, 91:033006, Feb 2015.

[8] Z. Bai, N.H. Christ, T. Izubuchi, C.T. Sachrajda, A. Soni, and J. Yu. $K_L - K_S$ Mass Difference from Lattice QCD. *Physical Review Letters*, 113(11), Sep 2014.

[9] Ziyuan Bai, Norman H. Christ, Xu Feng, Andrew Lawson, Antonin Portelli, and Christopher T. Sachrajda. Exploratory Lattice QCD Study of the Rare Kaon Decay $K \to \pi\nu\bar{\nu}$. *Physical Review Letters*, 118(25), Jun 2017.

[10] P. A. Baikov, K. G. Chetyrkin, and J. H. Kühn. Five-Loop Running of the QCD Coupling Constant. *Phys. Rev. Lett.*, 118:082002, Feb 2017.

[11] J.R. Batley et al. Precise measurement of the $K^+ \to \pi^+ e^+ e^-$ decay. *Physics Letters B*, 677(5):246–254, 2009.

[12] J.R. Batley, G. Kalmus, C. Lazzeroni, D.J. Munday, M.W. Slater, S.A. Wotton, R. Arcidiacono, G. Bocquet, N. Cabibbo, A. Ceccucci, and et al. New measurement of the $K^+ \to \pi^+\mu^+\mu^-$ decay. *Physics Letters B*, 697(2):107115, Feb 2011.

[13] J.R Batley, G.E Kalmus, C Lazzeroni, D.J Munday, M Patel, M.W Slater, S.A Wotton, R Arcidiacono, G Bocquet, A Ceccucci, and et al. Observation of the rare decay $K_S \to \pi^0 e^+ e^-$. *Physics Letters B*, 576(1-2):4354, Dec 2003.

[14] J.R. Batley, G.E. Kalmus, C. Lazzeroni, D.J. Munday, M. Patel, M.W. Slater, S.A. Wotton, R. Arcidiacono, G. Bocquet, A. Ceccucci, and et al. Observation of the rare decay $k_S \to \pi^0\mu^+\mu^-$. *Physics Letters B*, 599(3-4):197211, Oct 2004.

[15] Alexei Bazavov, Nora Brambilla, Xavier Garcia i Tormo, Pter Petreczky, Joan Soto, and Antonio Vairo. Determination ofsfrom the QCD static energy: An update. *Physical Review D*, 90(7), Oct 2014.

[16] K. G. Begeman, A. H. Broeils, and R. H. Sanders. Extended rotation curves of spiral galaxies: dark haloes and modified dynamics. *Monthly Notices of the Royal Astronomical Society*, 249(3):523–537, 04 1991.

[17] Lubos Bician et al. New measurement of the $K^+ \to \pi^+\mu^+\mu^-$ decay at NA62. In *Proceedings of 40th International Conference on High Energy physics — PoS(ICHEP2020)*, volume 390, page 364, 2021.

[18] T. Blum, P. A. Boyle, N. H. Christ, N. Garron, E. Goode, T. Izubuchi, C. Lehner, Q. Liu, R. D. Mawhinney, C. T. Sachrajda, and et al. $K \to \pi\pi$ decay amplitudes from lattice QCD. *Physical Review D*, 84(11), Dec 2011.

[19] T. Blum, P.A. Boyle, N.H. Christ, J. Frison, N. Garron, R.J. Hudspith, T. Izubuchi, T. Janowski, C. Jung, A. Jüttner, and et al. Domain wall qcd with physical quark masses. *Physical Review D*, 93(7), Apr 2016.

[20] Thomas Blum, Taku Izubuchi, and Eigo Shintani. New class of variance-reduction techniques using lattice symmetries. *Physical Review D*, 88(9), Nov 2013.

[21] Bugra Borasoy. Introduction to chiral perturbation theory. In Takhmasib Aliev, Namik Kemal Pak, and Meltem Serin, editors, *The Standard Model and Beyond*, pages 1–26, Berlin, Heidelberg, 2008. Springer Berlin Heidelberg.

[22] Fodor Z. Guenther J.N. et al Borsanyi, S. Leading hadronic contribution to the muon magnetic moment from lattice QCD. *Nature*, 593:51–55, 04 2021.

[23] P Boyle, A Jüttner, F Ó hÓgáin, and A Portelli. Latest Results on Lattice Calculation Concerning $K \to \pi\ell^+\ell^-$ Decays. *Journal of Physics: Conference Series*, 1526:012015, apr 2020.

[24] Peter Boyle, Azusa Yamaguchi, Guido Cossu, and Antonin Portelli. Grid: A next generation data parallel c++ qcd library, 2015.

[25] Peter A. Boyle, Norman H. Christ, Jonathan M. Flynn, Nicolas Garron, Chulwoo Jung, Andreas Jüttner, Robert D. Mawhinney, David Murphy, Christopher T. Sachrajda, Francesco Sanfilippo, and Hantao Yin. The kaon semileptonic form factor in Nf=2+1 domain wall lattice QCD with physical light quark masses. *Journal of High Energy Physics*, 2015.

[26] RichardC. Brower, Harmut Neff, and Kostas Orginos. The Möbius domain wall fermion algorithm. *Computer Physics Communications*, 220:1–19, 2017.

[27] Mattia Bruno, Mattia Dalla Brida, Patrick Fritzsch, Tomasz Korzec, Alberto Ramos, Stefan Schaefer, Hubert Simma, Stefan Sint, and Rainer Sommer. QCD Coupling from a Nonperturbative Determination of the Three-Flavor Λ Parameter. *Physical Review Letters*, 119(10), Sep 2017.

[28] Gerhard Buchalla, Andrzej J. Buras, and Markus E. Lautenbacher. Weak decays beyond leading logarithms. *Reviews of Modern Physics*, 68(4):11251244, Oct 1996.

[29] Andrzej J. Buras, Matthias Jamin, and Markus E. Lautenbacher. The anatomy of ϵ'/ϵ beyond leading logarithms with improved hadronic matrix elements. *Nuclear Physics B*, 408(2):209285, Nov 1993.

[30] Nicola Cabibbo. Unitary symmetry and leptonic decays. *Phys. Rev. Lett.*, 10:531–533, Jun 1963.

[31] Bipasha Chakraborty, C.T.H. Davies, B. Galloway, P. Knecht, J. Koponen, G.C. Donald, R.J. Dowdall, G.P. Lepage, and C. McNeile. High-precision quark masses and QCD coupling fromnf=4lattice QCD. *Physical Review D*, 91(5), Mar 2015.

[32] N. H. Christ, T. Izubuchi, C. T. Sachrajda, A. Soni, and J. Yu. Long distance contribution to the $K_L - K_S$ mass difference. *Physical Review D*, 88(1), Jul 2013.

[33] N. H. Christ, T. Izubuchi, C. T. Sachrajda, A. Soni, and J. Yu. Long distance contribution to the $K_L - K_S$ mass difference. *Physical Review D*, 88(1), Jul 2013.

[34] Norman H. Christ, Xu Feng, Andreas Jüttner, Andrew Lawson, Antonin Portelli, and Christopher T. Sachrajda. First exploratory calculation of the long-distance contributions to the rare kaon decays $K \to \pi\ell^+\ell^-$. *Physical Review D*, 94(11), Dec 2016.

[35] Norman H. Christ, Xu Feng, Antonin Portelli, and Christopher T. Sachrajda. Prospects for a lattice computation of rare kaon decay amplitudes. II. $K \to \pi\nu\bar{\nu}$ decays. *Physical Review D*, 93(11), Jun 2016.

[36] N.H. Christ, X. Feng, A. Portelli, and C.T. Sachrajda. Prospects for a lattice computation of rare kaon decay amplitudes: $K \to \pi\ell^+\ell^-$ decays. *Physical Review D*, 92(9), Nov 2015.

[37] M. A. Clark, Chulwoo Jung, and Christoph Lehner. Multi-grid lanczos. *EPJ Web of Conferences*, 175:14023, 2018.

[38] Andreas Crivellin, Giancarlo D'Ambrosio, Martin Hoferichter, and Lewis C. Tunstall. Violation of lepton flavor and lepton flavor universality in rare kaon decays. *Phys. Rev. D*, 93:074038, Apr 2016.

[39] Giancarlo D'Ambrosio, Gerhard Ecker, Gino Isidori, and Jorge Portolés. The decays $K \to \pi\ell^+\ell^-$ beyond leading order in the chiral expansion. *Journal of High Energy Physics*, 1998(08):004–004, aug 1998.

[40] Michele Della Morte and Andreas Jüttner. Quark disconnected diagrams in chiral perturbation theory. *Journal of High Energy Physics*, 2010(11), Nov 2010.

[41] S.-J. Dong and K.-F. Liu. Stochastic estimation with z 2 noise. *Phys. Lett. B*, page 130136, 1994.

[42] Simon Duane, A.D. Kennedy, Brian J. Pendleton, and Duncan Roweth. Hybrid monte carlo. *Physics Letters B*, 195(2):216–222, 1987.

[43] Giancarlo DAmbrosio, David Greynat, and Marc Knecht. Matching long and short distances in the form factors for $K \to \pi\ell^+\ell^-$. *Physics Letters B*, 797:134891, Oct 2019.

[44] Giancarlo DAmbrosio, David Greynat, and Marc Knecht. On the amplitudes for the CP-conserving $K^{\pm}(K_S) \to \pi^{\pm}(\pi^0)\ell^+\ell^-$ rare decay modes. *Journal of High Energy Physics*, 2019(2), Feb 2019.

[45] GIANCARLO DAMBROSIO and GINO ISIDORI. CP violation in kaon decays. *International Journal of Modern Physics A*, 13(01):193, Jan 1998.

[46] G. Ecker. Chiral perturbation theory. *Progress in Particle and Nuclear Physics*, 35:180, Jan 1995.

[47] Gerhard Ecker, Antonio Pich, and Eduardo de Rafael. $K \to \pi\ell^+\ell$ decays in the effective chiral lagrangian of the standard model. *Nuclear Physics B*, 291:692–719, 1987.

[48] Bradley Efron. Computers and the theory of statistics: Thinking the unthinkable. *SIAM Review*, 21(4):460–480, 1979.

[49] F. Englert and R. Brout. Broken Symmetry and the Mass of Gauge Vector Mesons. *Phys. Rev. Lett.*, 13:321–323, Aug 1964.

[50] Justin Foley, K. Jimmy Juge, Alan Cais, Mike Peardon, Sinad M. Ryan, and Jon-Ivar Skullerud. Practical all-to-all propagators for lattice qcd. *Computer Physics Communications*, 172(3):145162, Nov 2005.

[51] Christof Gattringer and Christian B. Lang. *Quantum chromodynamics on the lattice*, volume 788. Springer, Berlin, 2010.

[52] M. Gell-Mann. A schematic model of baryons and mesons. *Physics Letters*, 8(3):214–215, 1964.

[53] Paul H. Ginsparg and Kenneth G. Wilson. A remnant of chiral symmetry on the lattice. *Phys. Rev. D*, 25:2649–2657, May 1982.

[54] Sheldon L. Glashow. Partial-symmetries of weak interactions. *Nuclear Physics*, 22(4):579–588, 1961.

[55] Jeffrey Goldstone, Abdus Salam, and Steven Weinberg. Broken Symmetries. *Phys. Rev.*, 127:965–970, Aug 1962.

[56] M. Gu, A. Ruhe, R. Lehoucq, D. Sorensen, R. Freund, G. Sleijpen, H. van der Vorst, Z. Bai, and R. Li. *Hermitian Eigenvalue Problems*, chapter 4, pages 45–107.

[57] Maxwell T. Hansen, Fernando Romero-Lpez, and Stephen R. Sharpe. Decay amplitudes to three hadrons from finite-volume matrix elements. *Journal of High Energy Physics*, 2021(4), Apr 2021.

[58] Maxwell T. Hansen and Stephen R. Sharpe. Lattice qcd and three-particle decays of resonances. *Annual Review of Nuclear and Particle Science*, 69(1):65107, Oct 2019.

[59] F. Herzog, B. Ruijl, T. Ueda, J. A. M. Vermaseren, and A. Vogt. The five-loop beta function of Yang-Mills theory with fermions. *Journal of High Energy Physics*, 2017(2), Feb 2017.

[60] Peter W. Higgs. Broken Symmetries and the Masses of Gauge Bosons. *Phys. Rev. Lett.*, 13:508–509, Oct 1964.

[61] R.J. Hudspith. Fourier accelerated conjugate gradient lattice gauge fixing. *Computer Physics Communications*, 187:115119, Feb 2015.

[62] Gino Isidori, Guido Martinelli, and Paolo Turchetti. Rare kaon decays on the lattice. *Physics Letters B*, 633(1):75–83, 2006.

[63] Y. Iwasaki. Renormalization Group Analysis of Lattice Theories and Improved Lattice Action: Two-Dimensional Nonlinear O(N) Sigma Model. *Nucl. Phys. B*, 258:141–156, 1985.

[64] Y. Iwasaki and T. Yoshi. Renormalization group improved action for su(3) lattice gauge theory and the string tension. *Physics Letters B*, 143(4):449–452, 1984.

[65] David B. Kaplan. A method for simulating chiral fermions on the lattice. *Physics Letters B*, 288(3):342–347, 1992.

[66] David B. Kaplan. Chiral symmetry and lattice fermions, July 2019. Lectures delivered at the Frontiers in Lattice QCD Summer School Peking University.

[67] Makoto Kobayashi and Toshihide Maskawa. CP-Violation in the Renormalizable Theory of Weak Interaction. *Progress of Theoretical Physics*, 49(2):652–657, 02 1973.

[68] John Kogut and Leonard Susskind. Hamiltonian formulation of wilson's lattice gauge theories. *Phys. Rev. D*, 11:395–408, Jan 1975.

[69] Andrew Lawson. *Exploratory lattice QCD studies of rare kaon decays*. PhD thesis, University of Southampton, October 2017.

[70] Cristina Lazzeroni. 2021 na62 status report to the cern spsc. Status Report CERN-SPSC-2021-009 ; SPSC-SR-286, CERN SPS, March 2021.

[71] Christoph Lehner and Christian Sturm. Matching factors for $\Delta S = 1$ four-quark operators in RI/SMOM schemes. *Physical Review D*, 84(1), Jul 2011.

[72] LHCb collaboration. Observation of structure in the J/ψ-pair mass spectrum. *Science Bulletin*, 65(23):1983–1993, 2020.

[73] Martin Lüscher. *Computational strategies in lattice QCD.*, chapter 6.

[74] Martin Lüscher. Local coherence and deflation of the low quark modes in lattice qcd. *Journal of High Energy Physics*, 2007(07):081081, Jul 2007.

[75] G. Martinelli, C. Pittori, C.T. Sachrajda, M. Testa, and A. Vladikas. A general method for non-perturbative renormalization of lattice operators. *Nuclear Physics B*, 445(1):81105, Jul 1995.

[76] G. Martinelli and C.T. Sachrajda. A lattice study of nucleon structure. *Nuclear Physics B*, 316(2):355–372, 1989.

[77] Greg McGlynn. Algorithmic improvements for weak coupling simulations of domain wall fermions. In *Proceedings of The 33rd International Symposium on Lattice Field Theory — PoS(LATTICE 2015)*, volume 251, page 019, 2016.

[78] Matthew Moulson. Experimental determination of v_{us} from kaon decays, 2017.

[79] Herbert Neuberger. A practical implementation of the overlap dirac operator. *Physical Review Letters*, 81(19):40604062, Nov 1998.

[80] H.B. Nielsen and M. Ninomiya. A no-go theorem for regularizing chiral fermions. *Physics Letters B*, 105(2):219–223, 1981.

[81] E. Noether. Invariante Variationsprobleme. *Nachrichten von der Gesellschaft der Wissenschaften zu Göttingen, Mathematisch-Physikalische Klasse*, 1918:235–257, 1918.

[82] Antonin Portelli, Nils Asmussen, Peter Boyle, Felix Erben, Vera Gülpers, Raoul Hodgson, Joseph K.L. Lee, Michael Marshall, Fionn hgin, and David Preti. aportelli/hadrons: Hadrons v1.2, November 2020.

[83] Heinz J Rothe. *Lattice Gauge Theories*. WORLD SCIENTIFIC, 4th edition, 2012.

[84] Yousef Saad. *Iterative Methods for Sparse Linear Systems*. PWS Publishing, 1 edition, 1996.

[85] Andrei D Sakharov. Violation of CP invariance, C asymmetry, and baryon asymmetry of the universe. *Soviet Physics Uspekhi*, 34(5):392–393, may 1991.

[86] Yigal Shamir. Chiral fermions from lattice boundaries. *Nuclear Physics B*, 406(1):90–106, 1993.

[87] Yigal Shamir. Anomalies and chiral defect fermions. *Nuclear Physics B*, 417(1-2):167180, Apr 1994.

[88] R. F. Streater and A. S. Wightman. *PCT, spin and statistics, and all that*. 1989.

[89] C. Sturm, Y. Aoki, N. H. Christ, T. Izubuchi, C. T. C. Sachrajda, and A. Soni. Renormalization of quark bilinear operators in a momentum-subtraction scheme with a nonexceptional subtraction point. *Physical Review D*, 80(1), Jul 2009.

[90] Yung-Su Tsai. Decay Correlations of Heavy Leptons in $e^+ + e^- \to l^+ + l^-$. *Phys. Rev. D*, 4:2821–2837, Nov 1971.

[91] Hantao Yin and Robert Mawhinney. Improving DWF Simulations: Force Gradient Integrator and the Mobius Accelerated DWF Solver. In *Proceedings of XXIX International Symposium on Lattice Field Theory — PoS(Lattice 2011)*, volume 139, page 051, 2012.

[92] P.A. Zyla et al. Review of Particle Physics. *PTEP*, 2020(8):083C01, 2020.